UNIVERSITÀ DEGLI STUDI DI MESSINA

Dipartimento di
Scienze Chimiche, Biologiche, Farmaceutiche ed Ambientali

Dottorato di Ricerca in "Scienze Chimiche"

Doctor of Philosophy in "Chemical Sciences"

Analysis of food and food-related compounds by using advanced chromatography techniques

Ph.D. Thesis of:

Ivan **ALOISI**

Supervisor:

Prof. Peter Q. **TRANCHIDA**

Coordinator:

Prof. Paola **DUGO**

SSD CHIM/10

XXXIII Ciclo 2017-2020

TABLE OF CONTENTS

Chapter 1

1.0 Introduction and scope of the research

The objective of the research work, described in this Ph.D. thesis, is the development of modern analytical techniques, and improvement of established methods, for the detection, identification and characterization of complex food and food-related compounds.

In particular, the research was focused on the development and application of mono-dimensional gas chromatography (1D GC) and comprehensive two-dimensional gas chromatography (GC×GC) combined with different types of detectors (mainly mass spectrometers). Different food and food-related samples were subjected to study (i.e., vegetable oils, dietary supplements, food waste, etc.). A great deal of attention was focused on compounds potentially contained in dietary supplements (in particular, fatty acids and phytosterols).

Since the introduction of open-tubular capillaries (OTC) by Golay [1], GC has become one of the most powerful analytical techniques for the analysis of volatile and semi-volatile compounds. Nevertheless, considering that one 1D GC separations often rely on a single separation criterion, such as the different volatility of the analytes, if the vapor pressure of several analytes in a mixture do not differ sufficiently, then coelution(s) will occur. In this case, to achieve the separation of these coeluting compounds, it will be necessary to apply a further separation criterion, such as their different polarity. If each separation mechanism employed for the resolution of a complex mixture is defined as a separation “dimension”, then we are in the presence of a multidimensional approach. The most powerful multidimensional GC approach, capable of a very high resolving power, is represented by the GC×GC. The concept of GC×GC was introduced in the early 1990s by Liu and Phillips [2], bringing a great improvement to the GC field. The introduction of GC×GC can be considered at the same level of OTC, in terms of the revolutionary impact that it has had on the separation science field. Since its first appearance nearly thirty years ago, many

improvements have been made in the GC×GC field, in terms of practical/theoretical studies, hardware and software.

Here is a brief introduction regarding the food-related applications carried out during these three years of Ph.D. course.

Many vegetable oils were investigated by the use of comprehensive two-dimensional gas chromatography combined with high resolution time-of-flight mass spectrometry (HR ToFMS) for the untargeted analysis of high molecular weight constituents (sterols, triterpenic alcohols, tocopherols and squalene) and also for the generation of a high resolution time of flight mass spectrometry database containing the mass spectra of the main derivatized sterols compounds (section 5.1) [3].

A sample of extra virgin olive oil (focus was devoted to the phytosterol fraction), a mixture of pesticides and a mixture of fatty acid methyl esters were analyzed by the use of comprehensive two-dimensional gas chromatography-quadrupole mass spectrometry, employing common electron ionization energy (70eV) and "milder" electron ionization conditions (40, 25 and 20 eV). The effects of using lower source temperatures were also evaluated. The use of "milder" ionization energy led to a general increase in the relative abundance of higher-mass diagnostic fragments, while the reduction of source temperatures favored a further enhancement of the higher mass ions (section 5.2) [4].

Comprehensive two-dimensional gas chromatography-quadrupole mass spectrometry was also employed for the characterization of unconventional palm oils deriving from three endemic *Arecaceae* species coming from Reunion Island (section 5.3) [5].

For what concerns food waste, a complex sample of bio-oil, derived from the pyrolysis process of coconut fibers, was analyzed for the determination of an equivalent column set between cryogenic and flow-modulated comprehensive two-dimensional gas chromatography (section 5.4) [6].

The use of gas chromatography was exploited for the analysis of fatty acids in dietary supplements. Fatty acid derivatization was performed by using a direct derivatization protocol previously reported [7]. In detail, a robotic preparative station enabled automatic derivatization in a fully automatic manner. With regards to the GC separation, a medium-polarity ionic liquid column was used. Dual detection was

performed by splitting the eluate between a triple quadrupole mass spectrometer (in this case used as a single quadrupole) and a flame ionization detector. This choice allowed the possibility to obtain quali-quantitative results, in a single run (section 5.5).

During the Ph.D. course, I spent six months in Madrid (Spain) at CIAL (Instituto de Investigatión en Ciencias de la Alimentatión), using monodimensional and bidimensional thin layer chromatography for the separation of terpenes in orange extracts. The main objective of this research work (still in progress) was to investigate the principal bioactive terpenoids with acetylcholinesterase inhibitor activity derived from orange juice by-products (section 5.6).

The use of a novel commercial type of pneumatic modulator was exploited for the determination of fish oil fatty acids (section 5.7).

Finally, during the Ph.D. course, other applications, not related to food products, were carried out. The use of GC×GC coupled with HR ToFMS was exploited for target analysis and absolute quantification of organic sulphur compounds (OSCs) in coal tar. The method developed allowed the pinpointing of 60 OSCs, belonging to 14 different classes. Absolute quantitative information was obtained for 8 OSCs, which can provide a good albeit approximate idea on the concentration of each chemical class in the petrochemical sample under investigation [8].

A mixture of 64 fragrance allergens in cosmetics was employed for the evaluation of an equivalent column set between cryogenic and flow-modulated comprehensive two-dimensional gas chromatography [9]. The main objective of this study was to confirm the results attained previously on a sample of bio-oil [6].

Two review articles were also published in the context of current state of comprehensive two-dimensional gas chromatography. Here is a brief description.

The information on current trends in the field of the hyphenated technology GC×GC-MS, representing the most powerful analytical tool today-available for the analysis of mixtures formed of volatile compounds, were summarized [10]. Focus was devoted to various aspects of mass spectrometry, in particular to ionization methodologies. The information reported relates mainly to 2014-2017 period. The Scopus database was consulted, leading to a number of 343 papers, with these reporting on the use of 5 forms of MS. Regarding the MS types: low resolution (LR) ToFMS was by far the most popular choice (66%), followed by quadrupole (Q) MS

(20%). The third position was occupied by HR ToFMS (8%). Two remaining forms of MS (both multianalyzer types), namely quadrupole time-of-flight (QToF) and triple quadrupole (QqQ) MS, have been reported in only 12 and 6 investigations, respectively. For what concerns the process of ionization the electron ionization maintains its dominating role.

Recent application and instrumental trends relate to the combined period 2018 to 2019 were summarized in a recent review article [11]. The information related to the present review is reported in section 4.7.

References:

[1] M.J.E. Golay, in: Gas Chromatography, Academic Press, New York, USA, (1958).

[2] Z. Liu, and J.B. Phillips, J. Chromatogr. Sci. 29 (1991) 227.

[3] I. Aloisi, M. Zoccali, P. Dugo, P.Q. Tranchida, L. Mondello, Food Anal. Method. 13 (2020) 1523.

[4] P.Q. Tranchida, I. Aloisi, B. Giocastro, M. Zoccali, L. Mondello, J. Chromatogr. A. 1589 (2019) 134.

[5] Y. Caro, T. Petit, I. Grondin, P. Clerc, H. Thomas, D. Giuffrida, B. Giocastro, P. Q. Tranchida, I. Aloisi, D. Murador, L. Mondello, L. Dufossé, Nat. Prod. Res. 34 (2019) 93.

[6] I. Aloisi, T. Schena, B. Giocastro, M. Zoccali, P.Q. Tranchida, E.B. Caramão, L. Mondello, Anal. Chim. Acta. 1105 (2020) 231.

[7] G. Micalizzi, E. Ragosta, S. Farnetti, P. Dugo, P.Q. Tranchida, L. Mondello, F. Rigano, Anal. Bioanal. Chem. 412 (2020) 2327.

[8] I. Aloisi, M. Zoccali, P.Q. Tranchida, L. Mondello, Separations 7 (2020) 1.

[9] B. Giocastro, I. Aloisi, M. Zoccali, P.Q. Tranchida, L. Mondello, LC-GC North Amer. 38 (2020) 548.

[10] P.Q. Tranchida, I. Aloisi, B. Giocastro, L. Mondello, TrAC Trends Anal. Chem. 105 (2018) 360.

[11] P.Q. Tranchida, I. Aloisi, L. Mondello, LC-GC Eur. 33 (2020) 172.

Chapter 2

2.0 Theory of chromatography

2.1 Introduction

Chromatography represents a physical method of separation, in which the components of a sample are selectively distributed between two immiscible phases. The mobile phase, flowing through a stationary phase, carries the analytes. The separation occur thanks to the differences in the distribution coefficient of the individual sample components.

The "official" definitions of the International Union of Pure and Applied Chemistry (IUPAC) are: "Chromatography is a physical method of separation in which the components to be separated are distributed between two phases, one of which is stationary (stationary phase) while the other (the mobile phase) moves in a definite direction. Elution chromatography is a procedure in which the mobile phase is continuously passed through or along the chromatographic bed and the sample is fed into the system as a finite slug" [1].

The discovery of chromatography dates back to the early twentieth when Ramsey [2] separated a mixture of gases and vapors on adsorbents likes charcoal and Michail Tswett [3] observed that colored pigments of vegetable origin were individually separated in bands when they were injected in a column of glass filled with calcium carbonate. Tswett is credited as being the "father of chromatography" inasmuch that he coined the term chromatography (χρώμα, color and γραφή, graphy) and also because he scientifically described the process.

It is possible to classify column chromatographic separations in three different ways: by the physical state of the mobile phase and stationary phase; by the type of contact between the mobile phase and the stationary phase; or by the chemical or physical mechanism responsible for separating the analytes. Based on the mobile phase used, chromatography could be named as GC, liquid chromatography (LC), and

supercritical fluid chromatography (SFC). The classification of main column chromatography techniques is summarized in Figure 2.1.

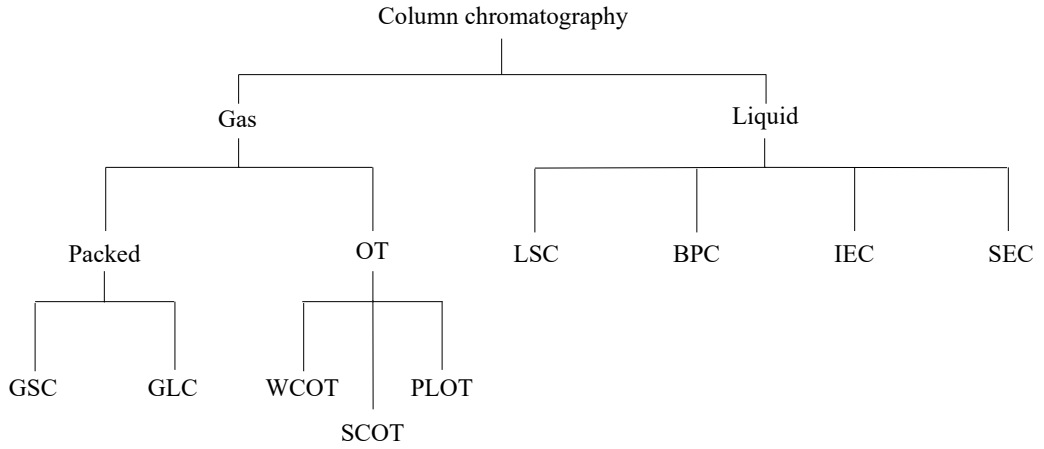

Figure 2.1. *Schematics of various chromatographic methods. Abbreviations: OT - open tubular; WCOT - wall coated open tubular; SCOT - support coated open tubular; PLOT - porous layer open tubular; LSC - liquid-solid chromatography; BPL - bonded-phase chromatography; IEC – ion exchange chromatography; SEC - size exclusion chromatography*

The detector, placed at the end of the column, provides a record of the chromatography as a chromatogram. Usually, the detector signals are proportionate to the amount of each analyte making possible, if required, quantitative analysis. Hence, the chromatogram generated is a plot of the sample concentration (y-axis) versus time (x-axis). It represents the individual component bands, separated by the chromatographic column and modified by a variety of physical processes into a peak shape. An example of chromatogram is reported in Figure 2.2.

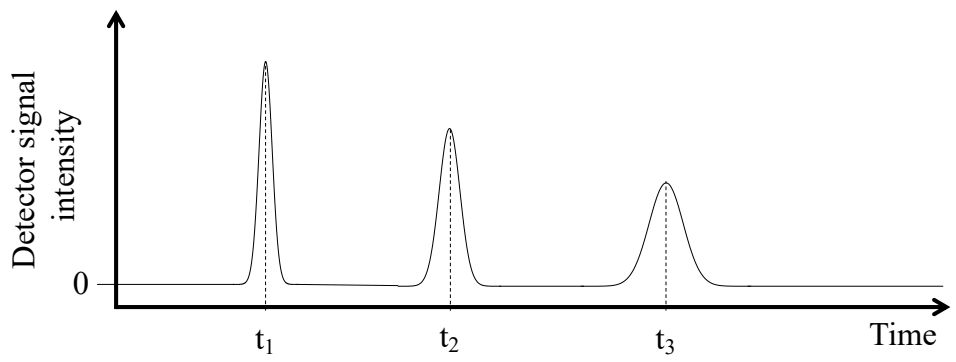

Figure 2.2. *Example of a chromatogram with three peaks isothermally eluted.*

Each chromatographic peaks represents at least one chemical substance. The position of a peak on the time scale of the total chromatogram give some qualitative information while the area under a peak is related to the amounts of individual substances separated in time space.

2.2 Fundamental chromatographic parameters

The primary purpose of chromatography is the separation of a sample in a series of chromatographic peaks, each representing, ideally, a single component. The most important chromatographic parameters are described as follows.

2.2.1 Retention

As shows in Figure 2.2, different analytes of a sample appear at the column outlet at different times. The first component eluted is the one that is not retained at all by the stationary phase. The time measured between the injection and the maximum of the first peak (t_M) is defined as *retention time of the unretained solute*, or in gas chromatography the *gas hold up time*. The time between the sample introduction and the maximum of the retained peak is the total retention time (t_R) of the analyte. This value is the sum of two time values:

$$t_R = t_M + t'_R$$

Eq. 2.1

Where t_M is the hold up time, while t'_R represent the time the molecules of the analyte spend in the stationary phase (otherwise defined *adjusted retention time*).

The retention time could be defined also with the following equation:

$$t_R = t_M(1 + k)$$

Eq. 2.2

where k is the capacity factor. The capacity factor is further defined as:

$$k = K\frac{V_S}{V_M}$$

Eq. 2.3

where K is distribution coefficient of the solute (expressing the distribution between the stationary and the mobile phases), V_S is the volume of the stationary phase, and V_m is the volume of the mobile phase in a chromatographic column. The distribution coefficient can be calculated:

$$K_D = \frac{C_S}{C_M}$$

Eq. 2.4

where C_s and C_m are the analyte concentration in the stationary and mobile phases, respectively. According to Eqs. 2.2 and 2.3, retention depends on different variables: (a) the chemical nature of the column phase and its temperature, as reflected by the distribution coefficient; (b) the ratio of the phase volumes in the column V_S/V_M; and (c) the value of t_M. These variables are optimized in order to maximize the component separation and the total time of analysis. Based on the retention time of an unretained component (t_M) and the column length it is possible to calculate the average linear velocity ($\bar{u}$) of the mobile phase:

$$\bar{u} = \frac{L}{t_M}$$

Eq. 2.5

The flow rate (F), is usually expressed as mL/min and through a column with internal diameter d_c is calculated by:

$$F = \pi d_c^2 e_u u$$

Eq. 2.6

where ε_u represent the fraction of the column occupied by mobile phase between the particles and in the pores. The so-called retention volume V_R is a product of the retention time and volumetric flow-rate:

$$V_R = t_R F$$

Eq. 2.7

Since retention times represent in some manner the nature of the solute, a means of their comparison must be available. Within a given chemical laboratory, relative retention times (the values relative to an arbitrarily chosen chromatographic peak) are frequently used:

$$a_{1,2} = \frac{t_{R2}}{t_{R1}} = \frac{V_{R2}}{V_{R1}} = \frac{K_2}{K_1}$$

Eq. 2.8

This equation is also a straightforward consequence of Eqs. 2.2 and 2.3. Since the relative retention represents the ratio of distribution coefficients for two different solutes, it is frequently used (for the solutes of selected chemical structures) as a means to judge selectivity of the solute-column interactions.

2.2.2 Separation

The success of a separation method is primarily dependent on increasing the differences in retention times of the individual sample components. The capacity of a chromatographic system to separate two analytes from each other is named selectivity. The selectivity factor α for two components is calculated by:

$$a = \frac{k_2}{k_1} = \frac{t_{R2} - t_M}{t_{R1} - t_M}$$

Eq. 2.9

where k_1 and k_2 represent the retention factors and t_{R1} and t_{R2} are the retention times of the two analytes. The selectivity factor is greater or equal to one. An additional variable of such a separation process is the width (w) of the corresponding chromatographic peak. By the peak width and the retention time it is possible to evaluate resolution. The term resolution (R) is used to express the degree to which adjacent peaks are separated, and is defined as:

$$R = \frac{t_{R2} - t_{R1}}{0.5(w_2 + w_1)} = \frac{2\Delta t_R}{w_2 + w_1}$$

Eq. 2.10

where w_1 and w_2 represent the peak widths of the two compounds at the base. The degree of separation between two chromatographic peaks improves with an increase in R. Thus, R is a quantitative measure of the effectiveness of a separation process. In Figure 2.3c a situation where two sample components are eluted too closely together is showed, so that the resolution of their respective solute zones is incomplete; Figure 2.3b represents a situation where the two components are resolved from each other through choosing a (chemically) different stationary phase that retains the second component more strongly than the first one; finally, Figure 2.3a shows the two peaks totally resolved, thus representing the most "efficient" handling of the two components.

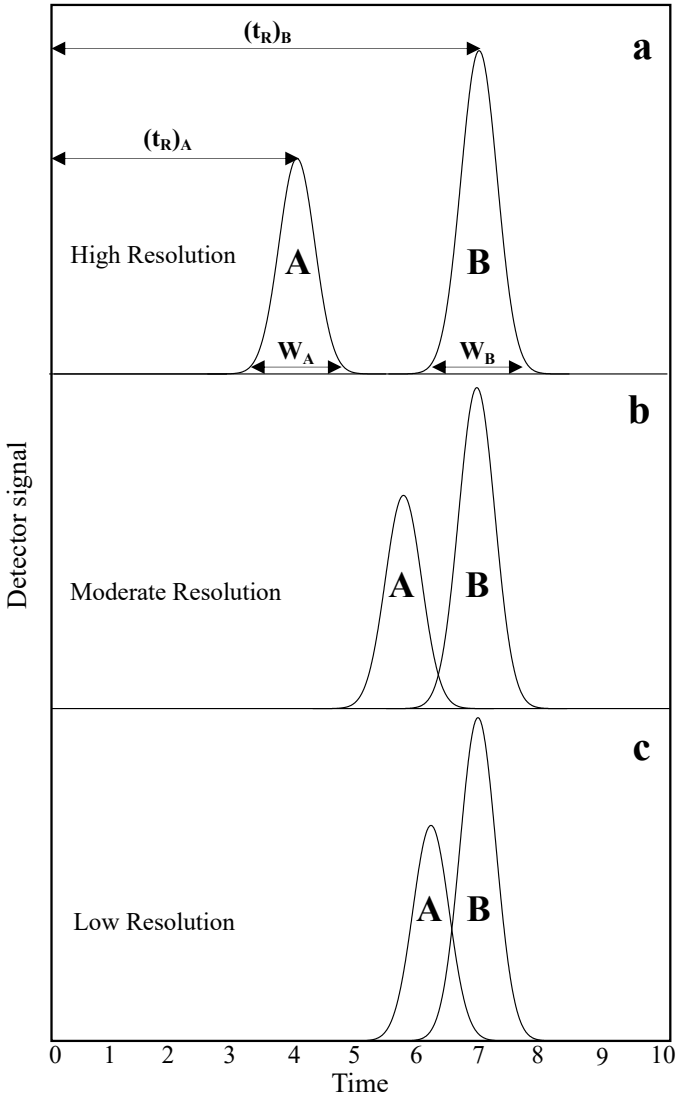

Figure 2.3. *Peak resolution.*

2.2.3 Column efficiency

In order to obtain optimal separations, sharp, symmetrical chromatographic peaks must be acquired; for this reason band broadening must be reduced. It is also suitable to measure the efficiency of the column, which is defined by the number of theoretical plates, *N*. The latter is calculated by:

$$N = 16\left(\frac{t_R}{w}\right)^2 = 5.54\left(\frac{t_R}{w_{1/2}}\right)^2 = 2\pi\left(\frac{h_p t_R}{A}\right)^2$$

Eq. 2.11

where $w_{1/2}$ represent the peak width at half-height, h_p peak height and A peak area. The equation 2.11 yields correct results only if the peak has a Gaussian shape. In case of asymmetric peaks an approximate value of *N* can be calculated by the following equation [4]:

$$N = 41.7\frac{\left({t_R}/{w_{0.1}}\right)}{T + 1.25}$$

Eq. 2.12

where $w_{0.1}$ is the peak width at 10% of the peak height and *T* is the tailing factor:

$$T = \frac{b_{0.1}}{a_{0.1}}$$

Eq. 2.13

where $a_{0.1}$ and $b_{0.1}$ are the sections (distances from the peak front to the maximum and from the maximum to peak end, respectively) of the peak width at 10% of the peak height.

The number of theoretical plates depends on column length *L*: the longer the column, the higher the number of the plates. Therefore, another term has been introduced relating the plate number to column length. This is the plate height *H* (HETP = height equivalent to a theoretical plate), which can be calculated:

$$H = \frac{L}{N}$$

Eq. 2.14

The width of a chromatographic peak is influenced by a series of parameters, which are taken into account in the van Deemter equation. The Van Deemter equation identifies three effects that contribute to band broadening in packed columns:

$$H = A + \frac{B}{\bar{u}} + C\bar{u}$$

Eq. 2.15

where *A* accounts for multiple paths, *B/u* for longitudinal diffusion, and *Cu* for solute mass transfer in the stationary and mobile phases, them being the experimental factors contributing to the broadening of a solute's chromatographic band. Factor *A* (Eddy diffusion) accounts for the fact that the solute molecules, while passing through the column, take random paths between the stationary phase particles. These different paths with different lengths will cause broadening of the solute band. Factor *B* (longitudinal diffusion) is related to the fact that the concentration of the analyte is lower at the edges of the band with respect to the center. Analytes diffuse out from the center to the edges, causing also band broadening. The effect of this factor is decreased when the velocity of the mobile phase is high. The factor *C* (resistance to mass transfer) depends on the fact that the analyte takes a certain time to equilibrate between the stationary and mobile phase. If the velocity of the mobile phase is high and the analyte has a strong affinity for the stationary phase, then the analyte in the mobile phase will move ahead of the analyte in the stationary phase and the band is broadened. The higher the velocity of the mobile phase, the worse the broadening becomes. Figure 2.4 represents the plot of the height of a theoretical plate as a function of mobile-phase velocity, the so-called van Deemter curve. The optimum flow rate and the contributions to the terms *A*, *B/u*, and Cu are also shown.

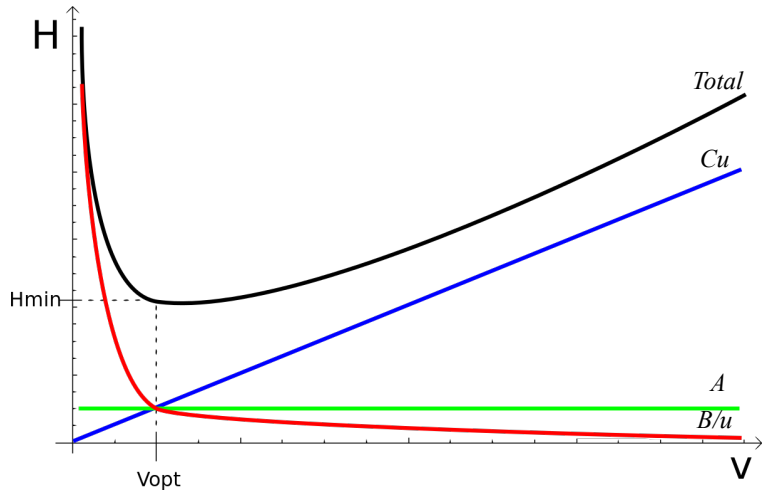

Figure 2.4. *Plot of the height of a theoretical plate as a function of mobile-phase velocity (using the van Deemter equation). The contributions to the terms A, B/u, and Cu are also shown.*

Since the theory of open tubular column was introduced in 1956 by M. J. E. Golay, the absence of any packing material inside the column modified the van Deemter equation excluding factor *A* (Eddy diffusion). This deduction was pointed out by Golay himself, who also suggested a new term to deal with the diffusion process in the mobile phase of open tubular columns [5]. Eq. 2.16 contains two C factors connected to the mass transfer in the stationary phase, C_S and another for the mass transfer in the mobile phase, C_M [6].

$$H = \frac{B}{\bar{u}} + (C_S + C_M)\bar{u}$$

Eq. 2.16

The efficiency of a separation system is well demonstrated by its peak capacity, n_c, which represent the number of solutes that can theoretically be resolved at the baseline on a given column. An estimate of a column's peak capacity for a retention time window from time t_1 to t_2 is given by:

$$n_C = 1 + \frac{\sqrt{N}}{4R}\ln\left(\frac{t_2}{t_1}\right) = 1 + \frac{\sqrt{N}}{4}\ln(1 + k_{max}) = 1 + \frac{\sqrt{N}}{4}\ln\left(\frac{V_{max}}{V_{min}}\right)$$

Eq. 2.17

where V_{min} and V_{max} are the smallest and largest volumes of mobile phase in which a solute can be eluted and detected [7]. This estimation is valid for isocratic elution. The peak capacity in gradient elution is generally higher and can be calculated by:

$$n_C = \frac{\sqrt{N}}{4}\left(\frac{t_2}{t_1} - 1\right) + 1$$

Eq. 2.18

References:

[1] L.S. Ettre, Pure Appl. Chem. 65 (1993) 819.

[2] W. Ramsey, Proc. Roy. Soc. A76 (1905) 111.

[3] M. Tswett, Ber. Dtsch. Botan. Ges. 24 (1906) 316 and 384.

[4] J.P. Foley, and J.G. Dorsey, Anal. Chem. 55 (1983) 730.

[5] M.J.E. Golay, in: Gas Chromatography, Academic Press, New York, USA, (1958).

[6] H.M. McNair, and J.M. Miller, in: Basic Gas Chromatography, Wiley & Sons, New York, (1998).

[7] J.C. Giddings, Unified Separation Science. Wiley-Interscience, New York, (1991).

Chapter 3

3.0 Gas chromatography

3.1 Introduction

Gas chromatography is a physical separation technique in which a gas is the mobile phase. Today, this methodology is used in scientific investigations, petroleum technology, environmental pollution control and in many scientific areas. The first paper reporting the use of GC was published in 1952 [1] by Martin and his co-worker James.

The technique is limited to volatile and semi-volatile (low-molecular-weight) compounds. The principle of separation is the relative affinity of the components to the stationary phase, while the mobile phase (a gas) migrates them through the system.

Ettre published several papers retracing the history of chromatography. Three of the most representative articles are: the first one regarding the work of Tswett, Martin, Synge, and James [2]; the second one highlighting the progress of GC instruments [3]; and the third, which contained over 200 references on the overall progress of chromatography [4].

The indispensable parts of the gas chromatographic system are represented in Figure 3.1. The column is the most important part of the instrumentation, because inside of it the physiochemical process of separation occurs. The separation column contains the stationary phase, while the mobile phase (the carrier gas) is flowing through this column from a pressurized gas cylinder. The rate of mobile-phase delivery is controlled by a pressure and/or flow-regulating unit (carrier gas flow controller).

Usually, in GC, the sample is introduced through the use of a syringe inside the sample injector. The whole sample, or a part of it, is transferred from the injector to the chromatographic column, where the separation occurs by the continuous redistribution between the mobile and the stationary phases. On the basis of their different affinities for the stationary phase, the individual components, eventually form their own concentration bands, which reach the column outlet at different times. A

detector is situated at the column outlet to identify and, if required quantify, the single components eluting from the column.

A typical gas chromatograph has three independently controlled thermal zones: the injector zone that ensures rapid volatilization of the introduced sample; the oven temperature that is controlled to optimize the separation process; and the detector zone that must be at temperatures where the individual sample components are measured in the vapor phase.

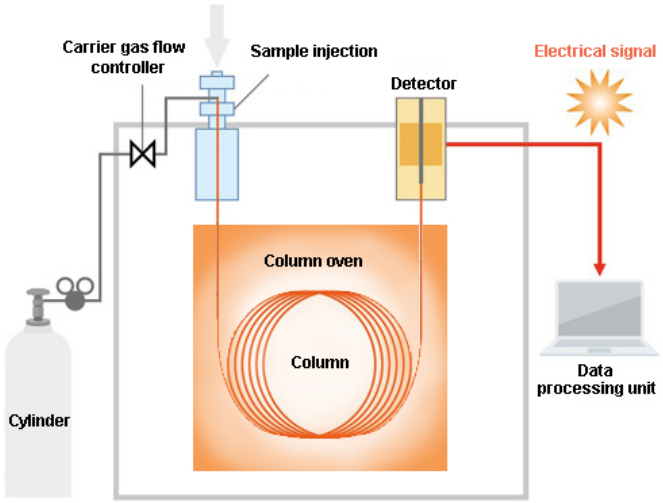

Figure 3.1. *The main components of a gas chromatograph.*

3.2 Columns

Gas chromatography columns can be divided into two main groups: packed columns, and OTC columns, showed in Figure 3.2.

A packed column (Figure 3.2a) is a tube, made from glass or metal, filled with a granular material. This kind of column is connected to the instrument through a gas-tight connection. The mobile phase flowing between the particles, while the sample molecules interact with the stationary liquid phase adsorbed on the inert granular material. Column inner diameters are 1-4 mm, and the lengths are 1-3 m, even if departures from these dimensions may exist for special applications. The granular packing can be either an adsorbent (if the method of choice is gas-solid chromatography) or an inert solid support that is impregnated with a defined amount of a liquid stationary phase (for gas-liquid chromatography). In either case, packing

materials with uniformly small particles are required, because the column performance is strongly dependent on the particle size. In fact, a distinct advantage of small particles is their closer contact with diffusing sample molecules and a greater number of the mentioned equilibrium units (i.e., theoretical plates). Regarding gas-solid chromatography, the solute molecules interact with the surface of solid adsorbents through relatively weak physical adsorption forces because the adsorption process must be reversible. Silica gel, alumina, zeolites, carbonaceous adsorbents, are some examples of suitable GC adsorbents.

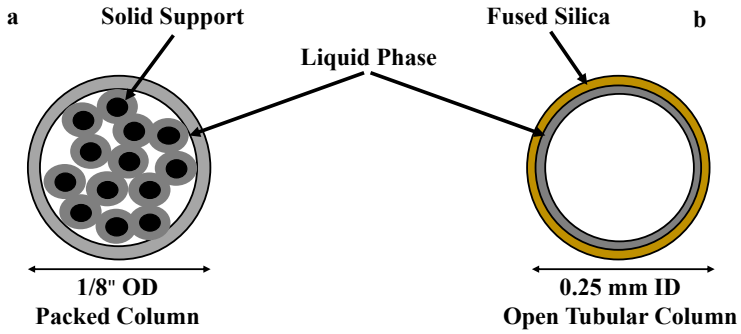

Figure 3.2. *Schematic representation of (a) packed column and (b) open tubular column.*

Gas-liquid chromatography has found considerable use in chemical analysis. The packing materials (solid supports) utilized in this method are similar to the described adsorbents even if they serve only as a supporting medium for the liquid stationary phase and do not participate directly in the separation process. The most commonly used solid supports are the diatomaceous earths that are fossil-originated minerals found in abundance in various parts of the world. The diatomaceous earths are basically siliceous materials that contain reactive surface structures, the silanol groups. Since such groups could adversely affect the chromatographic analyses, causing "tailing" of certain polar sample components, they are effectively blocked (deactivated) by a silylation reaction. The solid support is subsequently impregnated by a liquid stationary phase.

The theory of the OTC column, already discussed, was introduced in 1956 by M. J. E. Golay. A schematic representation of a capillary column is showed in Figure 3.2b. Thanks to the high separation efficiencies, OTC column have substantially improved

analytical separations. The absence of packing material inside the capillary column is the principal advantage. The stationary liquid phase is distributed as a thin film on the surface of the inner wall of the column. Usually, capillary columns have a length ranging from 10 to 100 meters and an internal diameter ranging from 0.1 mm to 0.5 mm. Capillary columns allow to obtain narrow chromatographic peaks and a high degree of resolution among the individual components of complex mixtures. In Figure 3.3 the improved resolution of a capillary column over a packed column is evident. The constituents of Calmus oil are separated from each other by the use of a capillary column (Figure 3.3a) and a packed one (Figure 3.3b). It is evident that packed columns allow the resolution of a limited number of compounds compared with a capillary column. The reason of an increase in separation power is connected to the high permeability to the carrier gas (absence of any column packing).

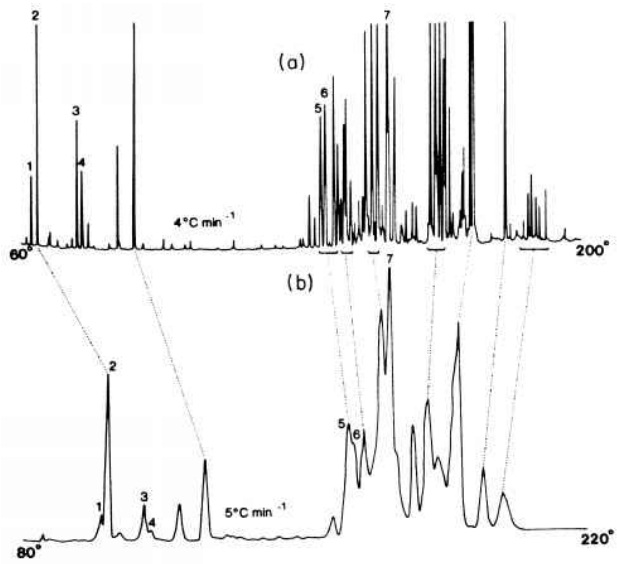

Figure 3.3. *Comparison between the resolution achieved with (a) capillary columns and (b) packed columns for a sample of Calmus oil. From K. Grob, and G. Grob, Pratical capillary gas chromatography – a systematic approach. J. High Resolut. Chromatogr. 3 (1979) 109.*

There is also a third type of a GC column: the porous layer, open tubular columns. This column has an inner diameter and a length similar to the wall-coated columns, but the inner wall is modified through a deposition of finely dispersed particles. The porous layer can be an adsorbent or a thin layer of the solid support impregnated with a liquid stationary phase. In this case, the efficiency is not as high as those of a

conventional capillary column, but the greater sample capacity is an advantage in some cases. The enhanced sample capacity is obtained because of a greater surface area of such columns and, consequently, a relatively larger amount of stationary phase.

3.3 Detectors

The detector plays a crucial role in the entire process of GC analysis. The success of GC as an analytical method is also connected to the early development of highly sensitive and reliable means of detection. At the column outlet the detector provides information regarding the distribution of individual peaks within a chromatogram (which compound?) and also their relative amounts (how much?).

In one of the first books about detectors, David described about 20 detectors that were already popular in the 1970s [5].

Detectors can be classified into two large families: universal and selective detectors. Universal detectors permit to measure nearly all components present in a mixture, although their response to the same quantities of different compounds is not similar. Instead, selective detectors generate a response only to mixture components that contain a unique structural feature in their molecular structure. To give an example, gasoline sample contains a huge number of compounds belonging to different classes. Near to all the compounds of gasoline can be detected by the use of an universal detector. Instead, using, for example, a nitrogen-selective detector, only a few peaks are recorded, that are nitrogen-containing compounds in gasoline, while the others mixture constituents are not detected.

An acceptable GC detector must have several analytical properties, such as sensitivity, linearity over an extensive concentration range, long-term stability, and ease of operation. A satisfactory sensitivity values allows detectors to determinate solute quantities between 10^{-6} and 10^{-9}g, and for some selective detectors it is possible to reach values of 10^{-15}g, representing some of the most sensitive measurement techniques available to the chemist.

Some detectors principles are correlated to the measurement of certain transport properties of the solutes (e.g. thermal conductivity), while others detectors work as transducers, measuring ultimately some product of a solute molecules (e.g. gas-phase ionization products).

Apart from the flame ionization detector (FID) and MS detector, which are reported in the following two subsections, a brief overview of other detectors is herein reported.

Almost all the first GC systems were equipped with a thermal conductivity detector (TCD). Nowadays, this detector is popular principally for packed columns and inorganic analytes, such as H_2O, CO, CO_2, and H_2. The operation of TCD is based on the measurements of the difference in thermal conductivity of pure carrier gas and the carrier gas plus solute.

The electron capture detector (ECD) is an instrument based on certain gas-phase ionization phenomena inside the ionization chamber. The ECD is a selective detector since only certain compounds exhibit appreciable affinities toward the low-energy electrons. Among the structures exhibiting strong electron affinities are various halogenated compounds, nitrated aromatics, highly conjugated systems, and metal chelates. The detector is extremely sensitive (amounts between 10^{-12} and 10^{-15} g can be detected) to various pesticides, herbicides, dioxins, freons, and other substances of great environmental importance.

The atomic emission detector (AED) is an instrument that allows to measure up to 23 elements: a He plasma chamber collects the GC effluent, and due to the high temperature encountered therein, the analytes are then decomposed to their constituent atoms. The AED is characterized by high level of sensitivity for almost all of the important elements, a linear range with an extension of three to five orders of magnitude, and an element versus carbon selectivity of four to five orders of magnitude [6].

The thermionic ionization detector (TID) is a selective instrument usually utilized for the detection of N and P-containing compounds (it is also defined as the nitrogen phosphorous detector, NPD). The TID is structurally similar to the FID, apart from the presence of a ceramic bead doped with an alkali metal salt, located above the jet. It is assumed that electronegative decomposition products, derived from compounds containing N or P, are ionized through extraction of an electron from the bead surface. Later, the negative ions are directed to a collector electrode. The application of TID is mainly for pesticides.

The helium ionization detector (HID) is a sensitive and universal instrument, utilized principally for compounds with no or a low FID response, and present in low

concentrations for the TCD. The HID promotes photon-induced ionization processes and has the capability to ionize compounds with an ionization potential of <19.8 eV [7].

3.3.1 Flame ionization detector

This detector is very popular GC detector, thanks to its high sensitivity (the minimum detectable amounts are in the order of 10^{-12} g/s), linearity, and ease of operation, in spite of the somewhat incomplete understanding of the physical (ionization) processes involved. For the early theories, it is possible to consult Sternberg et al. [8] and Sevcik et al. [9]. The detection process is based on the decomposition of the solute-neutral molecules in a flame into charged species and on the electrical measurement of the resultant changes of conductivity. A cross-sectional view of the FID is shown in Figure 3.4.

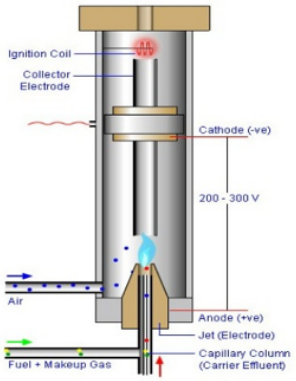

Figure 3.4. *Schematic representation of an FID.*

A small flame is sustained at the jet tip by a steady stream of pure hydrogen, while the necessary air (oxidant) is supplied through the diffuser. The column effluent is introduced at the detector base in a continuous manner, mixed with hydrogen and, finally, reaches the flame. Changes in conductivity between the electrodes are monitored, amplified by an electronical device, and recorded.

The carrier gas gives a small contribution to the flame conductivity; however, when organic solute molecules reach the flame, they are ionized, increasing the current in accordance with the solute concentration. With nearly all FIDs, this current increase is

linear with the solute concentration up to six orders of magnitude. The FID is also defined as a carbon counter, inasmuch that each carbon atom in the solute molecule gives a contribute to the signals (compounds with C—C and C—H bonds). Instead the presence of nitrogen, oxygen, sulphur, and halogen atoms tends to reduce the response of the detector.

Hydrocarbons are the compounds for which FID has the best response (high sensitivity). Instead, inorganic gases, carbon monoxide, carbon dioxide, and water are not detectable with this kind of detector.

3.3.2 Mass spectrometry

Mass spectrometry is one of the most interesting analytical techniques which dominate the life science scenery.

"The basic principle of mass spectrometry is to generate ions from either inorganic or organic compounds by any suitable method, to separate these ions by their mass-to-charge ratio *(m/z)* and to detect them qualitatively and quantitatively by their respective *m/z* and abundance. The analyte may be ionized thermally, by electric fields or by impacting energetic electrons, ions or photons. Ion separation is effected by electric and/or magnetic fields." This former definition of mass spectrometry dates back to 1968 [10].

Noteworthy is the importance on how to correctly define such a technique. In fact, never make the mistake of describing it as mass spectroscopy, inasmuch that the latter involves the absorption of electromagnetic radiation and the measurement of radiation intensity as a function of wavelength [11]. An explanation behind the use of such an incorrect terms finds its origin from the historical development of MS instrumentation.

In 1897, Joseph John Thomson, a physicist, demonstrated the existence of the electron and measured its *m/z* [12]. He later applied similar methods to the analysis of positive ions with positive ray parabolas [13]. In 1919, Aston, a student of Thomson, refined such an instrumentation by improving the use of electric and magnetic fields to focus ions on a photographic plate used as detector (focusing speed) [14]. Aston himself called that device mass spectrograph. After, Dempster constructed an instrument with a deflecting magnetic field angled at 180°. In order to detect different masses, it could have a variable magnetic field, and after focus them onto an electric

point detector [15]. Afterwards, the term mass spectrometer was coined for those type of instruments using a scanning magnetic field [16]. Aston and Dempster, along with the aforementioned Thomson, can therefore be considered as the pioneers of mass spectrometry.

Although the previously mentioned definition of mass spectrometry is still valid, some additional considerations have to be made. First of all, the energy directed to the analytes during the ionization processes can be varied, and this leads to the classification of the various ionization techniques on the basis of their relative "hardness" or "softness" features. Moreover, ions can also be mass separated in field-free regions (e.g., in time-of-flight analyzers). In such a case, the separation of ions within a given *m/z* range would be entirely governed by their masses, which will determine the time they spend into the drift region (a detailed discussion of the principles of time-of-flight mass analyzers is presented in section 3.3.2.3).

During the last decades there has been a remarkable growth in popularity of MS as a tool for both, routine analytical experiments, as well as advanced investigations. This is due to a number of features including relatively low cost, simplicity of design and extremely fast data acquisition rates. Although the sample is destroyed by the mass spectrometer, the technique is very sensitive and only trace amounts of material are used in the analysis.

Gas chromatography-mass spectrometry is the most popular analytical technique for the identification and quantitation of volatile and semi-volatile substances in complex matrices.

The potential of combining GC with MS for the determination of volatile compounds, contained in very complex samples, is well-known. The later introduction of very powerful data acquisition and processing systems, including automated database search techniques, guaranteed that the information content of the large quantities of data generated by GC-MS instruments was fully exploited. These early successes were the foundation of an increasingly diverse range of applications, utilizing many different mass spectrometric techniques. It is expected that a MS has the ability to form, separate and detect ions. To achieves these requirements three fundamental units are essential; an ion source, a mass analyzer and a detector [17] (see diagram scheme in Figure 3.5 and scheme in Figure 3.6).

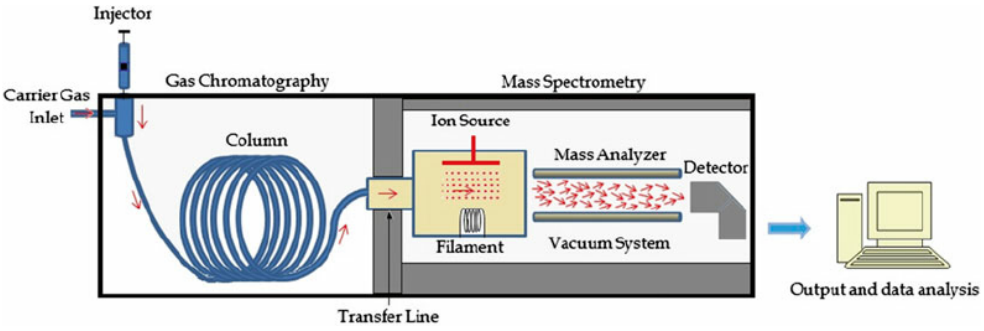

Figure 3.5. *Schematic representation of the main parts of a GC/MS instrument.*

The parts of the mass spectrometer are enclosed in a housing usually kept at relatively high vacuum (10^{-3} to 10^{-6} torr), which ensures that once the ions formed in the ion source begin to move towards the detector, they will not collide with other molecules.

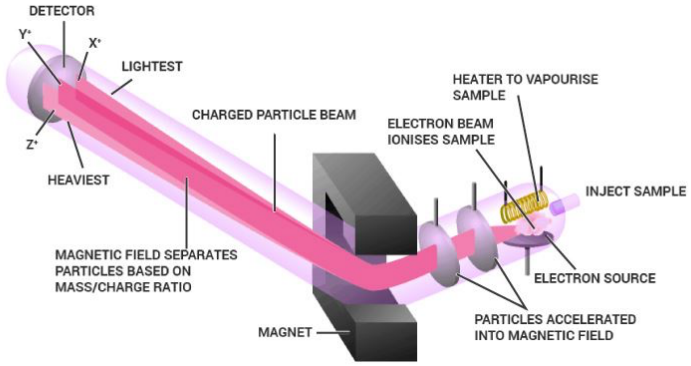

Figure 3.6. *Schematic representation of a mass spectrometry system.*

The collision of ions would result in further fragmentation or deflection from their desired path. Furthermore, the vacuum also protects metal and oxide surfaces of the ion source, analyzer, and detector from corrosion by air and water vapor, which could compromise the spectrometer ability to form, separate and detect ions. In brief, the sample has to be introduced into the ionization source of the instrument; volatile compounds are most commonly ionized by electron ionization (EI) sources.

In an electron ionization source a high energy beam of electrons is used to displace an electron from the organic molecule forming a radical cation ($M^{+\bullet}$), the molecular

ion. The ionization process normally supplies considerable energy to this first-formed ion, so that it is almost immediately fragmented. The product ions formed may themselves fragment to produce a characteristic fragmentation pattern, creating a cascade of ion forming reactions before leaving the ion source [18] (see Figure 3.7).

The collection of ions is then focused into a beam and accelerated into the magnetic field and deflected along circular paths according to the masses of the ions. By adjusting the magnetic field, the ions can be focused on the detector. The individual ion current intensities at each mass are sequentially recorded, generating a mass spectrum. The latter is an histogram of the relative abundance of the ions generated by ionization of the sample and their subsequent separation, based on their *m/z*. The mass spectrum is a fingerprint of the molecule conveying information about its molecular weight, and the relatives fragments that are generated during the fragmentation process.

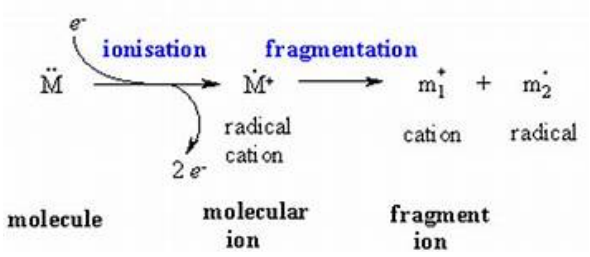

Figure 3.7. *Cascade of ion forming reactions.*

An MS generates an enormous amount of data, especially when allied to separation techniques such as GC. The raw data is stored in the form of a three-dimensional array with time, *m/z*, and intensity as independent axes, while as aforementioned, the mass spectrum itself is a two-dimensional representation of signal intensity versus *m/z*. The raw data is generated by repetitively scanning the mass analyzer over a particular mass range during the separation procedure and storing the intensity data for each scan separately. Alternatively, the mass analyzer is set to switch between a few selected ions, and only these ion intensities are stored during the chromatographic separation in selected ion monitoring.

In general mass spectrometers are classified on the basis of their mass analyzer; quadrupole mass spectrometry (QMS), triple quadrupole MS (QqQMS) and time-of -

flight MS (ToFMS) are three of the main mass spectrometry detection techniques often coupled with gas chromatography.

3.3.2.1 Quadrupole mass spectrometry

The principle of the quadrupole mass analyzer was described for the first time by Paul and Steinwegen in 1953 [19]. Ever since its introduction, the quadrupoles have been developed into commercially available instruments [20].

The mass analyzer comprises four parallel hyperbolic or cylindrical metal rods arranged in a square array (Figure 3.8); each pair of opposing rods is held at the same potential which is composed of a direct current (*DC*) and an alternating current (*AC*) component. If the applied voltage is composed of a DC voltage (*U*) on which an oscillating radio-frequency (*RF*) voltage ($Vcos(\omega t)$), is applied between one pair of rods, and the other, the field within the analyzer is created. A direct current voltage is then superimposed on the *RF* voltage (*V*) and the ions introduced into the quadrupole field undergo complex trajectories. At given values of the *DC* and *RF* potentials, only ions within a certain narrow *m/z* range will have stable trajectories and be allowed to reach the detector. This allows selection of a particular ion, or scanning by varying the voltages.

The motion of an ion traveling through the quadrupole is described by an equation established in 1866 by the physicist Mathieu, so-called Mathieu equation [21].

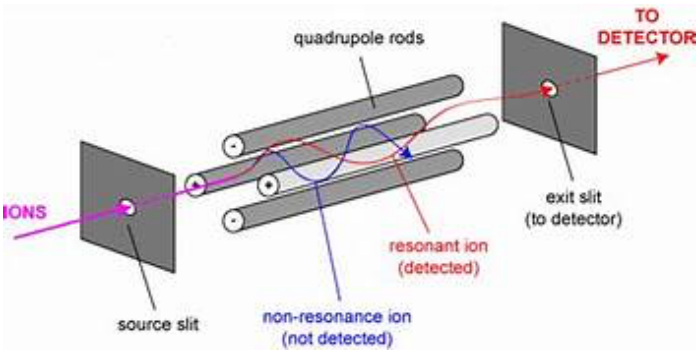

Figure 3.8. *Schematic representation of a quadrupole mass analyzer.*

The mass range is scanned by varying the *DC* and *RF* fields whilst keeping the voltage ratio and oscillator frequency constant. This produces a low resolution

spectrum. In general when the amplitude of *U* equals zero a wide band of *m/z* values will be transmitted, and as the value of *U/V* increases, resolution is enhanced so that at the stability limit only a single value of *m/z* corresponds to the trajectory, resulting in the transmission and collection of a single ion. In this manner QMS acts as a mass filter, and can be referred hereafter as a quadrupole mass filter.

Standard quadrupole analyzers have rods of 15 to 25 cm length and 10 to 20 mm in diameter. The *RF* is in the order of 1 to 4 MHz, and the *DC* and *RF* voltages are in the range of 10^2 to 10^3 V; ions of about 10 eV kinetic energy undergo approximately 100 oscillations during their passage.

A mass spectrum may be generated by scanning values of *U* and *V* with a fixed *U/V* ratio and constant drive frequency, or by scanning the frequency and holding *U* and *V* constant. The transmitted ions of certain *m/z* are then linearly dependent on the voltage applied to the quadrupoles, producing an *m/z* scale that is linear with time. The voltages applied to the rods are usually chosen to give equal peak widths over the entire mass range and unit resolution throughout the mass spectrum. The latter is then evaluated to determine the original structure of the analytes and compared with reference libraries for positive identification, providing an unparalleled qualitative ability.

3.3.2.2 Triple quadrupole mass spectrometry

Triple quadrupole mass spectrometry instruments follow a basic principle. The first quadrupole (Q_1) is set to transmit a particular *m/z*. The second quadrupole (q) is in truth an octapole or hexapole, and contains a gas-filled collision cell, within which fragmentation occurs through low-energy CID. In the third quadrupole (Q_3), the product ions produced from the precursor ion are analyzed (Figure 3.9).

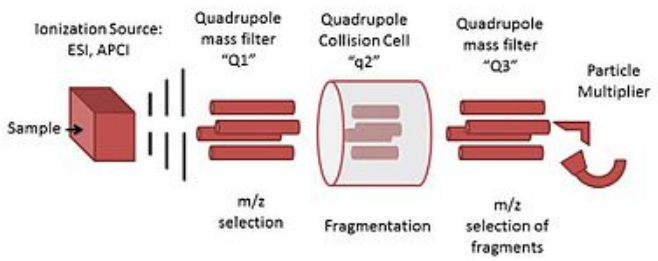

Figure 3.9. *Schematic representation of a triple quadrupole mass analyzer.*

Considering a precursor ion, m_1^+, which decomposes to give a product ion, m_2^+, and a neutral loss, *N*:

$$m_1^+ \rightarrow m_2^+ + N$$

MS/MS experiments can be classified according to which of these species (precursor, product ions or neutral loss) is detected. Therefore, five types of scanning mode are most commonly used, namely the scan (as a single quadrupole) the product ion scan, precursor ion scan, neutral loss scan and selected reaction monitoring (Figure 3.10).

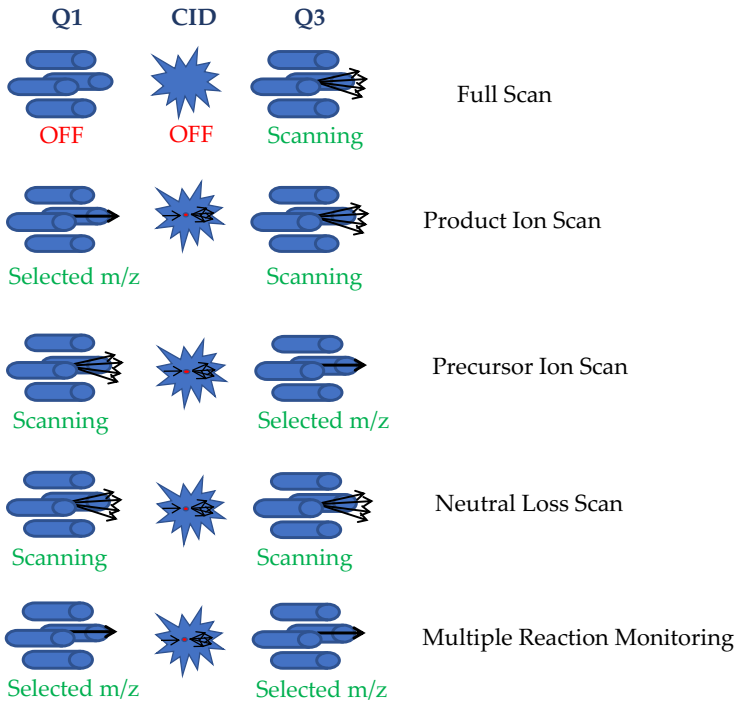

Figure 3.10. *Scan modes of triple quadrupole mass spectrometers.*

Usually, the scan is carried out by setting the first analyzer (Q_1) and the collision cell as a fly-through zone and performing a scan on a range of *m/z* values only in the second analyzer (Q_3)

The product ion scan is accomplished by setting the Q_1 to a particular *m/z* value, and performing a scan on a range of *m/z* values in the Q_3. This is the most common and well-known MS/MS mode, which is generally used for structural elucidation tasks.

Precursor ion scan is achieved by performing a scan in Q_1, while a specific *m/z* is set at Q_3. This mode is particularly useful when a given product ion, characteristic of a compound class, is known and thus all the compounds belonging to that class can be identified.

To perform a neutral loss scan, the two mass analyzers operate at the same scan speed, but Q_3 is shifted by a determined *m/z* value respect to Q_1. In this way, only ions which lose a neutral mass, corresponding to the *m/z* difference between the two analyzers, can be detected.

In the selected reaction monitoring mode, transitions of *m/z* values from a precursor to a particular ion produced upon dissociation are monitored. Since one or more pair of transitions can be monitored in the same time interval, that is a precursor to one or more product ions, this technique is often referred to as multiple reaction monitoring.

All these operating modes may be used for both qualitative and quantitative applications, depending on the specific case and needs. Concerning qualitative applications, they aims to two main purposes: i) the identification of unknown analytes compared to reference through the recognition of common fragmentation patterns, and ii) mapping the fragmentation paths that lead to a certain mass spectrum. Furthermore, the scanning of a precursor ion and that of a neutral loss are particularly useful in screening applications.

For what concerns quantitative analyses, the major reduction of chemical background is certainly a significant advantage. Additionally, the very rapid duty cycle (10 to 50 ms) of the QqQMS also makes it particularly suitable for high throughput analysis.

3.3.2.3 Time-of-flight mass spectrometry

The principle of time-of-flight analyzers was described by Stephens in 1946 [22]. Wiley and McLaren published in 1955 the design of a linear ToF mass spectrometer which later became the first commercial instrument [23].

The ToF analyzer allows to separate the ions, previously generated into the ion source, on the basis of the different velocity assumed inside the drift region. The heavier are the ions the more time they need for traveling the flight tube and reach the detector located at the end of the path. More in detail: after being formed into the ion

sources and accelerated by an electric field, ions arrive at the interface of the ToF in the form of ion packages. Specifically, they are accelerated towards the flight tube through a difference of potential applied between an electrode and the extraction grid. When leaving the acceleration region, all intact ions with the same charge will ideally have the same kinetic energy, and ions characterized by a distribution of masses present a distribution of their velocities accordingly. After, they enter into a field-free region where they will be separated according to their velocities, and reach the detector positioned at the other extremity of the flight tube. Provided that all the ions start their journey at the same time, or at least within a suitable short time interval, the lighter ones will arrive earlier at the detector than the heavier ones. Such an instrumental setup where the ions are traveling on a straight line from the point of their generation towards the detector is called linear TOF.

The fundamental requirement in ToF analyzers is a well-defined starting time for ions belonging to a given mass range. The time difference between the starting signal of the pulse and the time at which an ion hits the detector is the time of flight (t_{ToF}) and can be expressed as:

$$t_{ToF} = \frac{L}{v} = L\sqrt{\frac{m}{2qU_a}} \propto \sqrt{m/z}$$

Eq. 3.1

where L is the length of the field-free region, v is the ion velocity after acceleration, m is the mass of the ion, q the charge of the ion, U_a the accelerating electric potential difference, and z the charge state. This equation shows that, the lower the mass of an ion, the faster it will reach the detector, and vice versa. Summarizing, the physical property that is measured during an analysis is the flight time of the ion, which is then converted into a mass value.

An interesting advantage of these instruments is their powerful transmission efficiency which leads to very high sensitivity compared to quadrupole and sector analyzers. That is because all the mass range is simultaneously analyzed contrary to the scanning analyzers where ions are transmitted successively along a time scale.

Generally, the ToF analyzer is very fast, and a spectrum over a broad mass range can be obtained in the microseconds time interval. Thus, it is possible to produce

theoretically several thousand mass spectra over a very wide mass range in just 1 second. Actually, recorded spectra are generally the result of the summation of a number of individual “transient” spectra.

The resolving power of a time-of-flight analyzer depends on the mass and also on the length of the ion path inside the flight tube. Despite this, once a certain path length is exceeded, the system becomes less performing, since there is a loss of ions due to angular dispersion phenomena.

One of the main breakthroughs in the technological development of ToF analyzers arose from the design of the orthogonal acceleration ToF analyzer (oaToF). In an oaToF analyzers, pulses of ions are extracted orthogonally from a continuous ion beam. Specifically, ions fill the first stage of the ion accelerator in the space between the extraction plate and a grid. A pulsed electric field is then applied at a frequency of several kilohertz, which force ions to assume a direction orthogonal to their original trajectory, and then begin to fly towards the analyzer.

It is worthy to say that the duty cycle of an oaToF is far from 100% and it is generally lower than that of classical ToF analyzer. That is because the time required for the ion beam to fill the orthogonal acceleration region is lower than the time required for the sampled ions to hit the detector, and since new ions cannot be injected until the ions from the previous injection have reached the detector, the logical consequence is that a part of the ions produced in the source are lost in the first stage of the orthogonal accelerator.

The most significant advantages of oaToF analyzers are: i) high mass resolving power, and ii) mass accuracies even up to or below 1 ppm. Therefore, it is not surprising that oaToF instruments are currently widespread used in combination with GC and fast GC.

A further technological innovation was obtained through the development of the “reflectron” system, conceived by Mamryn in 1994 [24].

The simplest type of reflectron ToF analyzer (ReToF), which is called single-stage reflectron, usually consists of a series of equally spaced ring-shaped electrodes set at increasing potential which focus ions having the same *m/z* value but different kinetic energies in time. Ions with higher kinetic energy, and hence higher velocity, will penetrate the reflectron more deeply than ions with lower energy. Consequently, the

faster ions will spend more time in the reflectron and reach the detector at the same time of slower ions with the same *m/z*. Although the reflectron increases the flight path, though without increasing the dimensions of the mass spectrometer, the beneficial increase in mass resolution comes at the expense of sensitivity and mass range limitation. An oaToF mass spectrometer equipped with a reflectron is shown in Figure 3.11.

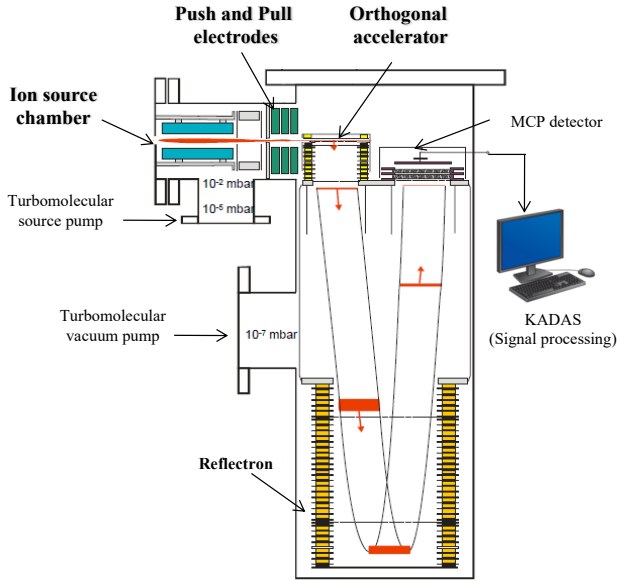

Figure 3.11. *Schematic representation of a time-of-flight mass spectrometer equipped with an orthogonal accelerator and a reflectron.*

The choice of operating ToF instruments in "linear" or "reflectron" mode depends on the species to be detected. For example, when operating in linear mode, the aim is usually to detect larger species, which will not be stable enough to survive along the strong electric field of the reflectron. Therefore, the given resolving power is much lower, as the width of the isotopic envelope do not allow for its decent resolution. The opposite is the case of ReToF, because especially in the presence of metastable fragmentations (i.e., in tandem MS), only fragments still having kinetic energies close to that of the precursor can be successfully and sensitively detected.

It is also possible to divide time-of-flight analyzers into two categories: low resolution systems (LR ToFMS) and high resolution systems (HR ToFMS).

The LR ToFMS system is characterized by a resolution of units of mass, and by an high acquisition frequency (i.e. 500 Hz). The duty cycle of a LR ToFMS is variable, with an approximate value of 30% [25], consequently the sensitivity is higher if compared to a scanning approach, such as qMS. The existence of a de-convolution software allows for the mass spectral resolution of partially co-eluted compounds during the chromatographic process. To ensure optimal de-convolution, a high spectral coherence is required, accompanied by an acquisition speed of about 20-30 spectra per peak. Quantification can be performed using the extracted ion chromatogram (EIC) technique, although there is low specificity due to the nominal mass resolution of LR ToFMS system.

The spectra generated by an HR ToFMS system are, on the other hand, characterized by higher resolution and high mass accuracy. Thanks to these capacities it is possible to generate highly specific chromatograms with the extracted ion, making a "pre-target" analysis possible. Obtaining fragments, with accurate mass values up to the forth decimal place, allows to obtain interesting information on the molecular structure. A high resolution mass spectrometer allows to obtain high mass accuracy, reducing the possibility of incorrect identification, due to the presence of isobaric interferences (same nominal mass and different molecular formula).

The term mass resolution, *R*, or simply resolution, usually refers to the ability of a mass spectrometer of separating two narrow mass spectral peaks. The ability of an instrument to distinguish between ions differing by a small increment in their *m/z* value (*Δm/z*) is called as resolving power:

$$R = \frac{m}{\Delta m} = \frac{m/_z}{\Delta m/_z}$$

Eq.3.2

Unit mass resolution means that only integer masses can be separated, that is, you can distinguish, e.g., mass 1000 from 1001.

The most commonly used method to measure the resolution follows the full width at half maximum (FWHM) definition, which uses the width of a peak at 50% of its height as a measure for *Δm* (Figure 3.12).

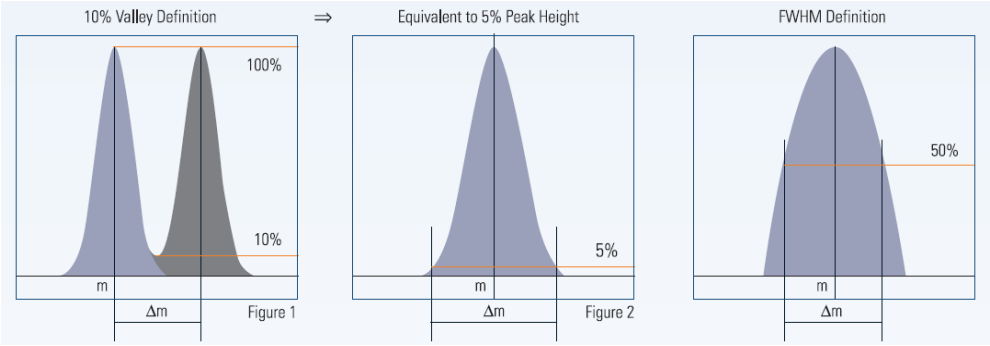

Figure 3.12. *Examples of different definitions of resolution.*

Instruments capable of low resolution operates at a R = 500–2000. High resolution refers to a R > 5000. However, there is no exact definition of these terms. Furthermore, one should be aware that increased settings of resolving power are usually obtained at the cost of transmission of the analyzer, thereby reducing the absolute signal intensity.

There are different ways to define and thus to calculate the mass of an atom, molecule or ion. Basically, an element is specified by the number of protons in its nucleus, i.e., the atomic number, which determines its place within the periodic table of the elements. Atoms with nuclei of the same atomic number but differing in the number of neutrons, i.e., by the mass number, are termed isotopes [26]. Those elements which do exist in the form of only one single naturally occurring stable isotope are termed monoisotopic elements. The distribution of the isotopic composition in a mass spectrum is named the isotopic pattern.

For stoichiometric calculations, chemists use the average mass, that is the result of the weighted average of the atomic masses of the different isotopes of each element in the molecule. In mass spectrometry, the nominal mass is generally used, the latter being calculated using the mass of the predominant isotope of each element rounded to the nearest integer value. However, the exact masses of isotopes are not exact whole numbers. They differ weakly from the nominal mass by a determined value, so-called mass defect, which is unique for each isotope. The monoisotopic mass is then calculated by using the exact mass of the most abundant isotope for each constituent element. It is very close to but not equal to the nominal mass of the isotope. As a consequence, almost no combination of elements in a molecular formula has the same calculated exact mass as any other one. The only exception is the carbon isotope ^{12}C, whose mass has been assigned precisely 12 u.

As an example, the molecular ions of nitrogen, $N_2^{+\bullet}$, carbon monoxide, $CO^{+\bullet}$, and ethene, $C_2H_4^{+\bullet}$, have the same nominal mass of 28 u, i.e., they are so-called isobaric ions. The isotopic masses of the most abundant isotopes of hydrogen, carbon, nitrogen, and oxygen are 1.007825 u, 12.000000 u, 14.003074 u, and 15.994915 u, respectively. Thus, the calculated exact masses are 28.00559 u for $N_2^{+\bullet}$, 27.99437 u for $CO^{+\bullet}$, and 28.03075 u for $C_2H_4^{+\bullet}$. This means they differ by several 10–3 u, and none of these isobaric ions measure precisely 28.00000 u.

The type of mass measured by mass spectrometry depends largely on the resolution and accuracy of the analyzer.

The mass accuracy indicates the deviation of the instrument's response between the measured accurate mass and calculated exact mass. It can be expressed as absolute mass accuracy, *Δm/z*:

$$\Delta m/z = m/z_{experimental} - m/z_{calculated}$$

Eq. 3.3

or, alternatively, as relative mass accuracy, *δm/m*, i.e., the absolute mass accuracy divided by the exact mass, and expressed as parts per million (ppm):

$$\partial m/m = (\Delta m/z)/(m/z) \times 10^6$$

Eq. 3.4

Accurate mass measurements allow to determine the elemental composition of an analyte, and thereby to confirm the identification of target compounds or to support the identification of unknowns. Assuming infinite mass accuracy, we should be able to assign the molecular formula of any ion simply through its exact mass. In reality, deviations between the accurate and exact mass of an ion always exist to some extent and, thus, we normally deal with errors in the order of one to several ppm depending on the type of instrument and the mode of its operation.

References:

[1] A.T. James, and A.J.P. Martin, Biochem. J. 50 (1952) 679.

[2] L.S. Ettre, Anal. Chem. 43 (1971) 20 A.

[3] L.S. Ettre, LC–GC 8 (1990) 716.

[4] L.S. Ettre, J. Chromatogr. 112 (1975) 1.

[5] D.J. David in: Gas Chromatographic Detectors, John Wiley & Sons, New York, (1974).

[6] L.L.P. van Stee, U.A.T. Brinkman, H. Bagheri, TrAC Trend. Anal. Chem. 21 (2002) 618.

[7] C.F. Poole, J. Chromatogr. A 1421 (2015) 137.

[8] J.C. Sternberg, W.S. Gallaway, D.T.C. Jones. Gas Chromatography, Third International Symposium , Instrument Society of America, Academic Press, (1962).

[9] J. Sevcik, R.E. Kaiser, R. Rieder. J. Chromatogr. 126 (1976) 361.

[10] K.H. Einführung, in: Massenspektrometrie, Weinheim, Verlag Chemie (1968).

[9-11] M. Jr. Jones in: Organic Chemistry, 2nd ed.; New York, W.W. Norton (2000).

[12] J.J. Thomson, Philos. Mag. 44 (1897) 293.

[13] J.J. Thomson, Philos. Mag. 13 (1907) 561.

[14] F.W. Aston, Philos. Mag. 38 (1919) 709.

[15] A.J. Dempster, Phys. Rev. 11 (1918) 316.

[16] A.O. Nier, Int. J. Mass Spectrom. Ion Proc. 100 (1990) 1.

[17] R. M. Smith in: Understanding Mass Spectra: a basic approach. Wiley & Sons, New York, (2004).

[18] F. W. McLafferty, F. Tureček in: Interpretation of Mass Spectra. University Science Books, Mill Valley, (1993).

[19] W. Paul, H. Steinwedel, Z. Naturforsch. A, 8 (1953) 448.

[20] R.E. Finnigan, Anal. Chem. 66 (1994) 969A.

[21] D.W. McLachlan in: Theory and Applications of Mathieu Functions. Oxford, Clarendon Press (1947).

[22] W.E. Stephens, Phys. Rev. 69 (1946) 691.

[23] W.C. Wiley, I.H. McLaren, Rev. Sci. Instrum. 26 (1955) 1150.

[24] B.A. Mamyrin, Int. J. Mass Spectrom. Ion Proc. 131 (1994) 1.

[25] E. de Hoffmann, V. Stroobant, in: Mass Spectrometry – Principles and Applications, John Wiley & Sons, Chichester, (2007).

[26] J.F.J. Todd, Int. J. Mass Spectrom. Ion Proc. 142 (1995) 211.

Chapter 4

4.0 Comprehensive two-dimensional gas chromatography

4.1 Introduction

Comprehensive two-dimensional gas chromatography can be considered as the most promising innovation in separation science since discovery of capillary columns. The first GC×GC application was reported in 1991, by Phillips and a co-worker [1]: a mixture of standard compounds eluting across a first-dimension column were subjected to sequential heart-cutting, at specific time intervals. Each entrapment process was followed by rapid release of the isolated fraction into a ^{2}D column.

Nowadays, 1D GC represent the most commonly applied method for the separation of volatile and semi-volatile compounds of real-word sample. However, in the last three decades it has become clear that the resolution of all constituents of a sample is often an unreasonable challenge by the use of a single column. Considering that 1D GC separation is mostly based on a single separation criterion, i.e. the different vapor pressure of each analytes, if this property of many analytes in a complex mixture do not differ enough, co-elution will occur. In this case, the application of a further separation criterion, such as their different polarity can lead to the resolution of many co-elution [2].

In general, the main advantages of GC×GC over 1D GC methods are essentially three: apart from the enhanced resolving power, a major beneficial characteristic is enhanced sensitivity through solute band re-concentration to make the technique particularly suitable for trace-level component detection (clearly, trace-amount volatiles must be totally resolved from interfering analytes). A further benefit is the ^{2}D chromatogram formation of chemically similar compound patterns. This aspect is of great help in the identification of unknowns, when no standard components are available, in the absence of a corresponding MS library spectrum, or when the resulting experimental MS spectra are very similar to others (e.g., homologous series of compounds, such as fatty acid methyl esters).

Considering that GC×GC has been on the analytical scene for nearly 30 years, it can now be defined as “well known”. During this period GC×GC has undergone great hardware and software evolution. For example, during the first 10 years FID was, by far, the most common form of detection. After that period, a rapid increase in the use of MS was observed [3-6].

For what concern the topics covered in the publications, over the past two-years (2018-2019), a clear dominance of applications research (i.e. food and beverage, energy, environmental, and biological) was observed. On a total number of 257 publications evaluated only the 10% of it deal with theory (6%) and instrumental evolution (4%). This confirm that GC×GC is becoming a mature technology. Such a tendency will probably continue, also in part as a result of the continuous evolution of MS. In fact, the availability of (powerful) MS reduces the requirements of an improved separation performance on the GC×GC side [7].

4.2 Concept of multidimensionality

The basic requirements for a multiple separation to be considered multi-dimensional were discussed by Giddings in 1987 [8].

Three conditions have to be fulfilled:

- The components of a mixture should be subjected to two (or even more) separation steps. All the steps have to be governed by different factors.

- Analytes that were resolved in the previous step should remain separated until the following separation process is completed.

- The second dimension must be significantly faster than the first dimension.

When two (or even more) independent separation mechanisms are used, this will result in an equal number of parameters to define the identity of an analyte [9]. Regarding GC×GC, each analyte is characterized by two independent retention times rather than by a single one (as in 1D GC).

A further condition requires the separate analysis of small fractions of eluate from the first column on the second one, in order to preserve the separation already fulfil on the first dimension.

When the dimension are based on different interaction mechanism, separation is defined as "orthogonal" [10]. The smallest correlation between the dimensions will cause redundant information which will influence all the separation. The concept of orthogonality is represented in Figure 4.1. Three different degree of correlation between two separation dimensions are illustrated. In a totally orthogonal separation, the peaks are distributed over the entire plane (a). The more the dimension are correlated, the more the distribution will be centered along the diagonal (b). If the correlation is total, the analytes will have the same retention into the two dimensions, leading to an equivalent ^{1}D separation along the diagonal (c).

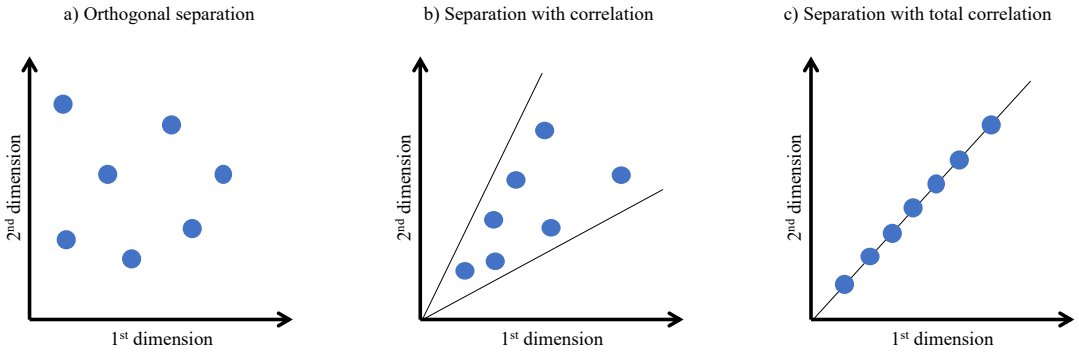

Figure 4.1. *Examples of different degree of correlation between two separation dimensions.*

In order to produce an efficient multidimensional system, the separation dimensions must be correctly selected. The concept of sample dimensionality (*S*), representing the number of independent variables describing properties of the sample compounds was first introduced by Giddings [11]. The dimension can be expressed at several levels: π-aromaticity interaction, chirality, hydrogen bonds, size or shape of molecules, volatility/number of carbon atoms, etc.

In a GC×GC approach, the usefulness of such a system for the separation of a complex mixture is illustrated in Figure 4.2. Let's suppose an hypothetical sample containing a large number of analytes that differ in shape, color, and size. Following

the concept of dimensionality from Giddings [11], the sample can be characterized by a dimensionality of three. In these conditions, there is virtually no chance to resolve all the analytes by the use of a conventional single dimension system. With such a ^{1}D system, the separation can be achieved according to size, but then color and shape will remain unresolved; or it can be carried out according to color, but then the size and shape will remain unseparated. Or, finally, the separation can be performed according to shape, but without separation between color and size. A viable approach to obtain the separation of nearly all the constituents of this sample is the use of an orthogonal ^{2}D separation system with a dimensionality that can match the dimensionality of the sample [11]. In that case, one can use most of the available separation space very efficiently in order to accommodate separated analytes and create highly structured elution pattern.

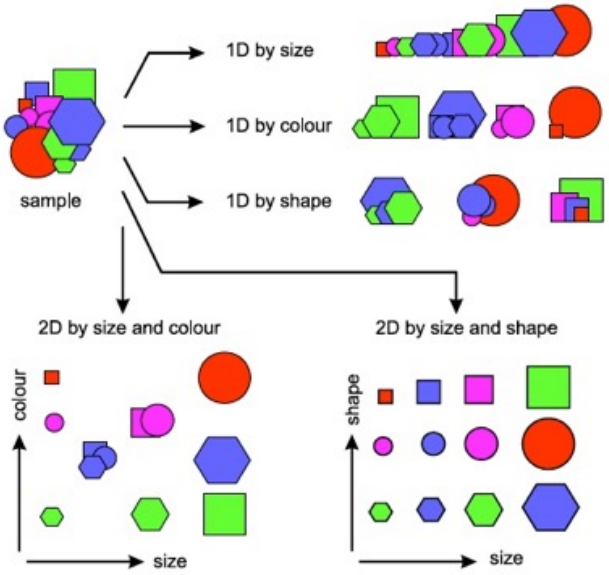

Figure 4.2. *Match between separation and sample dimensionality in GC×GC.*

A GC×GC analysis starts by the injection of a sample into the injector and by mixing it with the carrier gas, as in 1D GC. However, rather than entering the detector when exiting the GC column, the analytes reach in an interface, named the modulator, placed between the two separation columns. The role of the modulator (considered as the heart of a GC×GC system) is to guarantee high sampling rate and to transfer the sample from the ^{1}D to the ^{2}D columns [9], respecting the Giddings conservation rules discussed above.

The modulator can be considered as an on-line injector, capable of generating very narrow injection pulses on the second column head, accounting for a fast sampling of compounds eluting from the ^{1}D. The total ^{1}D chromatogram is thus "sliced" following a modulation period (P_M) of a few seconds and re-injected into ^{2}D column for a fast GC-type separation [12] (see Figure 4.3a).

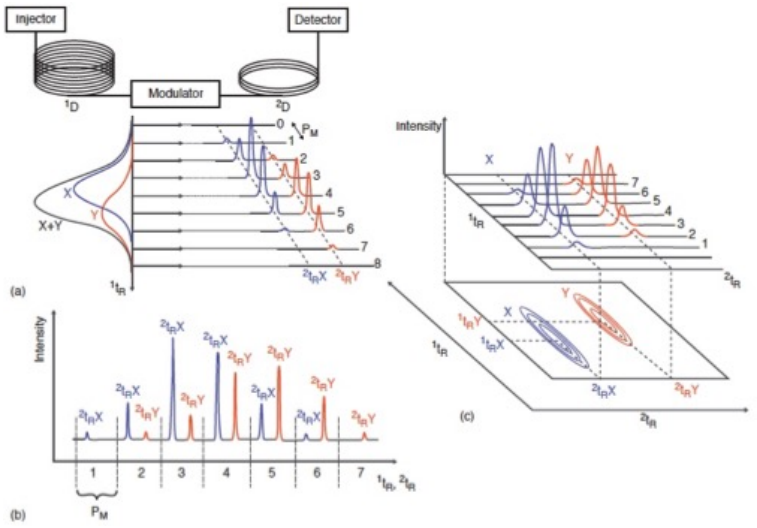

Figure 4.3. *Scheme of the column coupling in the GC×GC setup and of how data are handled (not to scale). (A) The modulator permit fast sampling of the analytes eluting out of ^{1}D and reinjection in ^{2}D. The modulation process is showed for two overlapping analytes (X and Y) coming out of ^{1}D at a defined first-dimension retention time ($^{1}t_R$). As the modulation process happens during a defined PM, narrow bands of sampled analytes are entering ^{2}D and appear to have different second-dimension retention times ($^{2}t_R$X and $^{2}t_R$Y). (B) Raw data signal as recorded by the detector through the entire separation process. (C) Construction of the two-dimensional contour plot from the collected high-speed secondary chromatograms of (B), in which similar signal intensities are connected by contour lines.*

Ideally, the separation of analytes re-injected into the ^{2}D by the modulation should be completed before the next modulation, in order to avoid overlap of peaks issued from different modulation cycles (an effect known as wraparound). However, as far as no new coelutions are generated from the wraparound effect, there is no reason to spend time to avoid wraparound in a separation procedure. Moreover, dedicated software can easily re-establish a clear picture of the separation space [13]. The main drawback of wraparound happens when peaks overlap and coelutions occur.

Usually, the second column analysis is much faster compared to the first one and a secondary GC oven is used to heat independently the ^{2}D column. As a result, the separation time into the ^{2}D column is about 100 times more rapid than that in the ^{1}D. Since the modulation occurs during the ^{1}D separation, the total analysis time of a GC×GC application is about the same as in 1D GC. Regarding the detector response, everything occurs as in 1D GC and a trace is monitored continuously. A series of high-speed secondary chromatograms of a length equal to P_M are recorded one after another (Figure 4.3b). They consist of slices that can be combined to describe the elution pattern by means of ^{2}D contour plots into the chromatographic separation plane (Figure 4.3c).

As already discussed, the larger peak capacity it is not the only advantage of GC×GC over 1D GC. Nowadays, GC×GC systems offer several features that cannot be obtained by 1D GC. For example, the capacity to provide structural composition of a sample in a way that 1D GC cannot (ordered structure in the bidimensional chromatogram) [4, 14-20]. GC×GC also has a unique class selectivity feature that allow to remove a majority of peaks of no interest from the two-dimensional separation space for the resolution of peaks of interest compared to 1D GC with equal peak capacity [4, 20, 21].

The main advantages of GC×GC, over 1D GC methods, are basically five:

1. speed – taking into account the number of peaks resolved/unit of time;
2. selectivity – two stationary phase of different selectivity are used;
3. separation – increased resolving power;
4. sensitivity – the isolation of chemical noise has a real influence on sensitivity. Moreover, the analyte band compression effect generated by the modulation improves *S/N* ratio (mainly using cryogenic modulation);
5. spatial order – the contour plot formation of chemically-similar compound patterns for homologous series.

4.3 Column configurations

For the construction of a GC×GC system it is possible to use the same equipment employed for 1D GC. Samples are introduced by an injector, allowing all conventional injection techniques to be used, into the first conventional capillary column where the first separation occurs; the eluate is then fractionated and re-injected through the modulator into the second capillary column coated with a different stationary phase for further separation. The two columns can be installed into the same GC oven or in two different one. The latter option allows to obtain an higher degree of flexibility during the method optimization. The detectors should have an high acquisition rate in order to accurately reconstruct the narrow chromatographic bands generated.

Moreover, the entire GC×GC process requires data elaboration and visualization (Figure 4.4). Dedicated software packages stack second-dimension chromatograms side by side, and considering the modulation time, derive the first and the second dimension retention times relative to each peak. The peak areas are obtained by the sum the area relative to each modulated peak. Regarding the signal intensity, it is considered as the height of the tallest modulated peaks and can be visualized in different ways: - by color plot (a); - by wireframe 3D plot (b); -by surface 3D plot (c).

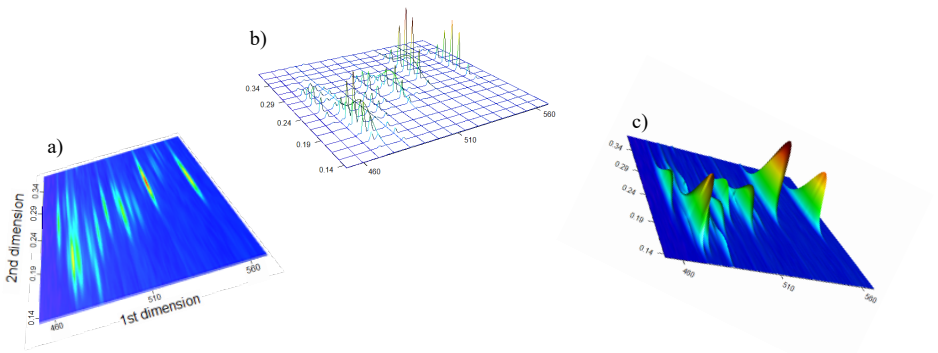

Figure 4.4. *Data visualization in* GC×GC.

Although the modulator is the key to successful GC×GC separations, the chromatographic columns play the most significant role in any GC analysis. The geometry together with the chemistry of the column represent two key factors of the potential resolution reachable with a particular system. In GC×GC the combination between column geometry and chemistry provide increased separation power. The

development of new column types provide several possibilities of combinations with specific selectivity behaviors [23].

In most GC×GC applications, operators exploit a difference in polarity between the two dimensions, using a nonpolar-polar or polar-nonpolar column combination. In order to comply with Giddings' rules 2 and 3 (see section 4.2), the second dimension has to work under fast GC conditions. Usually, the second dimension column measures between 80 and 200 cm long to maintain elution times that are under the P_M (i.e. 1-10 s) for nearly all analytes. The most used dimensions for the ^{1}D column are 30 m column length with 0.25 mm internal diameter (ID) and 0.25 μm film thickness (d_f). The most used column configuration combines a nonpolar ^{1}D column (i.e. dimethylpolysiloxane) with a more polar ^{2}D (i.e. polyethylene glycol), as shown in Fig. 4.5. This is probably due to the fact that an important reason for switching from 1D GC to GC×GC is to improve the separation resolution so much that analysts do not spend much time in optimizing the column set. For specific applications, different column combinations seem to emerge from the classical nonpolar/semipolar configuration [24,25].

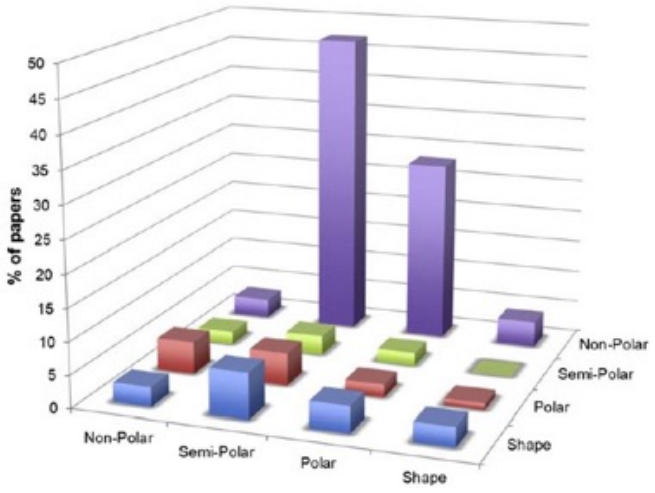

Figure 4.5. *Relative proportions of column combinations used in published GC×GC studies (2018).*

The most used combination of nonpolar ^{1}D and midpolar ^{2}D columns generates a structured elution pattern, where the saturated compounds are at the bottom, followed by alkenes, monoaromatic, diaromatic, and larger hydrocarbons, when going up along the second dimension axis, as shown in Fig. 4.6. Thanks to this column combination, group-type analysis is possible even using a simple detector such as FID.

By an inversion of the column configuration, with midpolar ^{1}D and nonpolar ^{2}D columns, the elution order will flip upside down. This reversed configuration is more suitable when semipolar and polar compounds represent the main part of the samples [2,26].

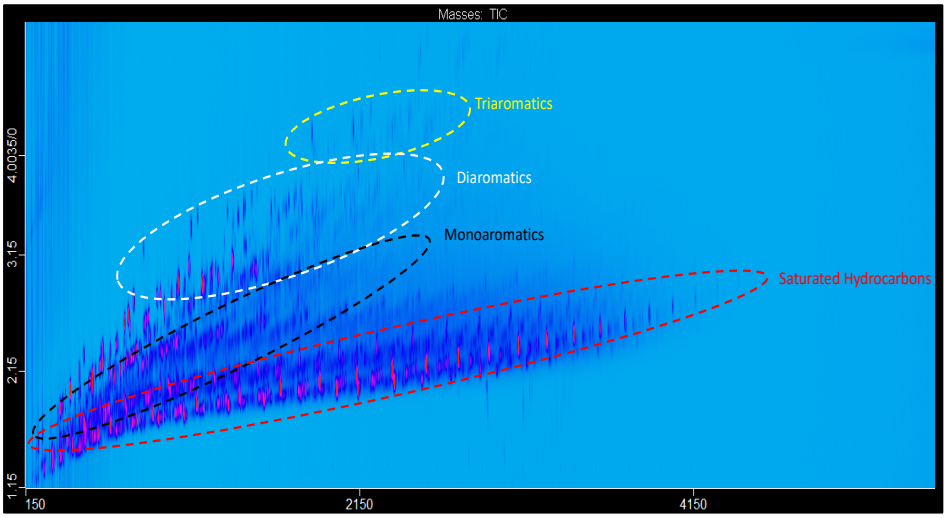

Figure 4.6. *GC×GC-HR ToFMS analysis of a commercial diesel sample on a normal column configuration. Red: saturated hydrocarbons; black: monoaromatics; white: diaromatics; yellow: triaromatics.*

4.4 Modulators

In order to generate a quality GC×GC separation, it is crucial to attain an effective transfer of the ^{1}D column effluent to the ^{2}D column. Moreover, it is important to maintain the separation which was obtained into the first dimension. To accomplish these two goals, a modulator interface is required [27]. Over the years many types of modulator have been developed.

Modulators enable continuous trapping, focusing and re-injection, without which GC×GC analysis cannot be achieved. The connection of two columns of differing stationary phase in series without a modulator do not allows a GC×GC separation [27].

In Figure 4.7 is evident the need for and the role of the modulator. If two columns with different stationary phase are connected in series the analytes separated on the ^{1}D column are not prevented from coelution at the exit of the ^{2}D column (Figure 4.7A-C). Figure 4.7A shows the ^{1}D separation, with three distinct analyte bands approaching the ^{2}D column. When the first two bands enter the ^{2}D column (Figure 4.7B), the black

band starts to catch up with the lighter one because it is less retained by the ^{2}D stationary phase, leading to coelution of the two bands at the outlet of the column. Consequently, the initial separation achieved into the ^{1}D is not preserved. Moreover, it is also possible a change of the elution order of the analytes due to different selectivity of the ^{2}D column (Figure 4.7C).

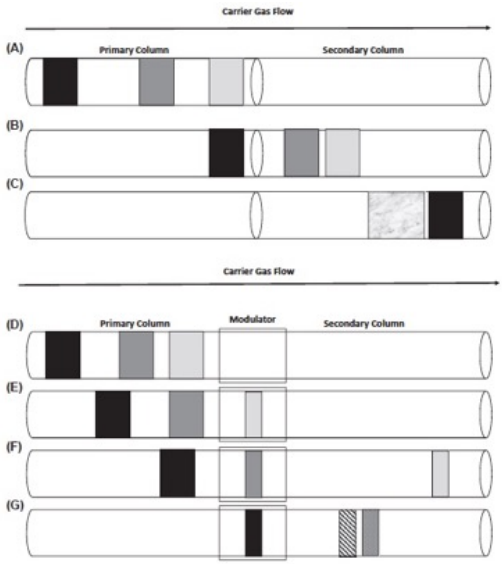

Figure 4.7. *The influence of the modulator is demonstrated when comparing (A-C) to (D-G). When the primary and secondary dimensions are connected in series without a modulator, analytes separated in ^{1}D can coelute or change elution order in the second column because of different retentivity of the ^{2}D column stationary phase (A-C). When a modulator is installed, the primary components of the ^{1}D effluent are periodically trapped, focused, and injected onto the head of the second-dimension column. The primary dimension separation is maintained because analytes that could be retained less in ^{2}D leading to a potential coelution (see the gray bands in panels A-C) are prevented from entering the ^{2}D column until the separation of the preceding band in ^{2}D is complete (D-G).*

When a modulator is placed between the two columns a proper GC×GC separation can be achieved (Figure 4.7D-G). Figure 4.7D show the same three analytes reaching the modulator after the ^{1}D separation. When the lower boiling point analyte band enters into the modulator (Figure 4.7E), in most cases, it is focused into a narrow band, which is then reinjected into the ^{2}D column (Figure 4.7F). In the meantime, the second analyte band is trapped by the modulator, avoiding possible coelution in the ^{2}D column. Focusing and reinjection of this analyte band (Fig. 4.7G) allows for further

separation into two separate bands in the second dimension, while the last analyte band eluting from the ^{1}D column is trapped by the modulator.

4.4.1 Modulation ratio and phase of modulation

In order to preserve the separation performed in the first dimension, the ^{1}D eluate must be sampled many times to avoid coelution of already separated components [2]. Each chromatographic peak must be sampled three or four time in order to meet this requirement [28,29].

The modulation period can be well described by the term modulation ratio (M_R) [29].

$$M_R = \frac{4\sigma}{P_M} = \frac{w_b}{P_M} = \frac{w_h \times 1.6985}{P_M}$$

Eq. 4.1

where the peak width at the base (w_b), defined as 4 times the ^{1}D column peak standard deviation (σ) or 1.6985 times the width at half height of the peak (w_h), is divided by the modulation period (P_M). To perform quantitative analysis of trace compounds a M_R value of at least three should be used, while a value of 1.5 is enough for semiquantitative analysis or for major components only [29].

For what concerns the phase of modulation, this is defined as the difference between the center of ^{1}D peak and the mean of the peak region sampled by the modulator. The phase of modulation influence the degree of resolution and the reconstructed peak width of the analyte eluting from the ^{1}D column [30]. There are two limiting situations, in-phase and 180 degrees out of phase modulation, respectively, and these are represented in Figure 4.8.

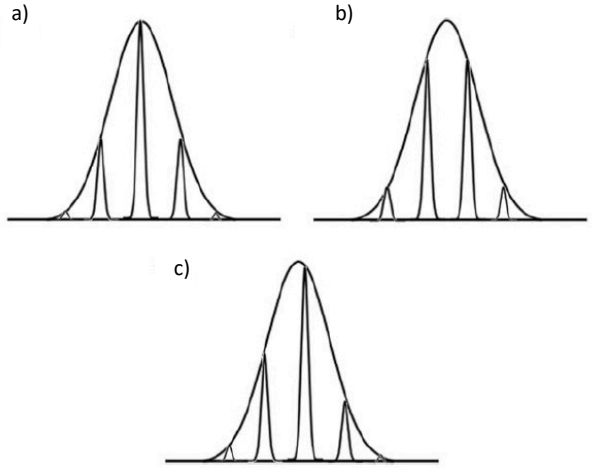

Figure 4.8. *GC peak pulses in GC×GC can have different phases. a) In-phase modulation, b) 180° out of-phase modulation, and c) any other phase modulation.*

The situation shown in Figure 4.8a represent a modulated ^{1}D peak gives from a symmetric pulse sequence with a single maximum peak centered. While in Figure 4.8b represent two equally tall symmetric maxima equidistant from the ^{1}D peak maximum [31]. Generally, any phase between these two limiting situations may be observed in actual two-dimensional separations due to the random nature of the distribution of peaks emerging from the ^{1}D column (e.g. Fig. 4.8c). Although ^{1}D resolution is affected by the modulation phase, it is not possible to modify this parameter to achieve the most appropriate phase. For this reason, it is recommended to use the peak area as a quantitative measure of response as it is independent of the modulation phase [31].

4.4.2 Types of modulator

Modulators can be broadly divided into two main categories: thermal modulators, and pneumatic or flow modulators. Thermal modulators can be divided into heater-based and cryogenic. In general, heater-based modulators works collecting analyte bands eluting from ^{1}D column at or slightly below the oven temperature and releasing them through an increment in temperature. Instead, cryogenic modulators (CM) collect analytes at very low temperatures realized with the use of cryogens and release them at/or slightly above the oven temperature.

Flow modulators (FM) can be divided into two subcategories: differential flow modulator and diverting flow modulator. Differential flow modulators is characterized by two independent carrier gas flows to achieve the modulation [32]. This kind of modulator is also known as: flow switching, or full transfer modulators [33]. Diverting flow modulator employ a stainless steel collection tube in order to collect the ^{1}D column effluent, which is subsequently flushed onto the ^{2}D column [32]. Usually, this modulator interface is classified as low duty cycle modulators [33].

4.5 Thermal modulation

The term “thermal modulator” is employed for all the devices that utilize a positive and/or negative temperature difference, with respect to the oven temperature to carry out the GC×GC process. All thermal modulators generate an increase in sensitivity (through a re-concentration effect) and are typically characterized by unit duty-cycle. Until 1998 (year of the first cryogenic and flow-based devices) all the modulators developed were thermal and were constructed by Phillips and co-workers [1, 34-41] or based on his early model [42].

4.5.1 Heater-based modulators

Heater designs depend on passive sorption of analytes by the use of thick coating of liquid stationary phases or adsorbent phases at or below ambient temperature, while utilizing active heating for the rapid desorption of the trapped analytes. One of the restrictions of heater designs with trapping performed at the oven temperature is the higher temperature limit of the stationary phase being used for modulation. Since extra heating is supplied for desorption, this restricts the highest GC oven temperature to the maximum operational temperature of the stationary phase minus the differential temperature employed [3]. This restriction becomes less critical if trapping is performed below the oven temperature.

4.5.1.1 Thermal desorption modulator (TDM)

As is well known, the transition from 1D GC to GC×GC was first reported in 1991 [1] when Phillips and a co-worker utilized a dual-stage TDM to reinject analytes from the ^{1}D column onto the ^{2}D one. Initially, the TDM was used as a sample introduction device in multiplex and high speed GC [34, 35, 43]. The dual-stage TDM was constructed using the head of the apolar ^{2}D column (1m × 0.1 mm ID × 0.5 μm d_f), looped outside of the GC oven at ambient temperature and coated with a film of electrically-conductive material (gold paint). The modulator was 15 cm long, divided equally between the two stages. The principle of its operation is shown in Fig. 4.9.

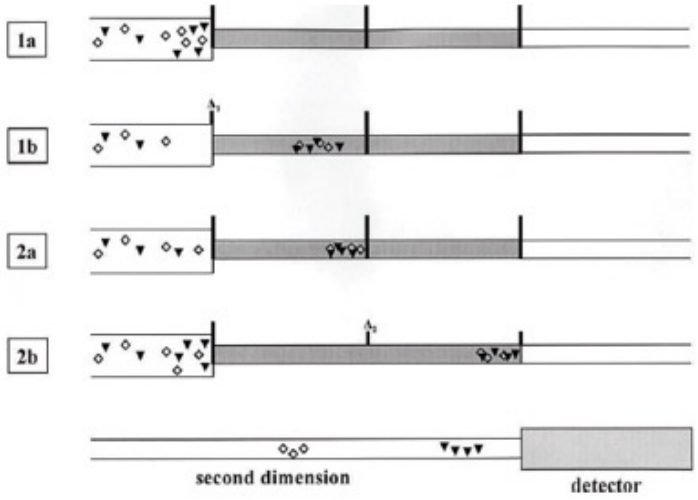

Figure 4.9. *Dual-stage thermal desorption modulation process on two compounds coeluting in the first dimension.*

The operating principle was the following (Fig. 4.9):

1) A narrow band of ^{1}D column (moderately polar, 21 m × 0.25 mm ID × 0.25 μm d_f) effluent, in this example containing two overlapping compounds, was formed at the modulator head (band compression I), at ambient temperature (stage 1a);
2) Re-injection was carried out through the use of an electrical pulse of 20-msec duration (Δ_1), directed to the first segment of the modulator (stage 1b), ending the first modulation stage;
3) The re-mobilized fraction, carried by the mobile phase, reached the second "cold" segment of the modulator (band compression II);

4) Meanwhile, another narrow chromatography plug begins to accumulate at the modulator head, which as rapidly cooled down to ambient temperature (stage 2a);
5) After 100 msec from the previous electrical pulse, a further eating shot (Δ_2) is directed to the second modulator segment, launching the narrow band onto the ^{2}D column (stage 2b), thus ending the second modulation stage;
6) Ideally, the different secondary-dimension selectivity will enable the delivery of two separated solute to the detector;
7) Two second after the first electric pulse, the next modulation process was initiated.

Although successful in achieving the first GC×GC separation, the design was not very robust due to frequent burnouts and the delicate nature of the thin conductive films [41].

Over the past ten years, the TDM was first revised by Górecki et al [44, 45] and by Hantao and coworkers, with updated materials, a simple design, and inexpensive commercial components [46].

4.5.1.2 Thermal sweeper modulator

One of the most noteworthy heater-based modulator, also because it was the first to be commercialized (Zoex Corporation), was the thermal sweeper [38-41]. This modulator was described for the first time in 1996 [38], subjected to further technical development over the years, and appeared in its final version in 1999 [41]. The thermal sweeper, illustrated in Figure 4.10, is based on the use of a slotted heater that rotate around a shaft to heat the modulator capillary. Analytes from the ^{1}D column accumulate at the first part of the modulator capillary coated with a thick film of the stationary phase (Figure 4.10A); Before breakthrough occurs, the slotted heater (280°C) rotates over the upstream end of the modulator capillary, generating a heart-cut (Figure 4.10B); The remobilized analytes would then be continuously refocused in the downstream portion of the modulator column that was still at oven temperature (Figure 4.10C). As the slotted heater rotated over the downstream part of the modulator

column, the focused band of analytes was ultimately injected into the ^{2}D column (Figure 4.10D).

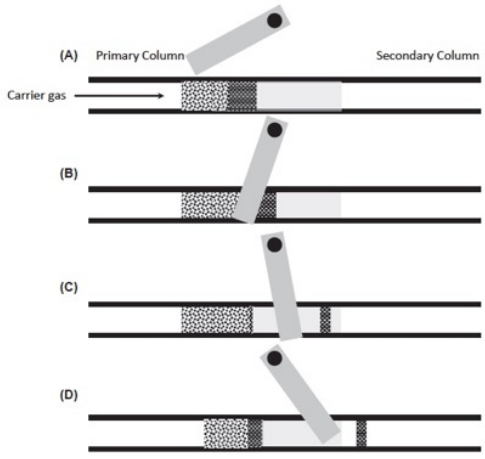

Figure 4.10. *Modulation process of the rotating thermal modulator.*

In order to generate sufficiently narrow modulated peaks, the temperature difference between the heater and the modulator capillary should be at least 100 °C [47]. This can be considered as a drawback, because limit the maximum GC oven temperature and consequently also the volatility range of compounds that could be modulated.

4.5.2 Cryogenic design modulators

The operating mechanism of CM consists on the use of cryogens for trap the analytes at temperatures significantly lower than the oven temperature.

Even if cryogenic modulation adds an important consumable cost to the system, it provide the best performance, overcoming the previous temperature limitations of the heater designs.

4.5.2.1 Longitudinal modulated cryogenic system (LMCS)

The first appearance of the LMCS dates back to 1997 [48]. Initially, the LMCS system was reported as a device capable of increasing GC *S/N* ratio [49]. In 1998, Kinghorn and Marriott connected a 30 m × 0.25 mm ID × 0.25 µm d_f non-polar column to a polar 0.6 m × 0.10 mm ID × 0.10 µm d_f column. The first 5 cm of the ^{2}D column was thread through an LMCS, with the movement of the trap occurring every 7.5 sec,

enabling GC×GC analysis of kerosene [50]. A representation of LMCS is reported in Figure 4.11.

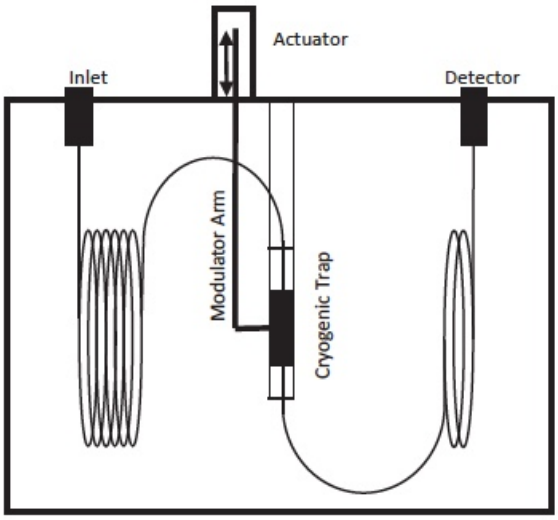

Figure 4.11. *Schematic representation of LCMS.*

In a comparison between the thermal sweeper and the LMCS, it was recognized that both systems generated very similar results regarding peak widths and symmetry [51]. Nevertheless, each system had its own limitations. The modulator capillary of the sweeper had problems related to trapping analytes at high temperatures, while for the LMCS system, analyte remobilization could suffer at lower oven temperatures, in particular, if a slow temperature program was utilized [51]. The poor remobilization capacity of high-boiling analytes resulting in severe band broadening [52]. Regulating the trap temperature in order to maintain a constant negative offset from the oven temperature rather than an isothermal temperature allows to improve the results [52].

4.5.2.2 Dual-stage jet modulators

The dual-stage, quad-jet modulator was firstly reported by Ledford in 2000 and it is still the most adopted modulator design [53]. As reported in Figure 4.12 the operating mechanism is based on the use of two hot jets and two cold jets to provide dual-stage modulation.

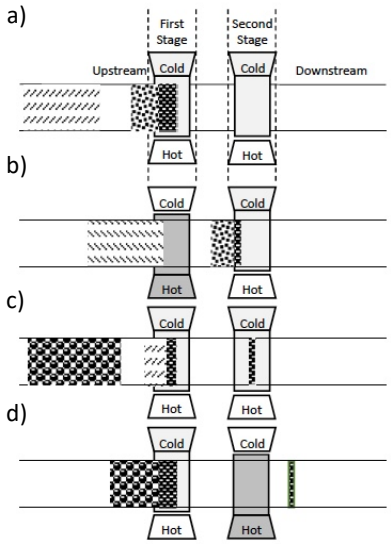

Figure 4.12. *Modulation process of the dual-stage, quad-jet thermal modulator.*

These jets were positioned to provide a transverse gas flow at the head of the ^{2}D column where modulation occurred [54]. Gas for the cold jets was cooled in a heat exchanger by the use of liquid nitrogen for cooling [54]. Instead, an electric heater allows to heating the gas flowing to the hot jets [54]. Analytes eluting from the ^{1}D column were trapped and focused at the first cold stage provided by the upstream cold jet (Figure 4.12a). The upstream hot jet was then pulsed, remobilizing the trapped analytes to the second stage where the downstream cold jet would refocus the band of analytes preventing any breakthrough (Figure 4.12b). Following the heat pulse, the upstream cold jet would reengage, allowing the upstream cold spot to start trapping the next fraction of the analytes (Figure 4.12c). The refocused band of the analytes in the second stage was remobilized and injected into the ^{2}D column when the downstream hot jet engaged while the upstream cold jet remained on to prevent breakthrough (Figure 4.12d). This modulator is available in both a liquid nitrogen variant with a modulation range of C_4 to C_{40} and a consumable-free variant with a modulation range of C_8 to C_{40}. The consumable-free variant uses a closed loop chiller instead of liquid nitrogen to cool the heat exchanger.

In 2001, Beens et al. proposed a dual-jet system, which was basically a simplified version of the quad-jet modulator, attained by eliminating the hot jets [55]. Instead of liquid N_2, pressurized liquid CO_2 was exploited as cooling agent, while the GC oven heat was used for analyte re-mobilization. A ^{2}D injection band width of 10 ms was

calculated for C_{14} alkane, which was claimed to be much better that the performance of both the thermal sweeper and LMCS. The not excessively low trapping temperatures generated by pressurized liquid CO_2 certainly minimized the need for heating jets, but also did not enable the entrapment of highly volatile compounds (e.g., C_5 and C_6).

4.5.2.3 Dual-jet loop modulator

After the introduction of the quad-jet modulator, Ledford et al. proposed a dual-stage interface, equipped with a cold and hot jet, named as loop-type modulator [56]. The two stages are created by looping a segment (1–1.5 m) of capillary column (modulator tube) through the pathway of a cold jet of N_2 gas (Figure 4.13).

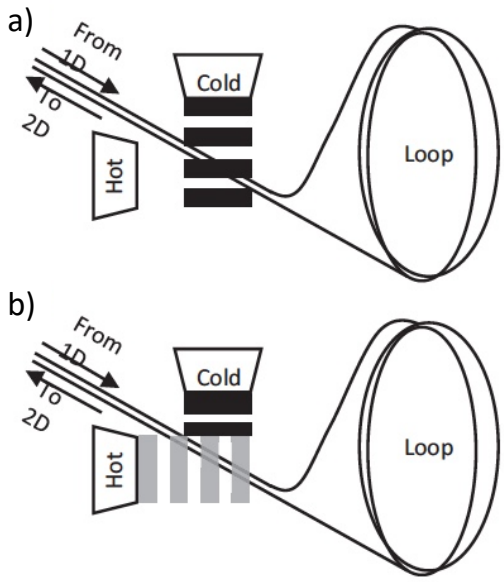

Figure 4.13. *Modulation process of the dual-jet loop modulator.*

Though the modulator loop can be created by using the last part of the first dimension or the initial segment of the second, such options are not advisable because breakages can occur when a capillary column is coiled tightly. Is better to use an uncoated column, or a segment of stationary-phase-coated capillary. The focusing gas, which is cooled in a heat exchange coil located in a small liquid-N_2 Dewar, flows continuously throughout the GC×GC analysis. The cold jet is directed vertically downward onto the modulator tube, thus generating two cold spots (Figure 4.13a); the

cold jet is diverted from the cold spots by a hot jet of nitrogen gas, which is activated for a brief period (i.e., 300–375 ms), in a periodic manner (i.e., every 4–6 s, corresponding to the modulation period). The hot jet is located perpendicularly to the cold one, and rapidly heats the cold spots, remobilizing the entrapped analytes (Figure 4.13b).

The loop-type modulator works essentially in the same manner as the quad-jet modulator, but through the use of only two jets: analytes entrapped in the upstream cold spot are injected in the modulator tube by activation of the hot jet. Before the analytes reach the downstream spot, the hot jet is deactivated, and a new cold spot is created. In this way the previously remobilized analytes are subjected to a further trapping step. Finally, the following activation of the hot jet injects the entrapped chromatography band onto the second dimension.

An important parameter for modulation in GC×GC, introduced by Tranchida et al., is the carrier gas velocity at the point of re-injection [57]. For loop-based thermal modulation, similar to other types of thermal modulation, the ^{1}D and ^{2}D columns are serially coupled. This means that the ^{2}D flow rate is directly influenced by the length, diameter, and flow rate of ^{1}D. To optimize the re-injection conditions, a bleed line can be added using a Y connector at the end of ^{1}D between the outlet of the modulator loop and ^{2}D column. Others have used this technique to improve the separation on the ^{2}D column [58,59].

Few years ago, Zoex Corporation has commercialized a loop-type modulator with no liquid N_2 requirements (ZX-2): cooling of the N_2 gas is achieved by using a refrigeration unit, with a reported minimum temperature of -90 °C, sufficient for the entrapment of C_7 alkane.

4.5.3 Other thermal modulators

Over the years, other thermal modulators have been developed that do not make use of cryogens, without compromise to the performance.

4.5.3.1 Solid-state modulator

The solid state modulator (J&X Technologies) appeared for the first time in 2016 ad thermal independent modulator (TiM) [60]. The TiM, shown in Figure 4.14, is placed outside of the GC oven and featured thermally independent heating and cooling stages [60]. Inside the modulator there are two heated zones (entry and exit zone) that can be programmed from ambient temperature to greater than 350 °C in order to guarantee the remobilization of analytes. The trapping zone is placed in the middle of the two heated areas and can be programmed from -50°C to 50 °C. The heating mechanism is based on the use of micathermic heaters to heat the aluminum chambers, while the cooling one is based on the use of a pair of three-stages thermoelectric coolers. Dual-stage modulation is achieved by the mechanical movement of the modulator column back and forth in a fashion opposite to longitudinally modulated cryogenic system (LMCS), in which the cold trap was moved along the column [48]. Moreover, the fact of being placed out of the GC oven is a figure in common also with the TDM [1].

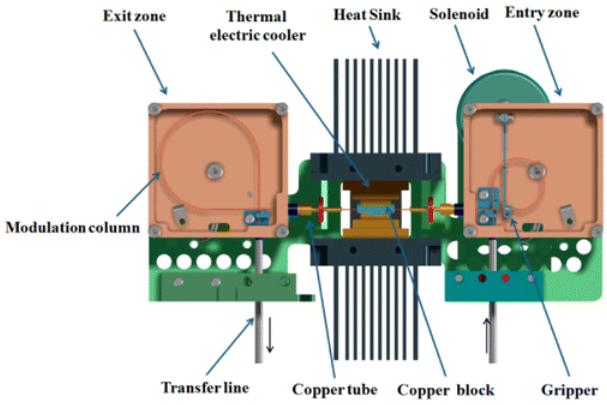

Figure 4.14. *Schematic representation of thermal independent modulator.*

Analytes eluting from the ^{1}D column were trapped inside the segment of the column exposed to the cooled zone. The first remobilization of the analytes was carried out by moving the column toward the heated entry zone, thereby exposing the trapped analytes to the elevated temperature. This movement also exposed the downstream segment of the modulator column to the cooling units. The remobilized analytes would

then reach the newly cooled zone for the second stage of trapping. Moving the column toward the exit zone exposed the trapped analytes once again to an elevated temperature and injected the band into the ^{2}D column. This simultaneously exposed the upstream segment of the column to the first stage of trapping once again. Initially relatively wide reinjection band widths were reported, due to the 0.25 mm ID modulator column used and the length of column between the second modulation stage and the ^{2}D column [60]. Use of an auxiliary carrier gas to increase the modulator flow rate to 3 mL min^{-1} reduced w_h to 20-25 ms for *n*-alkanes up to C_{24} when directly connected to an FID [60]. Volatility range was reported to be from C_6 to C_{24}, while w_h of 120 ms were reported for aromatic compounds [60]. The modulation range of the solid state modulator has been updated from the TiM to range from C_2 to C_{40+} depending on the modulator column installed.

Tranchida et al. evaluated the effects of the gas linear velocity on the modulation performance by using two different uncoated trapping capillaries (0.8 m × 0.25 mm ID and 0.8 m × 0.20 mm ID) [61]. The application was carried out on a standard solution of *n*-alkanes (C_9, C_{10}, C_{12}) and also on a sample of diesel fuel. The results demonstrated that the type of trapping capillary and the gas velocity have a great effect on modulation efficiency [61].

4.5.3.2 Single-stage modulator

Górecki, together with his research group, developed several designs for a consumable-free modulator [44, 45, 62, 63]. The first designs were based on the use of 15-cm segment of flattened coated Silicosteel capillary column, looped outside of the GC oven in order to achieve the entrapment of the analytes with the help of forced air cooling. The reinjection process was carried out through resistive heating [44, 45].

Regarding the single-stage modulator, it was introduced in 2015 [62]. This modulator, used a specially coated stainless steel capillary trap that could be passively or actively cooled. The analytes band re-concentration was accomplished with the aid of cooling from the compression of the trap between two ceramic cooling blocks. The ceramic cooling blocks were cooled through a copper heat transfer conduit that was

passively cooled by two heat sinks or actively cooled with the addition of a thermoelectric cooling unit between the heat transfer conduit and the heat sink.

4.6 Flow modulation

Flow modulator is any interface that uses gas flow to control and isolate part of the ^{1}D eluate, and redirect the isolate ^{1}D eluate via injection for the ^{2}D separation [27, 64].

In 2011 Tranchida et al. classified FM in two subcategories [65]: I) “in-line” valve systems, characterized by the presence of a switching valve with a direct connection with the first and second analytical column; II) “out-of-line” valve systems, those which derive from the Deans switch principle and are thus based on manipulation of the pressure between the two GC dimensions.

Another most recent classification, proposed by Synovec in 2019, described FM by two subcategories [32]: I) differential flow systems (including diaphragm valve-based), characterized by the presence of two different and individually adjustable flows in each dimension; II) diverting flow systems (including Deans’ switching), based on the use of valve (normally solenoid) to control gas pressure that lead to control of the transfer of eluate from the ^{1}D column to the ^{2}D column. Unlike differential flow system, the two column flows are inextricably connected with flow diversion, and hence communicate with each other, varying degree dependent upon system design.

In general, diverting flow modulators (defined also as low duty cycle modulators) direct only small portions of the ^{1}D column effluent to the head of the ^{2}D column, whereas differential flow modulator usually sample all of the ^{1}D effluent.

4.6.1 Differential flow modulators

Noteworthy is that the first differential flow modulator appeared for the first time in the same year as the LMCS [66]. In an experiment focused on chemometrics, Bruckner et al. employed four ports of a six-port diaphragm valve (located in the GC oven) to generate single stage flow modulation GC×GC analysis (Figure 4.15). A 4.9 m × 0.53 mm ID × 3.0 μm d_f apolar column and a 0.85 m × 0.18 mm ID × 0.15 μm d_f polar capillary were used in the first and second dimensions, respectively. The other

two valve ports were connected to an auxiliary pressure source and to a waste line. Excessively high gas flows in the ^{2}D column were avoided by the use of a split line (0.5 m × 0.180 mm ID fused-silica column). Single-stage flow modulation was carried out with a chromatography band being transferred onto the ^{2}D column for a 50 ms period at the beginning of each modulation process. At the end of the brief injection period, the valve was switched to the other position, and the ^{1}D column effluent was directed to waste (450 ms). The auxiliary pressure unit maintained elution conditions in the second dimension. The authors used a P_M of 0.5 s with 50 ms of re-injection (0.1 duty cycle). Apart from the sensitivity issue, due to the low duty cycle (95% of the ^{1}D column flow was directed to the waste), a major issue was related to the restricted operational temperature of the valve. The latter could not be operated at a temperature above 175 °C. An initial solution relative to the temperature limit concerns was to place the valve face-mounted external to the oven, extending the operating temperature range of the valve to 250 °C [67].

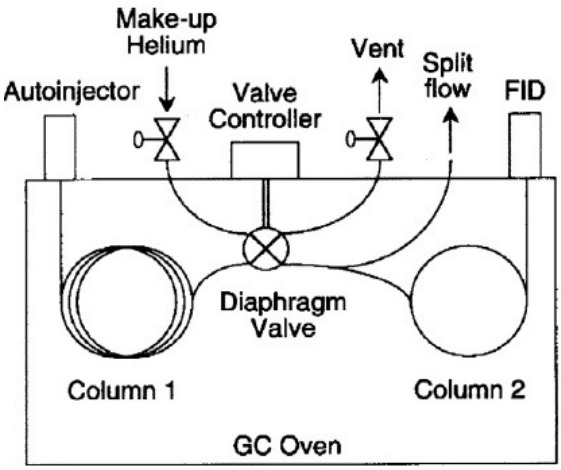

Figure 4.15. *Schematic representation of the first flow modulator device.*

In order to resolve the low duty cycle of the diaphragm valve-based modulation, Seeley and co-workers improved performance by the use of a sampling loop to collect the ^{1}D eluate, which provided a much higher fraction of the ^{1}D column eluate being transferred to the ^{2}D column, producing a clear improvement of detection sensitivity [68]. The device, developed by Seeley and co-workers, comprised a six-port, two-position, diaphragm valve, equipped with a 20 μL stainless-steel sampling loop,

connected to a waste line and an additional pressure source, and located between the detector platform and the GC oven (Figure 4.16). The part of the valve containing non-wetted components was situated outside the oven and was maintained at 125 °C by using a heater. Inside the oven, the interface was attached to a 10 m × 0.25 mm ID × 1.4 μm d_f (6% cyanopropylphenyl, 94% dimethylpolysiloxane) ^{1}D column and a 5 m × 0.25 mm ID × 0.25 μm d_f polyethylene glycol capillary or a 5 m × 0.25 mm ID × 0.50 μm d_f polyethylene glycol trifluoropropylmethyl polysiloxane capillary. The authors used the valve in the accumulation and injection states for 80% and 20% of the modulation period, respectively. In Figure 4.16 the valve is in the accumulation position. During the injection state, while the previously accumulated chromatography plug was launched onto the second dimension exploiting a high gas flow (15 mL/min), the ^{1}D column effluent (0.75 mL/min) was directed to waste.

As in the case of the previous reported modulator, the restricted operational temperature of the valve was a major issue and the modulator was unsuitable for analytes requiring a GC oven temperature above to 200°C.

Another disadvantage was related to the high ^{2}D column flows which did not allow the combination with mass spectrometry detectors. Moreover, this issue was partially resolved in a series of later flow modulated GC×GC studies by splitting the flow between two secondary analytical capillaries (GC×2GC) [69,70].

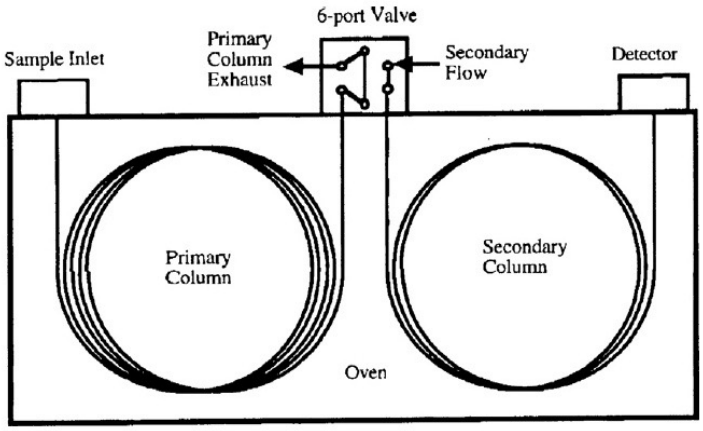

Figure 4.16. *Schematic representation of the first loop flow modulator device.*

In 2006, Seeley et al. introduced an interesting dual-stage flow modulator [71]. The flow modulator device (Figure 4.17) was constructed using three deactivated fused-

silica columns, two microvolume T-unions and a two-way solenoid valve (located outside the GC oven), connected to an auxiliary pressure source. The output ports of the solenoid valve were connected to the unions by using two fused-silica segments. One of the T-unions was linked to the ^{1}D column outlet, while the other directed the flow to the second dimension. A fused-silica segment, bridged between the two unions, acted as sample loop (volume= ~24 μL). A non-polar 15 m × 0.25 mm ID × 0.50 μm d_f capillary was used in the first dimension (flow: 1.0 mL/min), while two polar 5 m × 0.25 mm ID columns were employed in the second dimension, one with a 0.25 μm polyethylene glycol film and the other with a 0.50 μm poly(methyltrifluoropropylsiloxane) film.

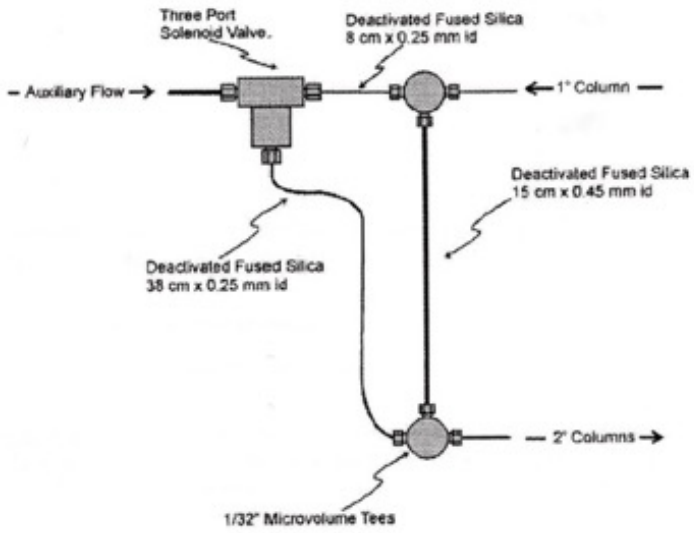

Figure 4.17. *Schematic representation of the out-of-line single loop, dual-stage flow modulator device.*

When the modulator was in the accumulation state, the auxiliary flow (20 mL/min) was directed to the "second-dimension" union, and the primary-column effluent (~17 μL/s) flowed freely within the loop; the accumulation period (1.4 s) was lower than the time necessary for the effluent to reach the bottom union (~1.5 s). When the solenoid valve was switched for a brief period (0.1 s), the auxiliary flow flushed the content of the loop onto the head of ^{2}D column. Unlike the modulators previously described, this device was stable at high GC temperatures. Moreover, this modulator had a unit duty cycle. The disadvantages related mainly to the complexity of method

optimization, the rather high second-dimension gas linear velocity, and the low modulation period. Following the original research of Seeley et al [71], a series of flow modulation GC×GC works were published [72-74].

In 2011, Tranchida et al. developed a differential flow modulator using a seven port valve with a flexible loop between ports to collect the sample [75]. The interface proposed by Tranchida, kept the characteristic and the advantages of the previously-described interface [71] plus the possibility to optimize flows, using a waste branch bridging the interface and a needle valve [76]. The interface, whose schematic representation is reported in Figure 4.18, comprises a metallic disc (2.5 cm diameter, 7 mm thickness), and internal rectangular channels (250 μm width/75 μm depth), connecting ports 1-2-3 and 4-5-6/7. A two-way electro valve is located outside the GC oven and is connected to an advanced pressure control (APC) unit. Two metallic branches connect the valve to the interface in positions 2 and 5. The primary and secondary columns are linked to positions 1 and 6, respectively. A 40 μL stainless-steel loop (20 cm × 0.71 mm OD × 0.51 mm ID) bridges positions 3 and 4; the size of the loop is chosen considering the modulation period, first-column flow and second-column dimensions. It is noteworthy that the flow exiting the loop is divided between the channels linked to ports 6 and 7. The operating mechanism is related to the Seeley modulator discussed above [71].

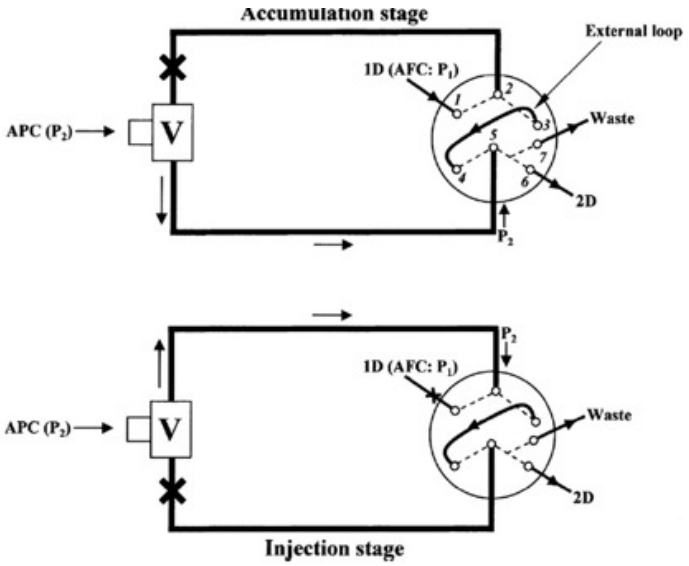

Figure 4.18. *Seven port flow modulator proposed by Tranchida et al. in the accumulation and reinjection mode.*

The first application was carried out by using a twin-oven flow modulation enantio-GC × polar-GC-FID employing a 40 μL stainless-steel loop for the analysis of spearmint essential oil. In particular, a chiral 20 m × 0.10 mm ID × 0.10 μm d_f capillary and a polyethylene glycol 2.5 m × 0.25 mm ID × 0.25 μm d_f column were connected to the interface, while a 0.13 m x 0.25 mm ID uncoated capillary was exploited as the waste line.

Using the same 7-port modulator, a proof-of-principle study was performed coupled with HR-TOFMS detection [77]. In this study, separation conditions were modified resulting in an initial flow rate of 3.4 ml/min and a duty cycle of ~40% at the beginning of the separation. At the end of the separation the flow rate was 2.1 ml/min with slightly lower duty cycle.

Moreover, Tranchida et al., in order to achieve lower carrier gas flow rates (6-8 mL/min) in the ^{2}D column, allowing the coupling with MS without compromising the sensitivity (unit duty cycle), used a matched lengths of deactivated fused silica, while still providing efficient re-injection of the ^{1}D eluate [78].

Further advancements were demonstrated using a design similar to Deans' switch at a flow rate of 4 ml/min on the ^{2}D separations in conjunction with qMS detection, while providing increased detection sensitivity relative to 1D GC [79]. The authors demonstrate that, the use of a long re-injection period (700 ms) enable efficient accumulation-loop flushing with a low flow. Different restrictor lengths in the connection linking the modulator to the auxiliary pressure source were used in order to extend the re-injection period without compromise the separation.

At the beginning of 2020, Synovec at al. described a simple flow modulator device (defined dynamic pressure gradient modulator) [80]. In this interface the ^{1}D and ^{2}D columns were linked through a tee union and connected to a pulse valve (Figure 4.19). An auxiliary gas source fed the valve (P_{aux}). Under suitable conditions of injector pressure (P_{inlet}), P_{aux} (both inlet and auxiliary pressures are ramped during the analysis), and valve open and close times, a 100% transfer GC×GC analysis could be achieved. When the valve was closed a fraction of the ^{1}D effluent was transferred onto the ^{2}D, while when it was opened, ^{1}D elution was interrupted (stop flow) and the ^{2}D separation proceeded. For example, a 90 compound mixture was subjected to a dynamic pressure gradient modulator GC×GC–FID analysis by using an apolar 10 m

× 0.18 mm, 0.18 µm d_f ^{1}D column, and a polar 1 m × 0.18 mm, 0.10 µm d_f ^{2}D column. The modulation period was only 750 ms, with a 60 ms valve close time. The applied P_{aux} generated a ^{2}D gas flow of 22.9 mL/min at the beginning of the analysis. Peak widths were narrow in time and variable, being in the range 20–180 ms.

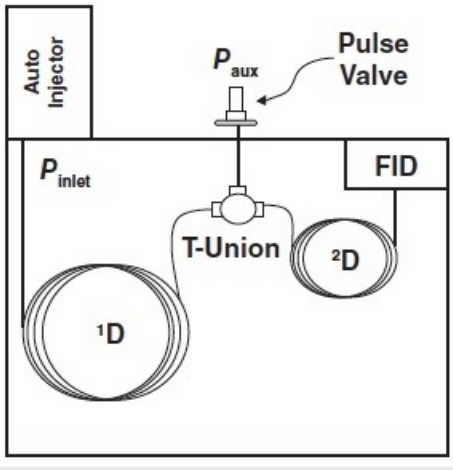

Figure 4.19. *Scheme of the* dynamic pressure gradient modulator.

In a further dynamic pressure gradient GC×GC–FID analysis on diesel fuel, the use of a longer ^{2}D column (2 m × 0.18 mm, 0.18 µm d_f) enabled the reduction of the ^{2}D flow to 8 mL/min. In this case, a modulation period of 2000 ms with a 150 ms valve close time was used. Very recently, dynamic pressure gradient GC×GC was combined with LR TOFMS, using a ^{2}D gas flow compatible with mass spectrometry detector [81]. In another investigation some modification have been made on the dynamic pressure gradient modulator for improved performance and this interface were combined with GC×GC and LR TOFMS. The system was tested on various sample, such as diesel fuel, derivatized cow serum, coffee, and river water [82].

4.6.2 Diverting flow modulators

The key factor for diverting flow devices came with the development of the Deans' switch in 1968 [83]. Diverting flow modulation employs the use of valves (normally solenoid) to control gas pressures that lead to control of the transfer of eluate from the ^{1}D column to ^{2}D column. Unlike differential flow modulation the two column flows are inextricably connected with flow diversion, and hence communicate with each

other, to a varying degree dependent upon system design, adding complexity to method development and application.

In 2018, Seeley et al. introduced a novel system based on the Deans switch principle and defined multi-mode modulator (MMM) [84]. A scheme of the MMM GC×GC system is shown in Figure 4.20. As can be observed, the MMM is of simple construction and is characterized by a deactivated metal joining capillary, connected on the ^{1}D side to a cross union and to a tee union on the ^{2}D side. The tips of the ^{1}D and ^{2}D columns are fixed near to one another within the joining capillary. Two metal capillaries link the unions to a solenoid valve (the normally opened [*NO*] port of the solenoid valve is connected to the tee union), which in turn receives a gas flow (F_S) from a pneumatic control module. The fourth port of the cross union is linked to an FID-connected restrictor (FID1). There are two flows entering the modulator, F_S and F_1 (^{1}D flow), and two flows exiting it, F_X (restrictor flow) and F_2 (^{2}D flow). When the valve is in the *NO* position, the ^{1}D flow is directed to the restrictor (low duty cycle) or stored in the joining capillary (high duty cycle); when the valve is in the normally closed (*NC*) position, effluent from the ^{1}D column is directed to the second one, and then subjected to FID monitoring (FID2).

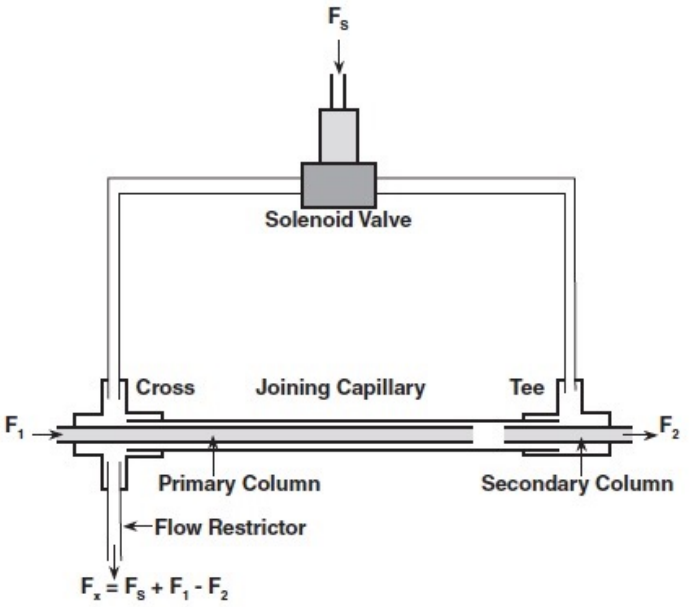

Figure 4.20. *Scheme of the MMM transfer system.*

Depending on the gas flows involved, and on the proximity of the ^{1}D and ^{2}D column tips within the joining capillary, the MMM could be operated as a low or high duty

cycle modulator. The MMM can be operated as either a differential flow modulator (full transfer) or a diverting flow modulator (low duty cycle). Under low duty cycle conditions, a 6% cyanopropyl phenyl + 94% polydimethylsiloxane 30 m × 0.25 mm, 1.4 μm d_f column was used in the first dimension (flow: 1.0 mL/min), and a polyethylene glycol 0.5 m × 0.18 mm, 0.18 μm d_f column in the second (flow: 0.9 mL/min). The modulation period was 1000 ms with a 75 ms injection time, meaning that only a low percentage of the ^{1}D effluent reached the ^{2}D. Very narrow peak widths at half height were reported for modulated *n*-octane (53 ms). Such MMM conditions were characterized by a duty cycle of 0.054 (ratio of the total area of the modulated pulses to that of the unmodulated peak), and were suitable for high-speed separations on short segments of micro-bore (≤ 0.18 mm ID) column, and for MS detection.
Under high duty cycle conditions, an apolar 40 m × 0.18 mm, 0.18 μm d_f column was used in the first dimension (flow: 0.50 mL/min), and a polyethylene glycol 5 m × 0.25 mm, 0.25 μm d_f column in the second (flow: 10.0 mL/ min). The modulation period was 1500 ms, with a 150 ms injection time. A fuel sample was subjected to analysis with w_h of approximately 80 ms. Such MMM conditions were characterized by a duty cycle of 1, and were suitable for high-speed separations on medium-length (5–8 m) segments of columns with an ID ≥ 0.25 mm. A flow of 10.0 mL/min can be considered as rather high for mass spectrometry, and possibly requires splitting prior to the ion source depending on the MS system used.

Based on MMM, a diverting flow modulator (namely flux modulator) was developed and commercialized by LECO. A representation of flux modulator is reported in Figure 4.21. The modulator operates by using an auxiliary gas flow which opposes the effluent from ^{1}D column, sending it to waste during the divert state. The auxiliary gas flow rate is higher than the ^{1}D flow and during the divert state it supplements the flow through ^{2}D column, as well as forcing the entirety of the ^{1}D column flow to waste. When the modulator changes his position to the inject state the majority of the auxiliary gas flow is directed straight to waste, thus enabling the flow from ^{1}D column to transfer directly into ^{2}D column.

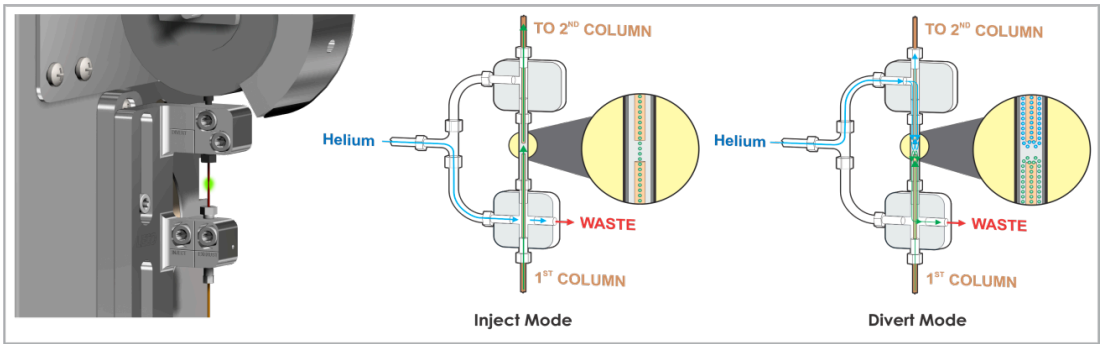

Figure 4.21. *Representation of flux modulator in the inject and divert mode.*

The flux modulator is characterized by a cross fitting to which ^{1}D column enters, and by a tee fitting to which ^{2}D column exits. The cross and tee are connected by a length of deactivated tubing which is crimped in the center. This crimp positions the columns at an appropriate distance from each other to ensure optimal transfer of analyte from ^{1}D to ^{2}D columns. The switching valve is then connected to a module for auxiliary flow control (3.5 mL/min) of the switching gas.

4.7 Recent application and instrumental trends

Recent application and instrumental trends herein reported will relate to the combined period 2018 to 2019. To obtain such information, a search process was launched by using the Scopus database and the keywords: “comprehensive two-dimensional gas chromatography”. The database provided a list of 136 papers for 2018 and 121 papers for 2019. It is obvious that, even though some published data were most probably missed, a total number of 257 works do give an overall view on the current situation.

With regard to the topics, a main one was defined for each publication, with a clear dominance of application research observed (77%), followed by reviews and perspectives (9%) (Figure 4.22). Among the applications (Figure 4.23), food and beverage (29%), energy (24%), environment (21%), and biological (9%) occupy the first four positions, with the first three being by far the most popular.

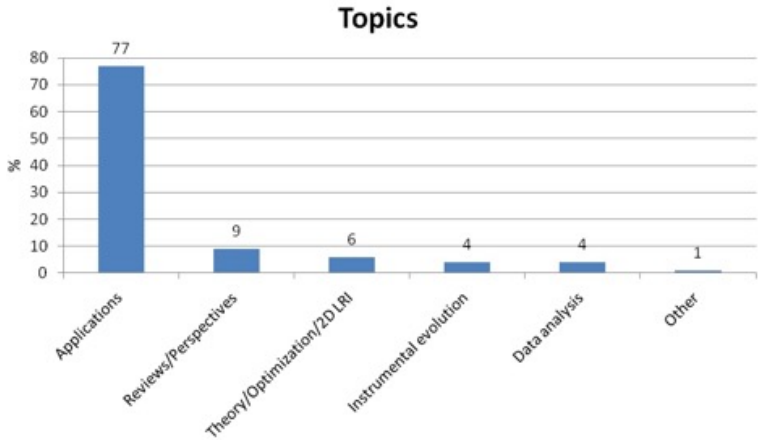

Figure 4.22. *Graph reporting the topics of GC×GC research published across the combined period 2018–2019. The % values have been rounded to the nearest integer.*

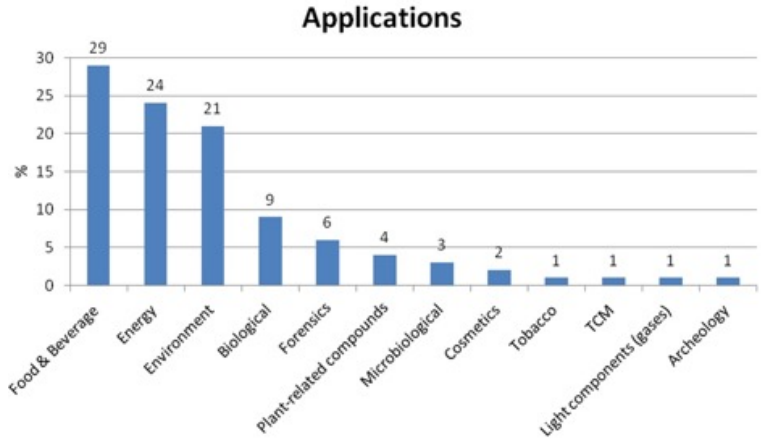

Figure 4.23. *Graph reporting the specific types of applications of GC×GC research published across the combined period 2018–2019. Abbreviation: TCM: traditional Chinese medicine. The % values have been rounded to the nearest integer.*

With regard to reviews and perspectives, these involve manuscripts covering both a specific GC×GC aspect or application (for example, metabolomics [85], modulation [32], environment [86]) and those describing GC×GC as an option within a specific research field (for example, analysis of S-containing compounds in petroleum [87], solid-phase microextraction [88]). Considering the sum of application research and reviews and perspectives, these represent 86% of the published work across the period 2018–2019. A third topic relates to theory and optimization (for example, retention time prediction [89], FM model [90], solid-state modulation optimization [61] and ^{2}D linear retention index (LRI) calculation [91, 92], represented by 6% of the published works. With regard to instrumental evolution and data analysis, these were

characterized by only 4% each of the published work. Technological advances have involved, among others, a miniaturized GC×GC system [93], the use of a micro-reactor prior to FID detection [94], a silver-based ionic liquid ^{2}D column [95], and different FM approaches [84, 96].

Proceeding onto the utilization of modulation approaches, specific information was attained from the majority of the 257 publications (for some papers we had access only to the abstract). As expected, CM was by far the most common choice (87%), followed by FM (10%), and solid-state modulation (3%).

GC×GC is becoming a mature technology, as can be concluded by observing recent literature, which is dominated by application research and with less space devoted to technological evolution. Such a tendency will probably continue, also in part as a result of the continuous evolution of MS. In fact, the availability of (powerful) MS reduces the requirements of an improved separation performance on the GC×GC side.

References:

[1] Z. Liu, and J.B. Phillips, J. Chromatogr. Sci. 29 (1991) 227.

[2] L. Ramos in: Comprehensive two dimensional gas chromatography, Wilson & Wilson's, (2009).

[3] J.B. Phillips, and J. Beens, J. Chromatogr. A 856 (1999) 331.

[4] M. Adahchour, J. Beens, U.A.Th. Brinkman, J. Chromatogr. A 1186 (2008) 67.

[5] J.V. Seeley, and S.K. Seeley, Anal. Chem. 85 (2013) 557.

[6] M.S.S. Amaral, Y. Nolvachai, P.J. Marriott, Anal. Chem. 92 (2020) 85.

[7] P.Q. Tranchida, I. Aloisi, L. Mondello, LC-GC Eur. 33 (2020) 172.

[8] J.C. Giddings, J. High Res. Chromatogr. 10 (1987) 319.

[9] P.J. Schoenmakers, P. Marriott, J. Beens, LC-GC Eur. 16 (2003) 335.

[10] C.J. Venkatramani, J. Xu, J.B. Phillips, Anal. Chem. 68 (1996) 1486.

[11] J.C. Giddings, J. Chromatogr. 703 (1995) 3.

[12] J.F. Focant, E. Reiner, K. MacPherson, T. Kolic, A. Sjödin, D.G. Patterson, Jr., S. Reese, F. Dorman, J. Cochran, Talanta 63 (2004) 1231.

[13] J.F. Focant, A. Sjödin, W.E. Turner D.G. Jr. Patterson, Anal. Chem. 76 (2004) 6313.

[14] J.M.D. Dmandja, Anal. Chem. 76 (2004) 167A.

[15] J.F. Focant, A. Sjödin, D.G. Patterson, Jr., J. Chromatogr. A 1040 (2004) 227.

[16] P.J. Marriott, P.D. Morrison, R.A. Shellie, M.S. Dunn, E. Sari, D. Ryan, LC-GC Eur. 15 (2003) 209.

[17] P.J. Marriott, and P.D. Morrison, LC-GC North Amer. 24 (2006) 1067.

[18] L. Mondello, A. Casilli, P.Q. Tranchida, P. Dugo, G. Dugo, J. Chromatogr. A 1019 (2003) 187.

[19] D. Ryan, R. Shellie, P.Q. Tranchida, A. Casilli, L. Mondello, P.J. Marriott, J. Chromatogr. A 1054 (2004) 57

[20] P.Q. Tranchida, G. Purcaro, L. Conte, P. Dugo, G. Dugo, L. Mondello, Anal. Chem. 81 (2009) 8529.

[21] J. Beens, J. Blomberg, P.J. Schoenmakers, J. High Res. Chromatogr. 23 (2000) 182.

[22] M. Adahchour, J. Beens, R.J.J. Vreuls, U.A.Th. Brinkman, TrAC Trends Anal. Chem. 25 (2006) 438.

[23] P. Schoenmakers, P. Marriott, J. Beens, LC-GC Eur. 25 (2003) 1.

[24] K.A. Perrault, L.M. Dubois, D. Cnuts, V. Rots, J.F. Focant, P.H. Stefanuto, Sep. Sci. Plus. 1 (2018) 726.

[25] M. Nasir, H.D. Bean, A. Smolinska, C.A. Rees, E.T. Zemanick, J.E. Hill, Sci. Rep. 8 (2018) 826.

[26] J.M.D. Dimandja, G.C. Clouden, I. Colón, J.F. Focant, W.V. Cabey, R.C. Parry, J. Chromatogr. A. 1019 (2003) 261.

[27] M. Edwards, A. Mostafa, T. Gorecki, Anal. Bioanal. Chem. 401 (2011) 2335.

[28] R.E. Murphy, M.R. Schure, J.P. Foley, Anal. Chem. 70 (1998) 1585.

[29] W. Khummueng, J. Harynuk, P.J. Marriott, Anal. Chem. 78 (2006) 4578.

[30] P. Marriott, R. Shellie, TrAC Trends Anal. Chem. 21 (2002) 573.

[31] R.C. Ong, P.J. Marriott, J. Chromatogr. Sci. 40 (2002) 276.

[32] H.D. Bahaghighat, C.E. Freye, R.E. Synovec, TrAC Trends Anal. Chem. 113 (2019) 379.

[33] J.V. Seeley, N.J. Micyus, S.V. Bandurski, S.K. Seeley, J.D. McCurry, Anal. Chem. 79 (2007) 1840.

[34] Z. Liu, and J.B. Phillips, J. Microcol. Sep. 1 (1989) 249.

[35] Z. Liu, M. Zhang, J.B. Phillips, J. Chromatogr. Sci. 28 (1990) 567.

[36] Z. Liu, S.R. Sirimanne, D.G. Patterson Jr., L.L. Needham, J.B. Phillips, Anal. Chem. 66 (1994) 3086.

[37] J.B. Phillips, and J. Xu, J. Chromatogr. A 703 (1995) 327.

[38] J.B. Phillips, and E. Ledford, Field Anal. Chem. Technol. 1 (1996) 23.

[39] H.J. de Geus, J. de Boer, J.B. Phillips, E.B. Ledford Jr., U.A.Th. Brinkman, J. High Resolut. Chromatogr. 21 (1998) 411.

[40] J. Blomberg, P.J. Schoenmakers, J. Beens, R.Tijssen, J. High Resolut. Chromatogr. 20 (1997) 539.

[41] J.B. Phillips, R.B. Gaines, J. Blomberg, F.W.M. van der Wielen, J.M.D. Dimandja, V. Green, J. Granger, D. Patterson, L. Racovalis, H.J. de Geus, J. de Boer, P. Haglund, J. Lipsky, V. Sinha, E.B. Ledford Jr., J. High Resolut. Chromatogr. 22 (1999) 3.

[42] H.J. de Geus, J. de Boer, U.A.Th. Brinkman, J. Chromatogr. A 767 (1997) 137.

[43] J.B. Phillips, D. Luu, J.B. Pawliszyn, Anal. Chem. 57 (1985) 2779.

[44] O. Panic, T. Górecki, C. McNeish, A.H. Goldstein, B.J. Williams, D.R. Worton, S.V. Hering, N.M. Kreisberg, J. Chromatogr. A 1218 (2011) 3070.

[45] D.R. Worton, N.M. Kreisberg, G. Isaacman, A.P. Teng, C. McNeish, T. Górecki, S.V. Hering, A.H. Goldstein, Aerosol Sci. Technol. 46 (2012) 380.

[46] V. Mucédola, L.C. Vieira, D. Pierone, A.L. Gobbi, R.J. Poppi, L.W. Hantao, Talanta 164 (2017) 470.

[47] J. Beens, H. Boelens, R. Tijssen, J. High Resolut. Chromatogr. 21 (1998) 47.

[48] P.J. Marriott, and R.M. Kinghorn, Anal. Chem. 69 (1997) 2582.

[49] R.M. Kinghorn, and P.J. Marriott J. High Resolut. Chromatogr. 21 (1998) 32.

[50] R.M. Kinghorn, and P.J. Marriott J. High Resolut. Chromatogr. 21 (1998) 620.

[51] P.J. Marriott, R.M. Kinghorn, R. Ong, P. Morrison, P. Haglund, M. Harju, J. High Resolut. Chromatogr. 23 (2000) 253.

[52] P. Haglund, M. Harju, C. Danielsson, P. Marriott, J. Chromatogr. A 962 (2002) 127.

[53] E.B. Ledford Jr., In 23rd International Symposium on Capillary Chromatography, Riva del Garda, Italy, 5−10 June 2000.

[54] E.B. Ledford Jr., C.A. Billesbach, J.R. Termaat, Transverse Thermal Modulation, United States Patent US20010037727A1, November 08, 2001.

[55] J. Beens, M. Adahchour, R.J.J. Vreuls, K. van Altena, U.A.Th. Brinkman, J. Chromatogr. A 919 (2001) 127.

[56] E.B. Ledford, C. Billesbach, J. Termaat, Pittcon 2002, 17–22 March 2002, New Orleans, LA, USA.

[57] PQ. Tranchida, M. Zoccali, F.A. Franchina, A. Cotroneo, P. Dugo, L. Modello, J. Chromatogr. A 1314 (2013) 216.

[58] G. Purcaro, C. Cordero, E. Liberto, C. Bicchi, L.S. Conte, J. Chromatogr. A 1334 (2014) 101.

[59] G. Purcaro, L. Barp, M. Beccaria, L.S. Conte, Food Chem. 212 (2016) 730.

[60] J. Luong, X. Guan, S. Xu, R. Gras, R.A. Shellie, Anal. Chem. 88 (2016) 8428.

[61] M. Zoccali, B. Giocastro, P.Q. Tranchida, L. Mondello, J. Sep. Sci. 42 (2019) 691.

[62] A.M. Muscalu, M. Edwards, T. Górecki, E.J. Reiner, J. Chromatogr. A 1391 (2015) 93.

[63] M.R. Jacobs, M. Edwards, T. Górecki, P.N. Nesterenko, R.A. Shellie, J. Chromatogr. A 1463 (2016) 162.

[64] J.V. Seeley, J. Chromatogr. A 1255 (2012) 24.

[65] P.Q. Tranchida, G. Purcaro, P. Dugo, L. Mondello, TrAC Trends Anal. Chem. 30 (2011) 1437.

[66] C.A. Bruckner, B.J. Prazen, R.E. Synovec, Anal. Chem. 70 (1998) 2796.

[67] A.E. Sinha, B.J. Prazen, C.G. Fraga, R.E. Synovec, J. Chromatogr. A 1019 (2003) 79.

[68] J.V. Seeley, F.J. Kramp, C.J. Hicks, Anal. Chem. 72 (2000) 4346.

[69] J.V. Seeley, F.J. Kramp, K.S. Sharpe, J. Sep. Sci. 24 (2001) 444.

[70] J.V. Seeley, F.J. Kramp, K.S. Sharpe, J. Sep. Sci. 25 (2002) 53.

[71] J.V. Seeley, N.J. Micyus, J.D. McCurry, S.K. Seeley, Am. Lab. 38 (2006) 24.

[72] M. Poliak, M. Kochman, A. Amirav, J. Chromatogr., A 1186 (2008) 189.

[73] M. Poliak, A.B. Fialkov, A. Amirav, J. Chromatogr., A 1210 (2008) 108.

[74] P.McA. Harvey, R.A. Shellie, P.R. Haddad, J. Chromatogr. Sci. 48 (2010) 245.

[75] P.Q. Tranchida, G. Purcaro, A. Visco, L. Conte, P. Dugo, P. Dawes, L. Mondello, J. Chromatogr. A 1218 (2011) 3140e3145.

[76] P.Q. Tranchida, A. Casilli, P. Dugo, G. Dugo, L. Mondello, Anal. Chem. 79 (2007) 2266.

[77] P.Q. Tranchida, S. Salivo, F.A. Franchina, L. Mondello, Anal. Chem. 87 (2015) 2925.

[78] P.Q. Tranchida, F.A. Franchina, P. Dugo, L. Mondello, J. Chromatogr. A 1359 (2014) 271.

[79] F.A. Franchina, M. Maimone, P.Q. Tranchida, L. Mondello, J. Chromatogr. A 1441 (2016) 134

[80] T.J. Trinklein, D.V. Gough, C.G. Warren, G.S. Ochoa, R.E. Synovec, J. Chromatogr. A 1609 (2020) Art. 460488.

[81] S. Schöneich, D.V. Gough, T.J. Trinklein, R.E. Synovec, J. Chromatogr. A 1620 (2020) Art. 460982.

[82] S. Schöneich, T.J. Trinklein, C.G. Warren, R.E. Synovec, Anal. Chim. Acta 1134 (2020) 115.

[83] D.R. Deans, Chromatographia 1 (1968) 18.

[84] J.V. Seeley, N.E. Schimmel, S.K. Seeley, J. Chromatogr. A 1536 (2018) 6.

[85] E.A. Higgins Keppler, C.L. Jenkins, T.J. Davis, H.D. Bean, TrAC, Trends Anal. Chem. 109 (2018) 275.

[86] A.M. Muscalu, and T. Górecki, TrAC, Trends Anal. Chem. 106 (2018) 225.

[87] Y. Han, Y. Zhang, C. Xu, C.S. Hsu, Fuel 221 (2018) 144.

[88] S. Huang, G. Chen, N. Ye, X. Kou, F. Zhu, J. Shen, G. Ouyang, Anal. Chim. Acta 1077 (2019) 67.

[89] R. Jaramillo, and F.L. Dorman, J. Chromatogr. A 1581–1582 (2018) 116.

[90] M. Giardina, J.D. McCurry, P. Cardineal, G. Semard-Jousset, C. Cordero, C. Bicchi, J. Chromatogr. A 1577 (2018) 72.

[91] M. Jiang, Anal. Chem. 91 (2019) 4085.

[92] D.M. Mazur, I.G. Zenkevich, V.B. Artaev, O.V. Polyakova, A.T. Lebedev, J. Chromatogr. A 1569 (2018) 178.

[93] J.J. Whiting, E. Myers, R.P. Manginell, M.W. Moorman, J. Anderson, C.S. Fix, C. Washburn, A. Staton, D. Porter, D. Graf, D.R. Wheeler, S. Howell, J. Richards, H. Monteith, K.E. Achyuthan, M. Roukes, R.J. Simonson, Lab Chip 19 (2019) 1633.

[94] J. Luong, Y. Hua, R. Gras, R.A. Shellie, Anal. Chem. 91 (2019) 11223.

[95] I.D. Souza, H. Nan, M.E.C. Queiroz, J.L. Anderson, Anal. Chem. 91 (2019) 4969.

[96] H. Cai, and S.D. Stearns, J. Chromatogr. A 1569 (2018) 200.

Chapter 5

5.0 Research in the field of food products

5.1 Analysis of the unsaponifiable fraction of vegetable oils by using cryogenically-modulated comprehensive two-dimensional gas chromatography-high resolution time-of-flight mass spectrometry and lipids high resolution database generation[†]

The aim of the research is the development of a GC×GC-HR ToFMS method for the profiling of the unsaponifiable fraction of vegetable oils. Twelve vegetable oils were analyzed, with particular attention devoted to the higher molecular weight compounds. Peak assignment was conducted by using commercial unit-mass MS databases, accurate mass data, literature and on-line freely-available mass spectral information, as well as an in-lab-constructed HR ToFMS lipid database. The primary purpose of the work was to generate a method for the characterization of extra-virgin olive oil. A further scope of the study was to evaluate the performance of the HR ToFMS system. The HR ToFMS accurate-mass lipid database was generated mainly by acquiring the mass spectra of vegetable oil constituents, well-resolved from both the matrix and column bleed background.

[†]This section has been adapted from the following publication: **I. Aloisi**, M. Zoccali, P. Dugo, P.Q. Tranchida, L. Mondello in "Fingerprinting of the Unsaponifiable Fraction of Vegetable Oils by Using Cryogenically-Modulated Comprehensive Two-Dimensional Gas Chromatography-High Resolution Time-of-Flight Mass Spectrometry", Food Analytical Methods 13 (2020) 1523-1529.

5.1.1 Introduction

The first GC×GC application was reported in 1991, by Liu and Phillips [1]. While the first publication regarding the use of GC×GC combined with MS appeared in 1999 [2]. The most common MS choice, in the GC×GC field, has been LR ToFMS, followed by QMS. Regarding to other forms of MS instrumentation, there have been a much lower number of applications involving QqQMS and HR ToFMS [3].

The present contribution is focused on HR ToFMS; a very powerful form of MS can be exploited in both untargeted and targeted GC-based experiments [4]. Qualitative information is attained through MS database matching and the study of accurate-mass ions (the molecular ion if present, along with others typical fragments). Pre-targeted analysis is performed by using highly-selective accurate-mass extracted-ion chromatograms; the spectrum data can also be investigated at a later stage to pinpoint previously-unsearched analytes (post-targeted analysis). Over the past few years, GC×GC experiments combined with HR ToFMS [with a 200-Hz spectral generation capability at a mass resolution of 25,000 (fwhm)] has been reported, dealing with the analysis of S-containing compounds in petrochemical samples [5,6]. The same HR ToFMS instrument has been used in order to carry out a qualitative analysis of the unsaponifiable fraction of milk lipids [7]. GC-HR ToFMS instrument was used to confirm the identification of several lipids, previously subjected to analysis by using GC×GC-QMS. Such a process was performed by a cross-comparison of the one- and two-dimensional chromatograms (the stationary phase used in the first GC×GC dimension was the same as that used in the GC experiment). Instead of deriving detailed lipid information from the mutual use of GC×GC-QMS and GC-HR ToFMS, in the present study it is attained directly from the GC×GC-HR ToFMS system. It is well-know that GC×GC with dual detection (FID and QMS) has been used to study the entire unsaponifiable fraction of extra-virgin olive (8 samples), sunflower and peanut oils [8]. In this case, pre-fractionation of the unsaponifiable fraction was not conducted due to the enhanced GC×GC separation space.

A main scope of the present study was to develop a method allowing a meticulous characterization of the unsaponifiable fraction of vegetable oil. The samples subjected to study were nine extra-virgin olive oils, as well as a soybean, peanut, and hazelnut oil. With respect to the previous GC×GC-FID/QMS study, the analysis time was

reduced by 43%, with more attention on the higher boiling point compounds, and also a lower amount of reagents/solvents were used to isolate the unsaponifiable fraction as previously described [9]. Finally, the performance of the HR ToFMS system (operated at a mass resolution of 25,000 fwhm) was evaluated under the challenging analytical conditions of a CM GC×GC-based experiment.

5.1.2 Experimental

Sample, standard compounds, and reagents

Nine genuine extra-virgin olive oils (EVOO1–9) were supplied by participants of a national project on olive oil. The others three oils (soybean, peanut, hazelnut) were part of an in-lab collection of vegetable oils. The BSTFA [N,O-bis(trimethylsilyl)trifluoroacetamide] + 1% TMCS (trimethylchlorosilane) kit was supplied by Merck Life Science (Merck KGaA, Darmstadt, Germany). Powdered anhydrous sodium sulfate, pyridine (anhydrous 99.8%), potassium hydroxide (KOH), diethyl ether (99.0%) and ethanol (LC grade) were supplied by Merck Life Science. Water was obtained from a Milli-Q SP Reagent Water System (Millipore, Bedford, MA, USA).

Sample preparation

Approximately one gram of exactly weighed vegetable oil was added to 10 mL of a 2 N KOH/EtOH solution, heated at 80°C, under reflux, and magnetic stirring (for about 20 min after solution clarification).

After, extraction was performed three times: the first with 20 mL of diethyl ether, and the other two with 15 mL of the same solvent. The extracts were combined and washed with 10 mL of distilled water (washing was performed about 15 times per sample). The washed solution was dried with anhydrous sodium sulfate, and the solvent was evaporated under low-pressure conditions at 37°C.

The unsaponifiable fraction isolated was dissolved in 500 μL of chloroform, and then treated with the derivatization mixture [200 μL of BSTFA (1% TMCS) and 200 μL of pyridine], and then heated at 70°C for 20 min. The derivatized sample was then ready for GC injection.

Instrumental conditions

CM GC×GC-HR ToFMS application was carried out on a Pegasus GC-HRT 4D system (LECO, Mönchengladbach, Germany). The first column was of low polarity, specifically an SLB-5ms [equivalent in polarity to poly(5%diphenyl/95%dimethyl siloxane)], with dimensions 30 m × 0.25 mm ID × 0.25 μm d_f; the second column was of intermediate polarity, namely an SLB-35ms, with dimensions 1.9 m × 0.10 mm ID × 0.10 μm d_f [equivalent in polarity to poly(35%diphenyl/65%dimethyl siloxane)]. Both analytical columns were from Merck Life Science. The connection between columns was made by using a Siltite mini union (Trajan, Ringwood, Victoria, Australia).

In order to focus attention on the higher boiling point compounds, the following method was developed: temperature program: 90°C-280°C at 15°C min^{-1}, and 280°C-360°C at 2.5°C min^{-1}; modulation period was 4 s: the hot jet was held for 1.4 s, and the cold jet for 0.6 s. Injector temperature: 360°C; injection mode and volume: split (10:1), 3 μL; He flow (constant): 2.4 mL min^{-1}; transfer line temperature: 360°C. Modulation heating and secondary oven temperatures: +15°C offset with respect to the temperature of the main GC oven; modulation cooling temperature: -60°C.

The HR ToFMS analyses were performed through electron ionization (70 eV), at a source temperature of 250°C. Masses were analyzed over a range of *m/z* 45-600, at a spectral production frequency of 120 Hz, using the high resolution mode (25,000 fwhm). The mass spectral databases used were NIST 11, Lipids (Wiley) and an in-lab-constructed high resolution MS lipid database.

5.1.3 Results & Discussion

The combination of CM GC×GC and HR ToFMS generates a powerful analytical platform, thanks to the high sensitivity, selectivity and resolving power, of both the GC and MS sides. Hence, GC×GC-HR ToFMS has the capability to perform in-depth investigations, and generate detailed fingerprints, of complex mixtures of volatile compounds.

The GC×GC-HR ToFMS method developed is characterized by a 44.7 min duration and a variable temperature gradient. The method allowed a detailed view of the heavier

molecular weight (MW) compounds, such as the sterols. Modulation period was 4 s, with cold and hot jet durations of 0.6 and 1.4 s, respectively. A total ion current (TIC) ^{2}D chromatogram of the EVOO1 sample is illustrated in Figure 5.1.1. A spectral production frequency of 120 Hz was used in order to obtain an effective deconvolution and, if request, reliable quantification.

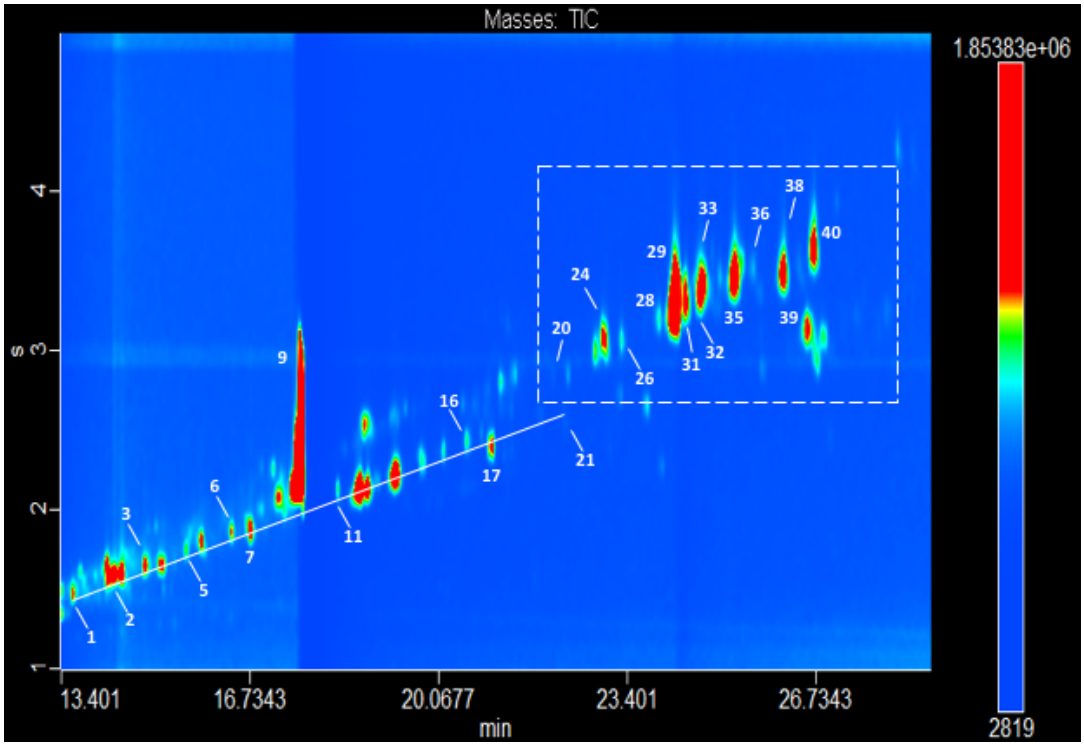

Figure 5.1.1. *TIC GC×GC-HR ToFMS chromatogram of sample EVOO1. For peak identification refer to Table 5.1.1.*

Qualitative information were achieved by exploiting commercial unit-mass MS databases, accurate mass data, literature and on-line freely-available mass spectral information. Furthermore, an in-lab HR MS lipid database (containing mainly derivatized sterol spectra) was constructed and used. Such a database was constructed through the analysis of a series of pure standard compounds and vegetable oils through CM GC×GC-HR ToFMS. An MS database search was launched; the identification was made only for compounds characterized by a minimum spectral similarity of 80%.

Finally, 8 linear saturated hydrocarbons and 2 linear alcohols, practically all eluted along a diagonal (Figure 5.1.1), and were tentatively-identified with good spectral similarities (Table 5.1.1). Compound numbering is related to elution order, and to the overall number of peaks assigned in all the vegetable oils. Considering the moderate degree of polarity of the 2D, the elution pattern can be related to the ^{2}D separation temperatures and to the fact that the alcohols are analyzed as trimethylsilyl ethers (polarity is greatly reduced): for example, heptacosane (peak 6 - $C_{27}H_{56}$) is subjected to lower ^{2}D temperatures compared to tetracosan-1-ol (peak 7 - $C_{27}H_{58}SiO$), leading to very similar retention times in the second column. The accurate mass data was not investigated for the linear hydrocarbons and alcohols due to the satisfactory spectral similarities and organized elution pattern; instead, the accurate mass data was helpful to support the identification of higher MW compounds, in particular sterols.

The larger peak of the ^{2}D fingerprint was the one corresponding to squalene (peak 9; similarity 928). Moreover, the mass error for squalene was 1.7 ppm. Regarding the most information rich part of the chromatogram (sterol-zone) enclosed in the rectangle in Figure 5.1.1, thirteen acceptable MS database matches (HR ToFMS database) were attained. Valuable MW information was also attained in nine cases, and among these (peaks 28, 31, 32, 33, 35, 40) further identity information was attained from the literature. In three cases (peaks 36, 38, 39) in which only an acceptable database match was attained, the literature was also consulted for MS information. For the remaining compound, cholesterol (peak 20), peak assignment of this low-concentration constituent was performed only by using the HR ToFMS database. Among the thirteen compounds which refer to the sterol zone, there are six desmethylsterols, one methylsterol, three dimethylsterols, two triterpenic alcohols and one triterpenic dialcohol.

Table 5.1.1. *Peak assignment, theoretical molecular ion, molecular ion error, and MS database similarity (match; values in bold relate to the HR ToFMS database) for the EVOO1 sample. Abbreviations: DesMeSt = desmethylsterol; TriTerpOH = triterpenic alcohol; DiMeSt = dimethylsterol; TriTerp2OH = triterpenic dialcohol; MeSt = methylsterol; TMS = trimethylsilyl ether.*

Peak/Compound	$[M]^+$	Molec. Ion Error (ppm)	Match
1. Tricosane			913
2. Tetracosane			959
3. Pentacosane			923
5. Hexacosane			949
6. Heptacosane			954
7. Tetracosan-1-ol-TMS			868
9. Squalene	410.390703	1.7	928
11. Nonacosane			920
16. Hentriacontane			913
17. Octacosan-1-ol-TMS			918
20. Cholesterol (DesMeSt-TMS)			**800**
21. Dotriacontane			820
24. Campesterol (DesMeSt-TMS)	472.409494	-2.4	**949**
26. Stigmasterol (DesMeSt-TMS)	484.409494	-0.7	**856**
28. Clerosterol (DesMeSt-TMS)[a]	484.409494	5.6	**869**
29. β-sitosterol (DesMeSt-TMS)	486.425144	-0.8	**920**
31. Δ^5-Avenasterol (DesMeSt-TMS)[a]	484.409494	-3.8	**899**
32. Parkeol (DiMeSt-TMS)[b]	498.425144	1.2	**847**
33. β-Amyrin (TriTerpOH-TMS)[a]	498.425144	1.7	**911**
35. Cycloartenol (DiMeSt-TMS)[a]	498.425144	5.8	**892**
36. α-Amyrin (TriTerpOH-TMS)[a]			**800**
38. 24-Methylenecycloartanol (DiMeSt-TMS)[a]			**936**
39. Erythrodiol (TriTerp2OH-TMS)[a]			**915**
40. Citrostadienol (MeSt-TMS)[a]	498.425144	-6.6	**931**
	aver.	3.0	**887**

[a] Diagnostic ions were consulted in: T.S.C. Li, T.H.J. Beverage, J.C.G. Drover, Phytosterol content of sea buckthorn (Hippophae rhamnoides L.) seed oil: Extraction and identification, Food Chem. 101 (2007) 1633–1639.

[b] The experimental spectrum was visually compared with that located in: Z. Xue, L. Duan, D. Liu, J. Guo, S. Ge, J. Dicks, P. Ó Máille, A. Osbourne, X. Qi, Divergent evolution of oxidosqualene cyclases in plants, New Phytologist 193 (2012) 1022-1038.

In general, mass accuracy for all 10 compounds (squalene is also considered) was satisfactory: an average value of 3.0 ppm (absolute value) was calculated. With regard to the HR ToFMS database similarity values, these were acceptable with an average calculated value of 887. The high-resolution mass spectrum of β-sitosterol (peak 29), the most abundant sterol in EVOO, is illustrated in Figure 5.1.2a. The HR ToFMS database match for this compound (920) was satisfactory and an accurate-mass molecular ion (-0.8 ppm) is evident. A high-resolution mass spectrum of parkeol (peak

32), a dimethylsterol, is shown in Figure 5.1.2b. In this instance, a spectral similarity of 847 and a mass accuracy of 1.2 ppm were obtained.

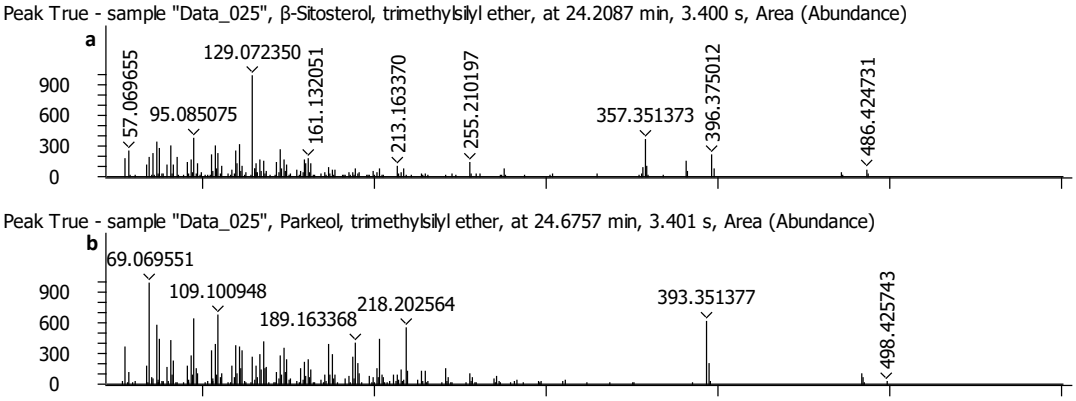

Figure 5.1.2. *Accurate-mass spectrum of: a) β-sitosterol, and b) parkeol.*

Considering the sterol zone in the other 8 EVOO samples, an additional two compounds were detected: campestanol (a desmethylsterol) and uvaol (a triterpenic dialcohol). All fifteen compounds have been previously related to olive oil [8-10].

In general, average mass accuracies for the 8 samples were in the range 2.1-4.9 ppm (absolute values), while the average spectral similarities varied in the range 868-903.

A bidimensional plot expansion showing the sterol zone of hazelnut oil (HO) is illustrated in Fig. 5.1.3a, compared with the EVOO samples the sterol zone fingerprint was entirely different. In such a respect, the sterol zone of sample EVOO9 is illustrated in Fig. 5.1.3b, aligned below that of HO. In the latter, a dehydration product of β-sitosterol, namely, stigmasta-3,5-diene (peak 19), was identified exploiting MW accurate-mass information and the HR ToFMS database. Stigmasta-3,5-diene is a stigmastadiene, a class of compounds formed through refining processes (e.g., deodorizing) [11].

Looking at Figure 5.1.3a, it is evident the presence of a circled zone in the HO chromatogram expansion (containing peak 19). This circled zone can be considered as a smaller fingerprint inside a larger one. This zone is totally absent in Figure 5.1.3b.

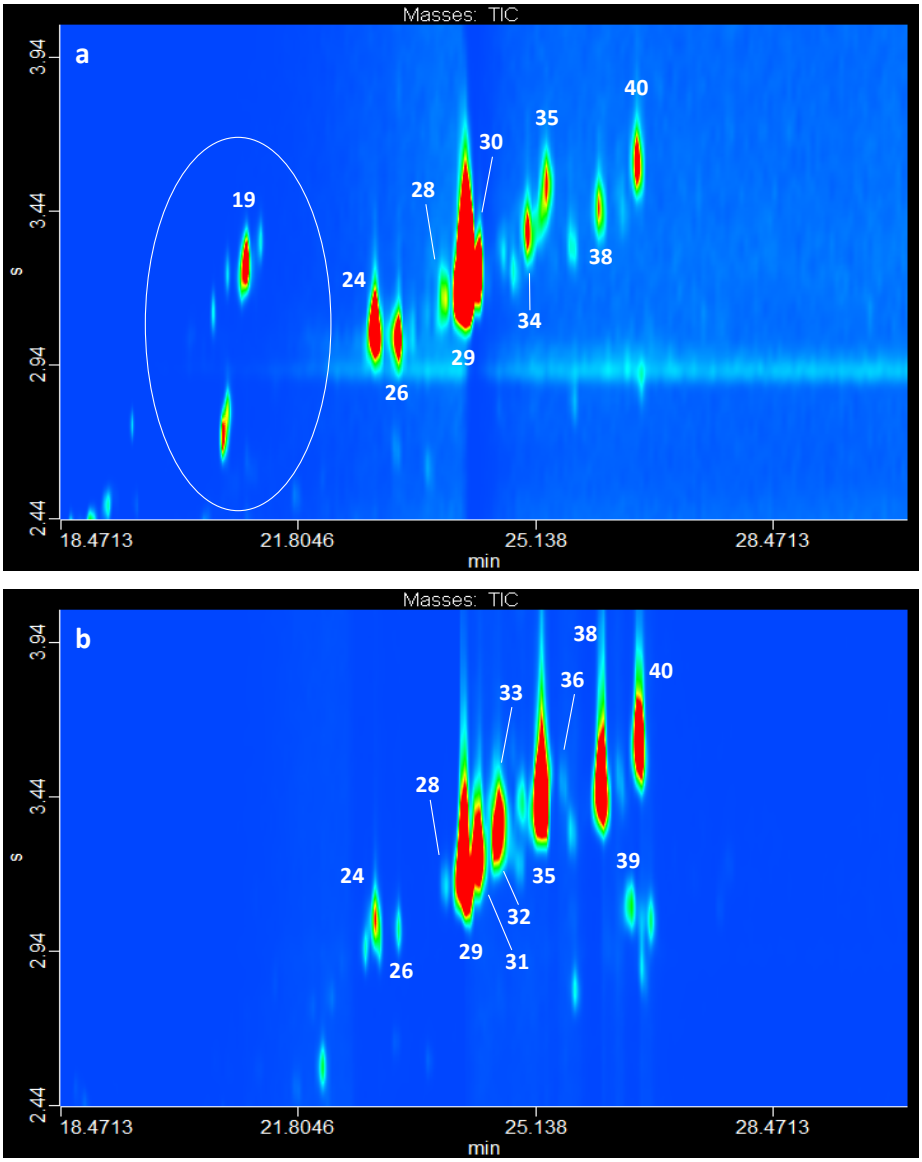

Figure 5.1.3. *TIC GC×GC-HR ToFMS chromatogram expansions of the HO (a) and EVOO9 (b) samples. For peak identification refer to Tables 5.1.2 and 5.1.3.*

Also for HO sample, mass accuracy and similarity values can be considered satisfactory. Average values of 3.0 ppm (absolute value) and 882, respectively, were calculated (Table 5.1.2).

Compared to EVOO1, only cholesterol was not found in EVOO9 (Table 5.1.3). Cholesterol must not be present in percentages exceeding 0.5% (with respect to the other sterols). Adulterations with palm oil or with a lipid of animal origin would lead to higher percentage values [8].

Table 5.1.2. *Peak assignment, theoretical molecular ion, molecular ion error, and MS database similarity (values in bold relate to the HR ToFMS database) for the hazelnut oil sample.*

Peak/Compound	$[M]^+$	Molec. Ion Error (ppm)	Match
7. Tetracosan-1-ol-TMS			954
8. Octacosane			852
9. Squalene	410.390703	0.2	916
11. Nonacosane			868
12. δ-Tocopherol-TMS			858
13. Hexacosan-1-ol-TMS			812
17. Octacosan-1-ol-TMS			832
18. α-Tocopherol-TMS			**863**
19. Stigmasta-3,5-diene	396.375053	2.2	**886**
24. Campesterol	472.409494	4.7	**909**
26. Stigmasterol	484.409494	2.1	**886**
28. Clerosterol[a]	484.409494	2.2	**885**
29. β-sitosterol	486.425144	3.7	**952**
30. Sitostanol (DesMeSt-TMS)[a]	488.440794	3.5	**880**
34. Δ^7-Stigmastenol[b]	486.425144	-1.3	**864**
35. Cycloartenol[a]	498.425144	7.4	**800**
38. 24-Methylenecycloartanol[a]			**883**
40. Citrostadienol[a]			**895**
	aver.	3.0	**882**

[a] Diagnostic ions were consulted in: T.S.C. Li, T.H.J. Beverage, J.C.G. Drover, Phytosterol content of sea buckthorn (Hippophae rhamnoides L.) seed oil: Extraction and identification, Food Chem. 101 (2007) 1633–1639.

[b] Diagnostic ions were consulted in: B. Xu, L. Zhang, H. Wang, D. Luo, P. Li, Characterization and authentication of four important edible oils using free phytosterol profiles estabilished by GC-GC-ToF/MS, Anal. Methods, 6 (2014), 6860-6870.

Table 5.1.3. *Peak assignment, theoretical molecular ion, molecular ion error, and MS database similarity (values in bold relate to the HR ToFMS database) for the EVOO9 sample.*

Peak/Compound	$[M]^+$	Molec. Ion Error (ppm)	Match
24. Campesterol	472.409494	1.3	**913**
26. Stigmasterol	484.409494	6.9	**867**
28. Clerosterol[a]	484.409494	1.7	**887**
29. β-sitosterol	486.425144	6.1	**921**
31. Δ^5-Avenasterol[a]	484.409494	3.5	**909**
32. Parkeol[b]	498.425144	3.5	**893**
33. β-Amyrin[a]	498.425144	0.2	**839**
35. Cycloartenol[a]	498.425144	5.7	**926**
36. α-Amyrin[a]		-	**800**
38. 24-Methylenecycloartanol[a]		-	**935**
39. Erythrodiol[a]		-	**863**
40. Citrostadienol[a]	498.425144	2.7	**938**
	aver.	3.5	**891**

[a] Diagnostic ions were consulted in: T.S.C. Li, T.H.J. Beverage, J.C.G. Drover, Phytosterol content of sea buckthorn (Hippophae rhamnoides L.) seed oil: Extraction and identification, Food Chem. 101 (2007) 1633–1639.

[b] The experimental spectrum was visually compared with that located in: Z. Xue, L. Duan, D. Liu, J. Guo, S. Ge, J. Dicks, P. Ó Máille, A. Osbourne, X. Qi, Divergent evolution of oxidosqualene cyclases in plants, New Phytologist 193 (2012) 1022-1038.

Stigmasterol (peak 26), which was one of the sterols with the lowest abundance in Fig. 5.1.3b, was reconstructed with 34 data points meaning that it possessed a peak width at the base of circa 280 ms. Such a number of data points is enough for an effective deconvolution. It is worthy of note that stigmasterol must be present in lower concentrations compared with campesterol (<4%). If the % of stigmasterol appear to be higher than that of campesterol, then there would be the presumed addition of soybean oil [8].

In general, for what concerns the other two vegetable oils, peanut oil (PO) and soybean oil (SO), apart from stigmasta-3,5-diene, found in both oils, additional peaks assigned in the sterol zone, and not found in samples EVOO1–9, were as follows: Δ^7-stigmastenol (a desmethylsterol) in both PO and SO, and brassicasterol (a desmethylsterol), 24-methylenecholesterol (a desmethylsterol), Δ^7-campesterol (a desmethylsterol), and Δ^7-avenasterol (a desmethylsterol) only in the SO. Even though not detected in samples EVOO1–9, the presence of Δ^7-stigmastenol and brassicasterol is regulated in extra-virgin olive oils, with maximum % values of 0.5% and 0.1%, respectively. Both were found in the previous GC×GC-FID/QMS study on EVOO samples [8]. In such a respect, the total number of assigned peaks in the sterol zone in the previous and present study reached 24 and 22, respectively.

5.1.4 Conclusions

A CM GC×GC-HR ToFMS approach for the detailed qualitative profiling of vegetable oils has been developed. The method, a relatively-rapid one, will be exploited for the analysis of 100 s of samples of EVOO for the creation of a sample-specific fingerprint, within the context of an EVOO research project. Apart from method development and application, a further objective of the present study consisted in the evaluation of the performance of the HR ToFMS system. Such instrumentation was found to be certainly suitable for the challenging circumstances of CM GC×GC analyses. In general, mass accuracy was acceptable, with poorer values observed for the less abundant compounds.

References:

[1] Z. Liu, and J.B. Phillips, J. Chromatogr. Sci. 29 (1991) 227.

[2] G.S. Frysinger, R.B. Gaines, J. High Res. Chromatog. 22 (1999) 251.

[3] P.Q. Tranchida, I. Aloisi, B. Giocastro, L. Mondello, TrAC Trend Anal. Chem. 105 (2018) 360.

[4] F. Hernández, T. Portolés, E. Pitarch, F.J. López, TrAC Trend Anal. Chem. 30 (2011) 388.

[5] P.Q. Tranchida, S. Salivo, F.A. Franchina, L. Mondello, Anal. Chem. 87 (2015) 2925.

[6] J.D. Byer, K. Siek, K. Jobst, Anal. Chem. 88 (2016) 6101.

[7] P.Q. Tranchida, S. Salivo, I. Bonaccorsi, A. Rotondo, P. Dugo, L. Mondello, J. Chromatogr. A 1313 (2013) 194.

[8] P.Q. Tranchida, S. Salivo, F.A. Franchina, I. Bonaccorsi, P. Dugo, L. Mondello, Anal. Bioanal. Chem. 405 (2013) 4655.

[9] P.Q. Tranchida, F.A. Franchina, S. Salivo, M. Russo, P. Dugo, L. Mondello, LC-GC North America 32 (2014) 24.

[10] D. Boskou, G. Blekas, M. Tsimidou, in: Olive oil, chemistry and technology, 2nd edn. AOCS Press, Champaign, Illinois, (2006).

[11] M. Amelio, R. Rizzo, F. Varazini, J. Am. Oil Chem. Soc. 75 (1998) 527.

5.2 Comprehensive two-dimensional gas chromatography-mass spectrometry using milder electron ionization conditions: a preliminary evaluation[†]

The present research is based on the use of GC×GC-QMS, using "milder" EI conditions. The term milder refers to the use of lower energy EI conditions (e.g., 20 eV), instead of the most common electron energy of 70 eV. The effects of using lower source temperatures were also evaluated. Within such an analytical context, GC×GC-QMS was applied to the analysis of a variety of different molecular-mass compounds with various polarities (sterols, linear alkanes, fatty acid methyl esters, vitamin E, squalene, a linear alcohol, and a group of fifteen pesticides).

In general, the results attained indicate that milder EI conditions, and lower source temperatures, generate mass spectra with a higher relative abundance of ions at higher *m/z* values, comprising the molecular ion, and reduced fragmentation at lower *m/z* values. The extent to which such a phenomenon occurred was obviously related to the chemical structure of each analyte. Spectral repeatability was also assessed, and was found to be satisfactory. Finally, with regard to analyte signal-to-noise ratios these were generally comparable in applications involving different electron ionization energies.

[†]This section has been adapted from the following publication: P.Q. Tranchida, **I. Aloisi**, B. Giocastro, M. Zoccali, and, L. Mondello in "Comprehensive two-dimensional gas chromatography-mass spectrometry using milder electron ionization conditions: a preliminary evaluation", Journal of Chromatography A, 1589, (2019) 134-140.

5.2.1 Introduction

In a recent review paper focused on the combination of GC×GC and MS, concerning the period between 2014-2017, it was found that 70-eV electron ionization was used in more than 90% of the published paper [1]. This form of ionization is an hard ionization technique leading to the excessive formation of low-mass fragment ions, and the reduced intensity, or the totally absence, of the molecular ion (MI). At the same time, the generation of highly-repeatable, analyte-specific mass spectral fingerprints and the fact that commercially-available MS databases contain 70-eV EI spectra are two big advantage.

The ionization energy (IE) is the lowest energy necessary to ionize a neutral compound. For nearly all of organic molecules the IEs are in the range 7-15 eV. Loss of an electron can occur from a lone electron pair, a π-bond, or a σ-bond, with the lone pair being the most favored location (followed by the π-bond). For example, the IEs of decane and naphthalene are 9.7 and 8.1 eV, respectively. However, there is a low probability that this minimum amount of energy will be transferred quantitatively to a molecule, leading to the formation of an ion. The ionization efficiency increases rather rapidly when the electron energy is enhanced, reaching a maximum value at around 70 eV for most organic compounds [2,3].

The combination of GC×GC with various forms of 70-eV EI single-analyzer MS, forms a three-dimensional technology [4-7], with five possible levels (or points) of identification: I and II) retention values on the two GC columns; III) the formation of chemical class patterns; IV) the entire mass spectral fingerprint; V) molecular mass. With regard to levels I, II and IV, these are always present, while level III depends mainly on sample composition (i.e., presence or not of homologous series of compounds), and level V on the presence of the MI. The latter occurrence is often hindered by the 70-eV EI process [1-3]. A four-dimensional technology, with more than five levels of identification, can be generated by using a dual-analyzer MS system [8].

An ideal ionization technology should maintain both the MS fingerprinting capability and the MI information; to get such an objective several “soft” ionization technologies have been exploited in the GC×GC-MS field. Some example are: photon ionization [9,10], chemical ionization [11], supersonic molecular beam EI [12-14],

atmospheric pressure chemical ionization [15], variable EI [16,17], and field ionization [18]. In particular, the use of photon ionization and supersonic molecular beam (SMB) EI have been strongly-emphasized forms of soft ionization for GC×GC-MS analyses [9,10,12-14].

Single photon ionization (SPI) is induced by using a pulsing laser, generating vacuum ultraviolet (VUV) photons with a sufficient-enough energy to promote soft and universal ionization [9]. A GC×GC-MS instrument, with the capability to provide both SPI and EI spectra, in an alternate manner during the same analysis, has also been described [10]. With regard to the SMB EI process, an approach also defined as "cold EI", the ionization of vibrationally-cooled compounds occurs in a fly-through EI ion source, producing particularly-evident MIs for analytes containing 15 or more atoms. Apart from soft ionization, other advantages of cold EI are represented by the possibility to operate at high gas flows (emphasized in flow modulation studies) and by a reduction of source-related peak tailing [12-14].

The combination of milder EI and modern MS instruments has been previously reported. For example, Shimma et al. carried out the analysis of polychlorinated biphenyls by the use of GC coupled with miniaturized HR ToFMS [19]. The applications were performed using an EI energy of 18 eV (several EI conditions were evaluated), because it enabled a more intense signal for the quantification ion of heptachlorobiphenyl. In a very recent study, Polet et al. used GC coupled with a quadrupole (Q)ToFMS system for the screening of doping agents in urine [20], using an EI energy of 18 eV. In this research both scan and MS/MS conditions were exploited.

In the field of comprehensive 2D GC, Wong et al. used GC×GC-QToFMS for the analysis of an oleoresin, using an EI energy of 30 eV, in order to increase the relative abundance of the molecular ions [21].

With regard to this research the use of GC×GC coupled with QMS under milder EI conditions (40, 25, 20 eV) is evaluated involving the unsaponifiable fraction of a sample of extra-virgin olive oil, and mixtures of pure standard compounds (linear alkanes, fatty acid methyl esters, and pesticides). A comparison between the conventional (70eV) and the soft-EI mass spectra results was carried out. Moreover, the combined effects of using a lower electron energy and a lower temperature into the

ion source were also evaluated. To the best of the authors' knowledge, the evaluation of such EI conditions, by using a standard EI source, has not been previously reported in the GC×GC-QMS field.

5.2.2 Experimental

Sample, standard compounds, and sample preparation

A sample of genuine extra-virgin olive oil was provided by a producer from the Italian region of Puglia.

The BSTFA [N,O-bis(trimethylsilyl)trifluoroacetamide] + 1% TMCS (trimethylchlorosilane) kit was supplied by Merck Life Science (Merck KGaA, Darmstadt, Germany). Powdered anhydrous sodium sulfate was purchased from Merck Life Science. The C_7–C_{30} alkane and C_{37} fatty acid methyl ester (FAME) mixtures, as well as the pesticides, were supplied by Merck Life Science. Solutions at the 100 ppm concentration level were prepared in hexane.

Isolation and derivatization of the unsaponifiable fraction of the olive oil was performed by using a previously-used procedure [22].

Instrumentation

All GC×GC-QMS applications were performed on a system formed of two Shimadzu GC-2010 gas chromatographs, and a QP2020 quadrupole mass spectrometer (Kyoto, Japan). Data were acquired by using the GCMS solution software (Shimadzu). Bidimensional chromatograms were generated by using the ChromSquare software v. 2.3 (Shimadzu).

The first gas chromatograph (GC1) was equipped with an AOC-20i auto-injector, and a split–splitless injector. The first-dimension column was an SLB-5ms [(silphenylene polymer which can be considered equivalent in polarity to poly(5%diphenyl/95% dimethylsiloxane)] with dimensions 30 m × 0.25 mm ID × 0.25 μm d_f. The second-dimension column (housed in the second oven - GC2) was an SLB-35ms [(polymer which can be considered equivalent in polarity to poly(35%diphenyl/65% dimethylsiloxane)] with dimensions 3 m × 0.25 mm ID × 0.25 μm d_f. A 1 m segment of the ^{2}D column was used to create the delay loop, leaving approx. a 1.5 m segment for the analytical separations. All the columns used were

provided by Merck Life Science. The connection between the columns was made by using a SilTite mini union (Trajan, Ringwood, Victoria, Australia).

- Extra-virgin olive oil unsaponifiable fraction: helium was supplied at the GC1 inlet at a pressure of 60 kPa (constant linear velocity mode); volume and mode of injection (360°C): 1 μL in the split mode (30:1); GC1 temperature program: 90-280°C at 15°C min^{-1}, 280-330°C at 2.5°C min^{-1}, 330-360°C at 15°C min^{-1}; GC2 temperature program: +20°C offset (until 360°C, when an isothermal period of 1.3 min began).
Modulation was performed by using a cryogenic modulator (under license from Zoex Corporation); modulation period was 3.5 s (the heating step was performed at 360°C, for 0.3 s).
Mass spectrometry conditions: the temperature of the interface was 330°C; the ion source temperature was 250°C, with analyte fragmentation induced by electron ionization at different energies (70, 40, 20 eV). A mass range of *m/z* 50-520 and a scan rate of 33 Hz were applied.

- Fatty acid methyl esters and linear alkanes: helium was supplied at the GC1 inlet at a pressure of 45.6 kPa (constant linear velocity mode); volume and mode of injection (310°C): 1 μL in the split mode (50:1); GC1 and GC2 temperature programs: 50-300°C at 5°C min^{-1}.
Modulation period was 2.5 s (the heating step was performed at 340°C, for 0.2 s).
Mass spectrometry conditions: the temperature of the interface was 300°C; the ion source temperature was 250°C (the linear alkanes were also analysed by using a source temperature of 150°C), with analyte fragmentation induced by electron ionization at different energies (70, 25, 20 eV). A mass range of *m/z* 50-500 and a scan rate of 33 Hz were applied.

- Pesticides: helium was supplied at the GC1 inlet at a pressure of 76.8 kPa (constant linear velocity mode); volume and mode of injection (310°C): 0.5 μL in the split mode (100:1); GC1 and GC2 temperature programs: 120-350°C at 5°C min^{-1}.
Modulation period was 2.5 s (the heating step was performed at 340°C, for 0.2 s).
Mass spectrometry conditions: the temperature of the interface was 310°C; the ion source temperatures were 250°C, 200°C and 150°C. Analyte fragmentation was induced by electron ionization at different energies (70 and 25 eV). A mass range of *m/z* 50-450 and a scan rate of 33 Hz were applied.

In general, autotuning processes were performed every time an ion source condition was modified (EI energy or ion source temperature). The detector voltages (DVs) varied between the different types of applications, and were obviously related to the tuning result.

5.2.3 Results & Discussion

The objective of the research was to evaluate mass spectral behaviours in GC×GC-QMS experiments, using milder ionization conditions. A series of applications were carried out at different EI energies. The DV values, set through the automatic tuning process, obviously tended to increase at lower EI energies, to contrast the reduction in analyte ionization efficiency, and thus in sensitivity. Below an EI of 50 eV, the ionization efficiency falls very rapidly [2,3]. All the DV values used in the present research were well below the maximum value recommended by the manufacturer (2.0 kV). The use of high DVs can, however, reduce the lifetime of the detector.

The scan rate was maintained constant in all the applications (33 Hz), it being sufficient for the generation of at least 10 data points per peak. The mass range varied slightly, in relation to the type of sample subjected to analysis. It is herein defined, in an arbitrary manner and with the scope to facilitate a comparative study, that an "evident" molecular ion is one with a mass spectrum relative abundance of minimum 2%.

Phytosterols

The unsaponifiable fraction of a sample of extra-virgin olive oil was subjected to GC×GC-QMS analysis, with initial focus on the phytosterols, under the form of TMS ethers. The GC×GC-QMS applications were carried out at EI energies of 70, 40 and 20 eV, and DVs of 0.85, 0.88 and 1.10 kV, respectively. In all three experiments analyte signal-to-noise ratios (*s/n*) were rather similar (TIC result), with both the background noise and peak intensities increasing with the DV value.

Chromatogram expansions, related to the 70-eV and 20-eV analyses, are shown in Figure 5.2.1.

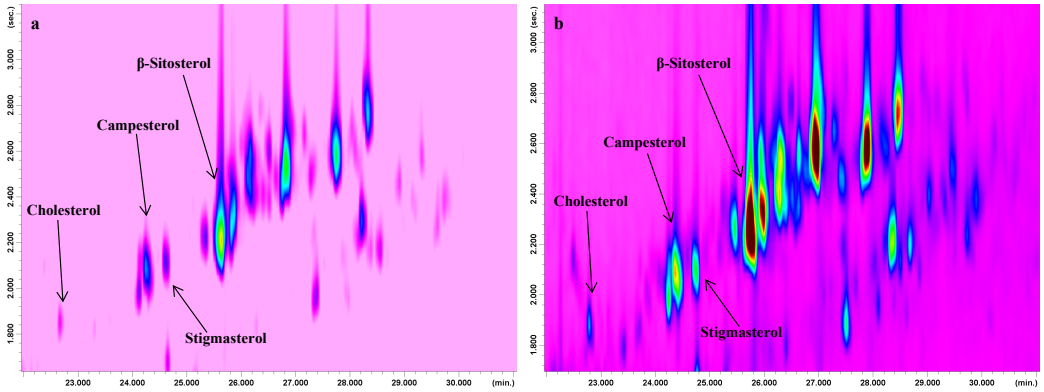

Figure 5.2.1. *Chromatogram expansions (reporting the sterol zone) relative to the GC×GC-QMS analysis of the unsaponifiable fraction of a sample of extra-virgin olive oil performed at EI energies of 70 eV (a) and 20 eV (b). Minimum z-axis intensity: -14371; maximum z-axis intensity: 3.5155e +07.*

Both chromatograms were obtained by setting the same values of minimum and maximum signal intensity (*z* axis values). As can be seen, both the background noise and the peak intensities are increased in the 20-eV analysis (Figure 5.2.1b). Four phytosterols, the presence of which is regulated in olive oils [23], are indicated in both expansions. The *s/n* values (n= 3), calculated for the four phytosterols (the most intense modulated peak was considered) were comparable (as can be derived from the total average values), and are listed in Table 5.2.1.

Table 5.2.1. *Signal-to-noise ratio values (n= 3) for four phytosterols attained under different EI energies, along with the total average s/n values.*

	70 eV	**40 eV**	**20 eV**
Cholesterol	157	147	114
β-Sitosterol	1901	1271	1783
Campesterol	673	807	822
Stigmasterol	271	228	205
Average s/n	*751*	*613*	*731*

Having concluded that, under milder EI scan conditions, and for the specific analytes in question, there were no substantial reductions in the *s/n* values, attention was focused on the mass spectral profiles. The averaged mass spectra for campesterol (the baseline noise was subtracted), under 70-, 40-, and 20-eV EI conditions, are shown in Figure 5.2.2. Attention was directed to seven ions (presumed identities are reported in the graph in Figure 5.2.3), comprising the MI, and spanning the mass spectrum.

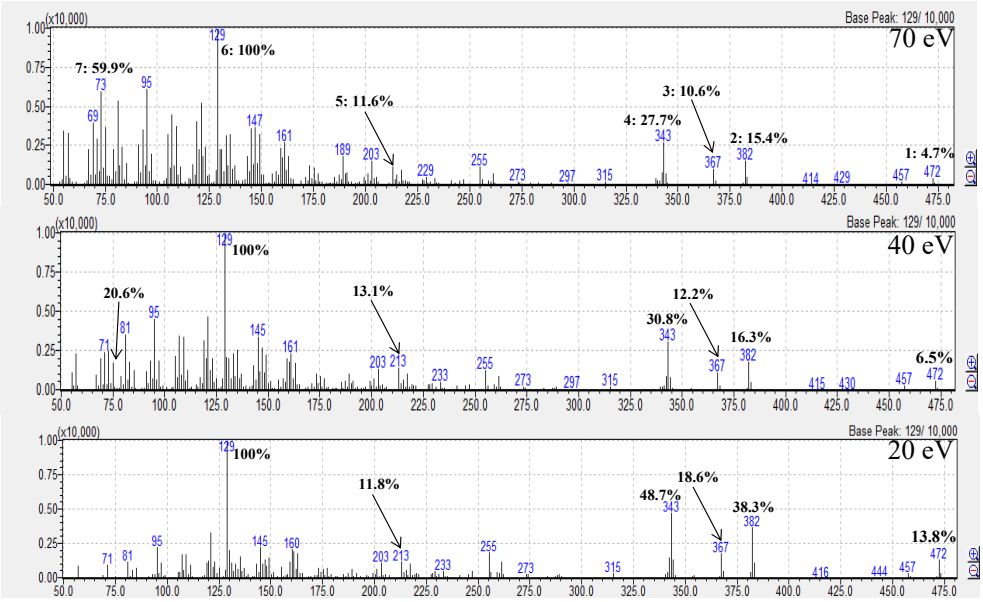

Figure 5.2.2. *Mass spectra for campesterol attained under 70-, 40- and 20-eV EI conditions; presumed identities of the indicated ions can be found in Figure 5.2.3.*

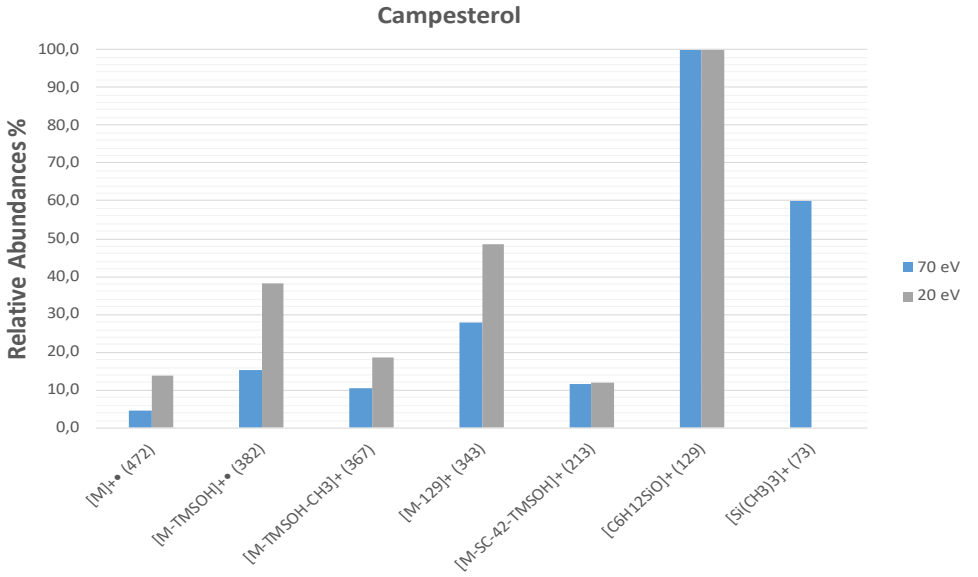

Figure 5.2.3. *Graph showing the relative abundances for seven ions present in the 70- and 20-eV EI mass spectra of campesterol.*

As can be readily seen, the differences between the 70-eV and 40-eV mass spectra are only slight, with the main one being a reduced fragmentation below *m/z* 129 in the 40-eV spectrum. On the contrary, the differences were much greater between the 70-eV and 20-eV mass spectra: in the latter, the relative abundance of the MI (*m/z* 472)

increased by a factor of nearly 3, while other high-mass diagnostic fragments (*m/z* 382, 367, 343) were also enhanced. Middle-mass ions, such as the *m/z* 213 and 129 (base peak) ions, remained basically unaltered, while fragmentation below *m/z* 129 is greatly reduced. For instance, the *m/z* 73 ion was the third most intense ion under 70-eV EI conditions, while it was not visible in the 20-eV EI spectrum. A similar (though not identical) trend was observed for the other three phytosterols, with the results attained under 70-eV and 20-eV conditions. Considering the four MIs, the average degree of enhancement was by a factor of 2.8. On the other hand, the average degree of relative abundance reduction for the ion $[Si(CH_3)_3]^+$at *m/z* 73 was by a factor of approx. 33 (campesterol was not considered). Characteristic sterol fragmentation pathways for two sterols tipical ions ($[M-129]^+$, and $[M-SC-42-TMSOH]^+$ at *m/z* 213) are illustrated in Figure 5.2.4 [24].

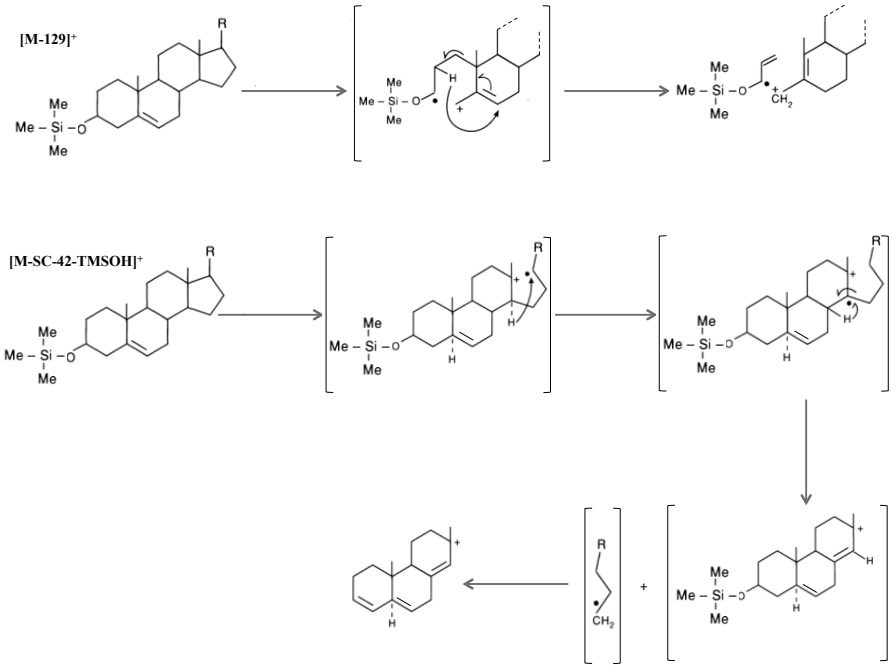

Figure 5.2.4. *Fragmentation pathways for two characteristic sterol ions ([M-129]$^+$, and [M-SC-42-TMSOH]$^+$ at m/z 213).*

Fatty acid methyl esters

On the basis of the results attained on the phytosterols, GC×GC-QMS applications under 70-eV and 20-eV EI conditions were carried out on a standard mixture of thirty-seven FAMEs. As previously observed for the phytosterols, *s/n* values of the FAMEs

in the two applications were similar, while substantial between-spectra differences were observed. Again, attention was directed to several ions across the mass spectra of the FAMEs. The results for five saturated FAMEs (C_{14}, C_{16}, C_{18}, C_{20}, C_{22}) are reported in Table 5.2.2, along with the presumed identity of the seven ions considered.

Table 5.2.2. *Relative abundances for seven ions present in the mass spectra of $C_{14:0}$, $C_{16:0}$, $C_{18:0}$, $C_{20:0}$, and $C_{22:0}$, along with the peak s/n values, under 70- and 20-eV EI conditions (the first value refers to the 70-eV EI result). Mass/charge values are reported in parenthesis.*

Ion	$C_{14:0}$%	$C_{16:0}$%	$C_{18:0}$%	$C_{20:0}$%	$C_{22:0}$%
1. $[M]^{+\bullet}$	1.4/3.0 (242)	2.4/3.7 (270)	1.7/5.2 (298)	2.9/6.7 (326)	3.6/10.0 (354)
2. $[M\text{-}OCH_3]^+$	2.0/4.1 (211)	2.5/2.8 (239)	1.4/1.9 (267)	1.1/2.1 (295)	0.7/0.8 (323)
3. $[M\text{-}C_3H_7]^+$	7.4/9.5 (199)	6.0/9.5 (227)	6.8/10.1 (255)	4.5/9.4 (283)	3.8/7.6 (311)
4. $[M\text{-}C_5H_{11}]^+$	1.5/0.7 (171)	3.6/4.5 (199)	1.2/2.0 (227)	2.2/3.6 (255)	1.4/0.9 (283)
5. $[M\text{-}C_7H_{15}]^+$	15.0/24.3 (143)	6.0/4.6 (171)	5.9/7.9 (199)	4.9/5.9 (227)	5.7/9.1 (255)
6. $[CH_3CH_2COOCH_3]$	85.5/62.8 (87)	84.7/67.3 (87)	90.7/65.5 (87)	92.0/67.3 (87)	85.1/74.2 (87)
7. $[CH_2COHOCH_3]^{+\cdot}$	100/100 (74)	100/100 (74)	100/100 (74)	100/100 (74)	100/100 (74)
s/n	*103/139*	*158/189*	*100/92*	*69/53*	*87/47*

Higher-mass ions were more intense in the 20-eV EI spectra, while the opposite occurred for the lower mass ones (e.g., $[CH_3CH_2COOCH_3]^+$). For the $[M\text{-}C_5H_{11}]^+$ ion the relative abundances were always increased in the 20-eV applications, except for $C_{14:0}$ and $C_{22:0}$; for the $[M\text{-}C_7H_{15}]^+$ ion, the relative abundances were always lower in the 70-eV applications, except for $C_{16:0}$. Considering the five MIs of the saturated FAMEs, the average degree of enhancement was by a factor of 2.4. Additionally, in 2 cases the MI was characterized by an intensity lower than 2.0% under 70-eV EI conditions, and was always well over such an intensity level under milder EI conditions. The overall average *s/n* values, for the five saturated FAMEs, were 103 and 104, in the 70-eV and 20-eV applications, respectively (single TIC *s/n* values are reported in Table 5.2.2). Characteristic fragmentation pathways for methyl stearate, involving all the ions listed in Table 5.2.2, are illustrated in Figure 5.2.5 [25].

The mass spectra of the unsaturated FAMEs also differed, with the results for $C_{14:1\omega5}$, $C_{18:1\omega9}$, $C_{20:1\omega9}$, $C_{18:2\omega6}$, and $C_{20:2\omega6}$, listed in Table 5.2.3. Specifically, the relative abundances of three diagnostic ions were considerably increased using the milder EI conditions: average degrees of enhancement were by factors of 11.2, 6.1,

and 2.3, for the ions $[M]^{+\bullet}$, $[M\text{-}OCH_3]^+$ (plus $[M\text{-}32]^{+\bullet}$), and $[M\text{-}CH_2COHOCH_3]^{+\bullet}$, respectively.

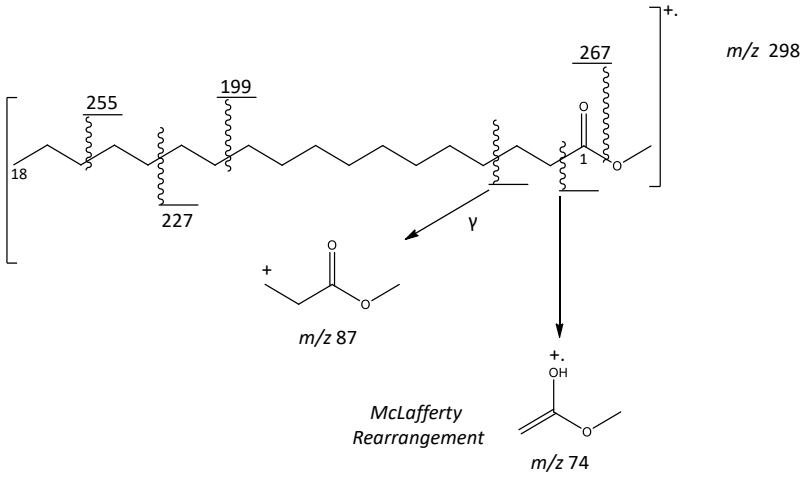

Figure 5.2.5. *Fragmentation pathways for methyl stearate.*

Table 5.2.3. *Relative abundances for three diagnostic ions present in the mass spectra of $C_{14:1\omega5}$, $C_{18:1\omega9}$, $C_{20:1\omega9}$, $C_{18:2\omega6}$, and $C_{20:2\omega6}$, along with the peak s/n values, under 70- and 20-eV EI conditions (the first value refers to the 70-eV EI result). Mass/charge values are reported in parenthesis.*

Ion	$C_{14:1\omega5}$%	$C_{18:1\omega9}$%	$C_{20:1\omega9}$%	$C_{18:2\omega6}$%	$C_{20:2\omega6}$%
1. $[M]^{+\bullet}$	0.9/5.4 (240)	0.1/2.7 (296)	0.3/2.3 (324)	0.8/2.3 (294)	0.7/8.6 (322)
2. $[M\text{-}32]^{+\bullet}$	5.9/30.9 (208)	5.9/47.5 (264)	6.2/20.1 (292)		
3. $[M\text{-}OCH_3]^+$				1.1/5.5 (263)	1.0/9.1 (291)
4. $[M\text{-}CH_2COHOCH_3]^{+\bullet}$	12.9/37.8 (166)	3.7/10.9 (222)	5.9/15.1 (250)	2.9/4.8 (220)	1.3/1.6 (248)
s/n	*72/91*	*50/53*	*46/25*	*25/21*	*44/33*

Moreover, in all cases the MI was characterized by an intensity lower than 1.0% under 70-eV EI conditions, and was always over the 2.0% level under milder EI conditions. As an example, the mass spectra for the FAME $C_{14:1\omega5}$ (molecular mass = 240.22 u), under hard and milder EI conditions, are reported in Figure 5.2.6. As can be readily seen, all the diagnostic ions are more intense under 20-eV conditions, while the fragmentation profile is modified (rather than being reduced) at the low masses (below *m/z* 100). The overall average TIC *s/n* values, for the five unsaturated FAMEs, were 47 and 45, in the 70-eV and 20-eV applications, respectively (single *s/n* values are reported in Table 5.2.3).

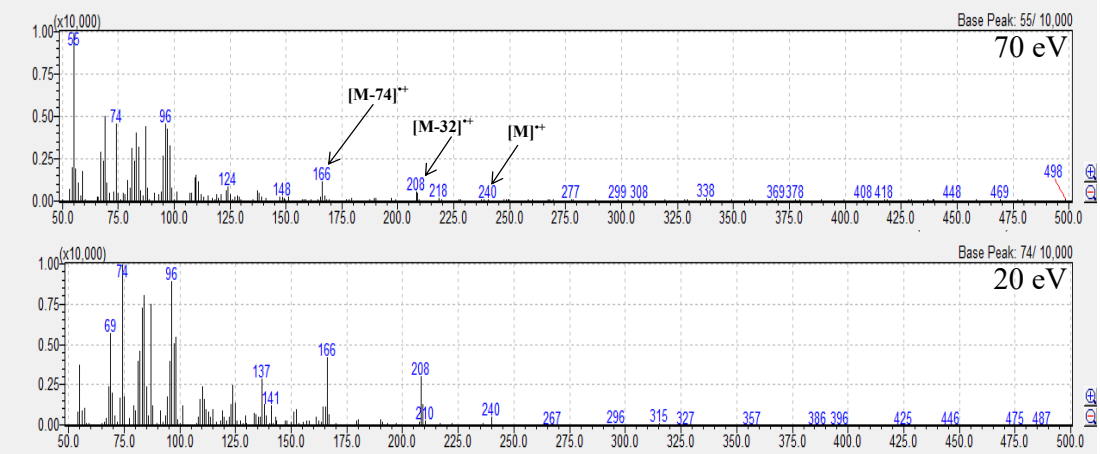

Figure 5.2.6. *Fragmentation pathways for methyl stearate.*

Hydrocarbons, pesticides, and other compounds

The mass spectral behaviour of linear alkanes, under 70-eV conditions, is well known, inasmuch that only the lower mass compounds present a distinguishable MI. Moreover, the intensity of the latter tends to diminish as the chain length increases [26]. A standard C_7-C_{30} series of linear alkanes was subjected to GC×GC-QMS analysis, under hard and milder EI conditions; the relative abundances for the molecular ions, within the C_{10}-C_{20} range, are illustrated in the graph in Figure 5.2.7. As can be seen, the intensity of the $[M]^{+\bullet}$ ion gradually decreases with an increase in chain length, under both ionization conditions. Alkane C_{12} was the heaviest with an evident molecular ion (2.0%), under hard ionization conditions, while C_{17} was the heaviest alkane with an evident molecular ion (2.1%), under milder ionization conditions. Considering the average MI abundances, these were 1.1% and 3.6% under 70- and 20-eV EI conditions, respectively.

To evaluate mass spectral repeatability, a 20-eV MS database was constructed by using the spectra of the C_{10}-C_{20} alkanes; after, two consecutive GC×GC-QMS analyses were performed, an MS database search carried out, with an overall calculated average MS similarity of 95% (min. 92%; max. 97%).

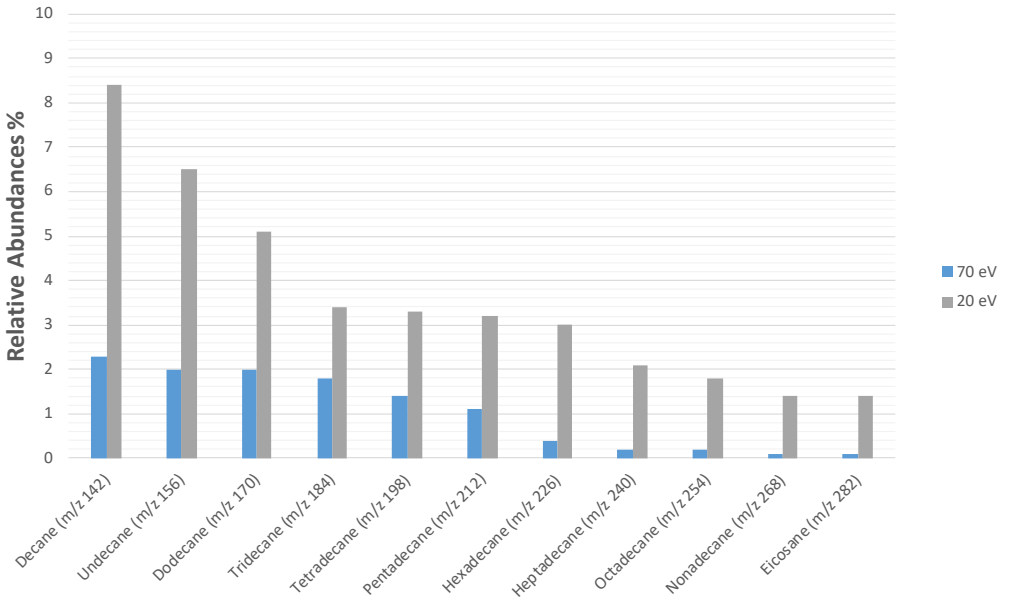

Figure 5.2.7. *Graph showing the relative abundances for the molecular ions present in the mass spectra of linear alkanes in the range C_{10}-C_{20}, under 70- and 20-eV EI conditions.*

Considering further compounds contained in the unsaponifiable fraction of extra-virgin olive oil, squalene is the most abundant constituent, and is a branched (six methyl groups) triterpene hydrocarbon with 6 double bonds ($C_{30}H_{50}$). With respect to linear hydrocarbons, branched ones generate more stable secondary and tertiary cations, normally leading to a low-intensity MI [26]. In fact, under 70-eV EI conditions, its MI reached an intensity of 0.1%; under milder EI conditions, however, it increased to a value of 2.0%. Additionally, MIs of very low intensity were observed for the TMS-derivatized aliphatic alcohol 1-octanosol (molecular mass = 482.49 u) under both ionization conditions; however, under milder ionization conditions the intensity of the diagnostic ion $[M\text{-}CH_3]^+$ was greatly increased, while the presence of lower MW fragments was considerably reduced. Finally, vitamin E, in the form of (TMS-derivatized) α-tocopherol was characterized by an evident MI (*m/z* 502; 13.3%) under 70-eV EI conditions; under milder EI conditions, the MI reached an intensity of 54.5%, while the ion at *m/z* 237 became the base peak.

At this point of the research, the effects of two other MS operational conditions on the fragmentation process were investigated: the use of an EI energy slightly higher

than 20 eV and the influence of the ion source temperature. As previously seen, in the initial applications the mass spectral differences between the 70- and 40-eV applications were limited. With regard to the source temperature, it is well-known that lower values promote reduced fragmentation, due to a reduction of the thermal vibrational energy [3, 26]. The linear alkanes were again subjected to GC×GC-QMS analyses, this time under 70- and 25-eV EI energies, and at source temperatures of 250°C and 150°C. The 70 eV/250°C results essentially confirmed those previously observed (Figure 5.2.7), in relation to the relative abundances of the C_{10}-C_{20} MIs (Table 5.2.4).

Table 5.2.4. *Relative abundances for the molecular ions present in the mass spectra of linear alkanes in the range C_{10}-C_{20}, along with average values, under 70- and 25-eV EI conditions and ion source temperatures of 250°C and 150°C (the first value always refers to the 70-eV EI result).*

Alkane	$[M]^{+\bullet}$% - 250°C	$[M]^{+\bullet}$% - 150°C
C_{10}	2.2/2.7	8.9/11.8
C_{11}	1.7/2.0	8.6/9.0
C_{12}	1.7/1.7	7.8/9.2
C_{13}	1.4/1.6	7.5/8.4
C_{14}	1.1/1.2	6.8/8.0
C_{15}	0.9/1.0	6.3/8.7
C_{16}	0.8/0.8	6.4/7.3
C_{17}	0.7/0.8	5.4/7.3
C_{18}	0.6/0.8	5.1/7.2
C_{19}	0.5/0.6	4.5/6.9
C_{20}	0.4/0.6	4.9/7.3
Average	*1.1/1.3*	*6.6/8.3*

Furthermore, the use of 25 eV/250°C conditions enabled only slight increases in the MI relative abundances: the average MI abundances were 1.1% and 1.3% under 70- and 25-eV EI conditions, respectively (Table 5.2.4). On the other hand, the use of a source temperature of 150°C had a significant impact on the relative abundances of the MIs, with average values reaching 6.6% and 8.3% under 70- and 25-eV EI conditions, respectively (Table 5.2.4). For example, the MI of undecane (*m/z* 156) passed from a relative abundance of 1.7% to one of 9.0%, under 70 eV/250°C and 25 eV/150°C conditions, respectively. Although the scope of the present research is not a comparative one with other ionization technologies, it is noteworthy that the MI was

the base peak in the spectrum of undecane with very limited fragmentation, when using GC×GC-SPI MS [10]. Moreover, in a flow-modulation GC×GC-SMB EI MS application on diesel fuel, the spectrum for a $C_{11}H_{24}$ hydrocarbon (presumably a branched alkane) was characterized by a base peak at *m/z* 156, while the general fragmentation profile was maintained [26].

Table 5.2.5. *Relative abundances for the molecular ions present in the mass spectra of 15 pesticides, along with average values, under 70- and 25-eV EI conditions and ion source temperatures of 250°C, 200°C and 150°C.*

Compound	$M^{+\bullet}$	70 eV (250°C/200°C/150°C)	25 eV (250°C/200°C/150°C)
Dichlobenil	172	12.7/12.5/12.1	11.0/11.3/12.0
Pebulate	203	1.6/3.0/4.5	2.1/2.8/6.8
MCPA* methyl ester	214	57.3/64.1/69.8	70.6/77.0/93.2
Bromoxynil methyl	290	4.7/4.4/4.0	8.8/6.6/8.2
Chlorbufam	223	6.7/8.1/9.6	5.3/9.2/13.6
Terbacil	216	0.9/1.4/1.5	1.0/2.5/4.4
Dimethachlor	255	0.2/0.3/0.7	0.6/0.7/1.1
Orbencarb	257	0.3/0.6/0.9	0.2/0.6/1.0
Fluthiamid	363	0.4/1.1/2.1	0.5/1.2/2.4
Dimepiperate	263	0.7/1.6/3.0	0.8/1.9/3.1
Siduron isomer I	232	0.9/2.0/1.4	1.3/2.3/3.0
Nitrofen	284	46.0/42.7/54.5	42.2/43.9/57.2
Anilofos	367	0.4/0.7/1.0	0.5/0.7/0.5
Mefenacet	298	1.0/2.3/3.3	1.5/2.0/4.6
Fenoxaprop-P-ethyl	361	40.4/37.4/39.4	61.8/48.3/73.1
Average		*11.6/12.1/13.8*	*13.9/14.1/18.9*

Finally, a mixture containing 15 pesticides was subjected to GC×GC-QMS analyses, under 70- and 25-eV EI energies, and at source temperatures of 250°C, 200°C and 150°C. Due to the differences in analyte chemistries, fragmentation behaviors varied greatly. However, distinct trends were again observed, with MI abundances reported in Table 5.2.5: the impact of using a source temperature of 150°C, compared to one of 200°C, was far greater than that observed between source temperatures of 200°C and 250°C.For example, under 25 eV EI conditions and at source temperatures of 250°C, 200°C and 150°C, the average relative abundances of the MIs were 13.9%, 14.1%, and 18.9%, respectively. The combined use of a 25-eV EI energy and a source temperature of 150°C enabled an increase in the average MI

abundances of over 7%, with respect to 70 eV/250°C conditions (11.6% →18.9%). In general, an increase in the abundance of higher mass ions, and a decrease of the lower mass ones, were observed. It must be noted, however, that source contamination increases when operating at lower temperatures, especially when high-boiling analytes are involved. Furthermore, source-induced peak tailing can also occur [26].

5.2.4 Conclusions

The research herein described can be considered as a preliminary evaluation of the use of milder EI conditions, using CM GC×GC-QMS. The results attained on various groups of chemically-diverse compounds can be considered as positive inasmuch that, compared to 70-eV EI, a general increase in the relative abundance of higher-mass diagnostic fragments was observed, along with a reduced relative abundance of the lower-mass fragments. Moreover, it was seen that a reduction of the source temperature favored a further enhancement of the higher mass ions. Such characteristics are beneficial not only for the purpose of identification, but also for more selective targeted analysis, using extracted ions and selected-ion-monitoring. Apart from the outcome of the investigation, which was in part expected, a further underlying objective was to emphasize the need for highly-informative and sensitive softer ionization approaches.

References:

[1] P.Q. Tranchida, I. Aloisi, B. Giocastro, L. Mondello, TrAC Trends Anal. Chem. 105 (2018) 360.

[2] J.H. Gross, in: Mass Spectrometry - A Textbook 2nd Edition, Springer-Verlag Berlin Heidelberg, (2011)

[3] E. de Hoffmann, V. Stroobant, in: Mass Spectrometry - Principles and Applications Third Edition, John Wiley & Sons Ltd, Chichester, England, (2007).

[4] N. Ochiai, T. Ieda, K. Sasamoto, Y. Takazawa, S. Hashimoto, A. Fushimi, K. Tanabe, J. Chromatogr. A 1218 (2011) 6851.

[5] D. Megson, R. Kalin, P.J. Worsfold, C. Gauchotte-Lindsay, D.G. Patterson Jr., M.C. Lohan, S. Comber, T.A. Brown, G. O'Sullivan, J. Chromatogr. A 1318 (2013) 276.

[6] L. Mondello, A. Casilli, P.Q. Tranchida, M. Lo Presti, P. Dugo, G. Dugo, Anal. Bioanal. Chem. 389 (2007) 1755.

[7] W. Welthagen, S. Mitschke, F. Mühlberger, R. Zimmermann, J. Chromatogr. A 1150 (2007) 54.

[8] M. Zoccali, P.Q. Tranchida, L. Mondello, Anal. Chem. 87 (2015) 1911.

[9] W. Welthagen, S. Mitschke, F. Mühlberger, R. Zimmermann, J. Chromatogr. A 1150 (2007) 54.

[10] M.S. Eschner, T.M. Gröger, T. Horvath, M. Gonin, R. Zimmermann, Anal. Chem. 83 (2011) 3865.

[11] J.D. Byer, K. Siek, K. Jobst, Anal. Chem. 88 (2016) 6101.

[12] M. Kochman, A. Gordin, T. Alon, A. Amirav, J. Chromatogr. A 1129 (2006) 95.

[13] M. Poliak, A.B. Fialkov, A. Amirav, J. Chromatogr. A 1210 (2008) 108.

[14] U. Keshet, A.B. Fialkov, T. Alon, A. Amirav, Chromatographia 79 (2016) 741.

[15] D. Megson, X. Ortiz, K.J. Jobst, E.J. Reiner, M.F.A. Mulder, J-C. Balouet, Chemosphere 158 (2016) 116.

[16] M.S. Alam, C. Stark, R.M. Harrison, Anal. Chem. 88 (2016) 4211.

[17] L.M. Dubois, K.A. Perrault, P.H. Stefanuto, S. Koschinski, M. Edwards, L. McGregor, J.F. Focant, J. Chromatogr. A 1501 (2017) 117.

[18] W. Genuit, H. Chaabani, Int. J. Mass Spectrom. 413 (2017) 27.

[19] S. Shimma, S. Miki, M. Toyoda, J. Environ. Monit. 14 (2012) 1664.

[20] M. Polet, W. Van Gansbeke, P. Van Eenoo, Anal. Chem. Acta. 1042 (2018) 52.

[21] Y. Foo Wong, T.M. Uekane, C.M. Rezende, H.R. Bizzo, P.J. Marriott, J. Chromatogr. A 1477 (2016) 91.

[22] P.Q. Tranchida, S. Salivo, F.A. Franchina, I. Bonaccorsi, P. Dugo, L. Mondello, Anal. Bioanal. Chem. 405 (2013) 4655.

[23] Regulation 2568/91 and modifications, European Commission, 11th July 1991.

[24] L.J. Goad, T. Akihisha, in: Analysis of Sterols, Chapman & Hall, London, (1997).

[25] J.H. Gross, in: Mass Spectrometry - A Textbook 2nd Edition, Springer-Verlag Berlin Heidelberg, (2011).

[26] A. Amirav, A. Gordin, M. Poliak, A.B. Fialkov, J. Mass Spectrom. 43 (2008) 141.

5.3 Chemical characterization of unconventional palm oils from *Hyophorbe indica* and two other endemic *Arecaceae* species from Reunion Island[†]

Chemical characteristics of novel seed oils, yet not investigated, from three endemic *Arecaceae* (palm) species from Reunion Island are described. Fatty acid profiles are performed using CM GC×GC-QMS. Carotenoid contents are determined by high performance liquid chromatography mass spectrometry. The results of the investigations emphasize the particular composition of the unconventional red seed oil from *Hyophorbe indica*. Characteristic features of this oil reveal a high degree of unsaturation (50%) of polyunsaturated fatty acids, with a high content (17%) of omega-3, which is possibly a unique fatty acid composition in the *Arecaceae* family. The two other palm oils from *Dictyosperma album* and *Latania lontaroides* contain high level of saturated fatty acids very similar to that of the edible palm oil. *H. indica* oil is also very rich in valuable carotenoids; in particular, lutein, β-carotene and lycopene are detected in a high content (respectively 45, 23 and 35mg kg^{-1} in oil).

[†]This section has been adapted from the following publication: Y. Caro, T. Petit, I. Grondin, P. Clerc, H. Thomas, D. Giuffrida, B. Giocastro, P.Q. Tranchida, **I. Aloisi**, D. Murador, L. Mondello, L. Dufossé in "Chemical characterization of unconventional palm oils from *Hyophorbe indic*a and two other endemic Arecaceae species from Reunion Island", Natural Product Research, 34, (2020) 93-101

5.3.1 Introduction

The plant kingdom contains various bioactive hydrocarbon compounds such as lipids with an incredible variety of structures and functions. In this respect, vegetable seeds are original and abundant sources of valuable lipids (fatty acids, carotenoids, etc.). Polyunsaturated fatty acids (PUFAs) are found mostly in plant seed oils and are important substrates for the biosynthesis of cellular hormone-like compounds (eicosanoids) at least. A large number of studies have shown positive health benefits associated with consumption of Omega-3 (ω3) PUFAs on infant development, coronary artery and cardiovascular diseases [1, 2], arthritis [3], inflammatory and autoimmune disorders [4], and cancer [5, 6]. Some particular seed oils are also rich in unsaponifiable derived lipids with varying biological properties, such as the carotenoids. Carotenoids are fat-soluble pigments found in seed oils. They are isoprenoidic type of compound usually consisting of a forty carbon atoms skeleton [7]. Carotenoids that contain oxygen in their structure are known as xanthophylls, whereas those that lack oxygen are called carotenes. Some carotenes, such as α- and β-carotene, are converted by the body into retinol, or vitamin A1. Some carotenoids can act as antioxidants by scavenging oxygen and peroxyl radicals. Recently, their importance has grown due to the beneficial health properties that have been ascribed to them [8, 9].

Five vegetable oils dominate the world market, e.g. palm, soybean, canola, sunflower seed, and palm kernel oil. Edible palm oil is derived from the fruit of the oil palm tree, primarily the African palm *Elaeis guineensis*. In its natural, unprocessed state, crude palm oil is dark red in color due to a high content of carotenoids, including β-carotene and lycopene [10]. Recent literature has emphasized the necessity of investigating unconventional, or underutilized minor plant oils, like those from rice bran [11], Allanblackia [12, 13], pequi [14], and pistachio oil [15] to meet the increasing global demand for edible oils and biodiesel [10]. Furthermore, consumers are looking for novel vegetable oils that have unique health-promoting properties. Unconventional oils are often harvested from wild plants, and each unconventional oil has its own challenges that must be overcome to enable large-scale production: low seed yield or oil content, strong flavor of the oil, presence of minor toxic compounds, etc. [10].

Reunion Island in the western Indian Ocean arose two million years ago from a volcanic hot spot and its diversity of habitats and microclimates have encouraged the diversification of a highly endemic flora. Given that the presence of bioactive polyunsaturated fatty acids and valuable carotenoids in plant seeds could offer new additional values to a prospective crop, we investigated the chemical characteristics (e.g. fatty acid and carotenoid contents) of novel seed oils, yet not investigated, from ripe fruit of three endemic plant species of Reunion Island belonging to the *Arecaceae* family. *Arecaceae* are part of a botanical family of perennial plants. These are climbing plants, shrubs, trees and stemless plants, all commonly known as 'palms' such as the well-known African species *Elaeis guineensis* (Jacq.) producing the edible palm oil. To date, over 181 genera including around 2600 species are listed, most of them restricted to tropical and subtropical climates. In Reunion island, 55 species of *Arecaceae* were identified and some of them are endemic, including the following three species: *Hyophorbe indica Gaertn* (local name: 'palmiste poison'), *Dictyosperma album* (Bory) Scheff. (local name 'palmiste blanc'), and *Latania lontaroides* (Gaertn.) H.E. Moore (local name: 'latanier rouge') (Figure 5.3.1). As far as we know, the chemical characterization of the seed oil (i.e. the oil content, fatty acid composition, carotenoid content…) extracted from these three endemic palms which grow inside the forest or along the coasts of the Reunion Island have not been previously investigated.

Figure 5.3.1. *Photograph of the plant, ripe fruit, seeds and extracted seed oil of the three endemic Arecaceae species of Reunion island: a) Hyophorbe indica Gaertn.; b) Dictyosperma album (Bory) Scheff.; c) Latania lontaroides (Gaertn.) H.E. Moore.*

5.3.2 Experimental

Samples collection

The ripe fruits from the three endemic plant species were wild collected in the forest area of the Reunion Island. The endemic species were authenticated by the botanist Hermann Thomas of the National Park of La Réunion.

Oil extraction from seeds

The ripe fruits were cleaned and oven-dried at 60 °C during 24 to 48 hours. The shell was cracked to remove the seeds (kernels) and dried at 60 °C for 2 hours. The seeds (1.9 – 3.8 kg) were first milled in a laboratory grinder for 30 seconds in order to obtain a fine powder. Oil extraction was then carried out using cyclohexane (99.8% purity, Carlo Erba) from 50-60g of dried seed powder by pressurized liquid extraction under nitrogen at 90 °C under 100 bar with a Dionex ASETM300 apparatus (Dionex, USA). The following experimental conditions were applied for the pressurized liquid extraction: temperature 90 °C, cells were preheated 6 min, 17 min static time, 5 min dynamic time. The cycle was repeated 5 times. This program ensures complete extraction of the neutral lipids from the sample. A flush volume of 100% of the cell was used and finally the cell was purged for 120 sec with nitrogen to collect the extract in the collection vial. The solvent was finally driven off at 40 °C using a rotary evaporator (RC 600, KNF Neuberger, France) to obtain the extracted lipids. All quantitative determinations were performed in triplicate.

Fatty acids (FAs) analysis by cryogenic-modulation two-dimensional gas chromatography-quadrupole mass spectrometry (CM GC×GC-QMS)

Derivatization FAMEs was performed as follows: 100 μL of a solution of KOH/MeOH 2N was added to 10 mg of oil sample, dissolved in 1 mL of *n*-hexane and was left to react for 5 min at room temperature. The reaction mixture was shaken for 2 min using a vortex mixing. The upper hexanic phase, containing FAMEs, was subjected to CM GC×GC-QMS analysis. All CM GC×GC-QMS analyses were carried out using a system consisting of two independent Shimadzu GC-2010 gas chromatographs, and a QP2020 quadrupole mass spectrometer (Kyoto, Japan). The

first gas chromatograph (GC1) was equipped with an AOC-20i auto-injector, and a split-splitless injector (310°C). The first column was an SLB-5ms [(silphenylene polymer, which can be considered equivalent in polarity to poly (5%diphenyl/95% dimethylsiloxane)] with dimensions 30 m × 0.25 mm ID × 0.25 μm d_f. The second column was an SLB-35ms [(polymer which can be considered equivalent in polarity to poly (35%diphenyl/65% dimethylsiloxane)] with dimensions 3 m × 0.25 mm ID × 0.25 μm d_f. A 1.5 m segment of the column was used to create the modulator loop, leaving a 1.5 m segment for the analytical separation. All the columns used were kindly provided by Merck Life Science (Merck KGaA, Darmstadt, Germany). The connections between ^{1}D and ^{2}D columns, were made by using two SilTite mini unions (Trajan, Ringwood, Victoria, Australia). Carrier gas (helium) was supplied at a pressure of 60.3 kPa. Sample (1 μL) was injected in the split mode (30:1). Temperature programs were set at 110-320°C, and 3°C/min. Modulation was performed by using a cryogenic fluid-free modulator (under license from Zoex Corporation); modulation period was 2.5 sec (the heating step was performed at 340°C, for 0.5 s). For quadrupole MS analysis, the sample was analyzed in the full scan mode with a scan speed of 20,000 amu/sec, a mass range of 45-500 *m/z* and a sampling frequency of 33 spectra/sec. The temperature of the interface was set at 310°C and the ion source temperature was set at 200°C, with analyte fragmentation induced by electron ionization (70 eV). Data were acquired by using the GC-MS solution software (Shimadzu). The MS database used was the Lipids GC-MS library v.1.0 (Shimadzu). Bidimensional chromatograms were generated using the ChromSquare software v. 2.3 (Shimadzu). FAMEs were identified by comparison of their retention times with those of pure reference standards. The fatty acid profile of the oil was obtained by relative quantification from CM GC×GC-QMS peak areas.

Extraction of the unsaponifiable fraction of the oils

Carotenoid analyses were performed on the unsaponifiable fractions of the oils. Firstly, the unsaponifiable fraction was extracted from oils (4 g) using diethyl ether (3 × 100 mL) after saponification of the oil by using 50 mL KOH/EtOH (1M) under reflux for 1 hour according to ISO standard 3596-1. Organic layer was washed with water (2 × 40 mL), aqueous solution of KOH 0.5M (1 × 40 mL), water, KOH/H_2O,

and water (4 × 40 mL) up to neutral. The organic phase was dried over anhydrous sodium sulfate, filtered and the solvent was removed on a rotary evaporator at 40 °C to obtain the unsaponifiable fraction of the oil. All quantitative determinations were achieved in triplicate.

Carotenoids determination by High Performance Liquid Chromatography-Photodiode Array detector-Mass Spectrometry (HPLC-PDA-MS)

The oil samples were fully diluted in 1 mL of a methanol (MeOH)/ Methyl-tert-butyl-ether (MTBE) (1:1) mixture, and if necessary, they were further diluted with the same solvent mixture, passed through a 0.2 um nylon filter before injection into the HPLC-PDA-MS system. The carotenoid analyses were carried out using a Nexera X2 liquid chromatography system (Shimadzu, Milan, Italy), consisting of a CBM-20A controller, four HPLC-30AD dual-plunger parallel-flow pumps, a DGU-20 A5R degasser, a CTO-20AC column oven and a SIL-30AC autosampler. A 0.1 mm ID stainless steel tubing (zero dead volume) was employed for column connection and a SPD-M30A photodiode array detector (PDA). The HPLC system was coupled to an LC-QMS-2020 mass spectrometer through an APCI source (Shimadzu, Kyoto, Japan). Data acquisition was performed by means of the LabSolutions software (Version 5.91, Shimadzu Corporation). Separations were carried out on a YMC C30 column (250 mm × 4.6 mm ID, 5 μm particle size). The mobile phases were A (MeOH/MTBE/H_2O, 81:15:4) and phase B (MeOH/MTBE/H_2O, 16:80.4:3.6); a linear gradient was used changing from 99 to 66% A in 30 min, maintaining this condition for 5 min, changing from 66 to 44% A in 15 min, keeping this condition for 5 min, changing from 44 to 22% A in 15 min and from 22 to 0% A in 5 min, returning to the initial conditions (99% A) in 5 min, and keeping this condition for 5 min. The flow rate was set at 0.8 mL/min, the column temperature was maintained at 35 °C, the UV/vis spectra were acquired between 220 and 700 nm and the chromatograms were processed at 450 nm. The LC-QMS-2020 detection was achieved through an APCI interface operated in positive and negative mode; detector voltage, 1.05 kV; interface temperature: 350 °C; DL temperature, 300 °C; heat block temperature, 300 °C; nebulizing gas flow (N_2), 2.0 L/min; drying gas flow (N_2), 5.0 L/min; scan range (positive and negative mode), 300-1200 *m/z*; event time, 0.2 s. The different carotenoids were characterized using

their UV-vis and mass spectra, their available standards and their elution order. Quantitative data were obtained by HPLC-DAD using external calibration curves from carotenoids standards, in the concentration range from 1 to 100 µg/mL at five concentrations levels. The results were obtained from the average of three determinations and the CV% was below 7% in all the LC measurements. Standard purity was above 98% and the R coefficient for the calibration curves was always above 0.9992, with LOD and LOQ values of respectively for β-carotene 0.07 and 0.1, for lutein of 0.06 and 0.18, for lycopene of 0.08 and 0.3, µg/mL. The carotenoid concentrations are expressed in ppm (mg/kg of oil).

5.3.3 Results & Discussion

The chemical characteristics of the seed oils extracted using a pressurized liquid extraction process with cyclohexane are presented in Table 5.3.1. The seed oil content ranged from 3.1% to 8.8% (*w/w*). The kernels of *Dictyosperma album* (Bory) Scheff. showed the highest oil content (8.8%) whereas *Hyophorbe indica* Gaertn. seeds had the lowest oil content (3.1%) among the studied *Arecaceae* species. Interestingly, the *H. indica* seed oil exhibited the highest content of unsaponifiable fraction (13.4 g/100g oil). The content of unsaponifiable lipids from commercial vegetable oils generally reaches 0.2 to 2.0 g/100g oil.

Table 5.3.1. *Compositional characteristics of the oils extracted from the three endemic Arecaceae species from Reunion Island.*

Plant species	Seed oil content (g/100g seed DM)[a]	Color of the extracted oil	Unsaponifiable content in oil (g/100g oil DM)[a]
Hyophorbe indica Gaertn.	*3.09 ± 0.19*	*dark orange-red*	*13.41 ± 1.50*
Dictyosperma album (Bory) Scheff.	*8.81 ± 0.08*	*dark green*	*2.76 ± 0.22*
Latania lontaroides (Gaertn.) H.E. Moore	*8.68 ± 0.29*	*pale green*	*0.74 ± 0.31*

[a]*Mean value and standard deviation of triplicate samples. DM: Dry material.*

For example, the study conducted on oil extracted from *Phoenix canariensis* date seeds (*Arecaceae*) indicated that the unsaponifiable matter content was 1.8 g/100g of seed oil [16]. The level of unsaponifiable fraction of the seed of *H. indica* was thus considered as very exceptional; in fact, a value around 13.4 (g/100g oil) is higher than the unsaponifiable fraction content of the avocado oil and shea butter (from 10 to 12

g/100g oil) which are commonly used in cosmetics for their moisturizing and softening properties (hair, scalp, skin, face, etc.). Interestingly, oil from *H. indica* also presented a dark orange-red color indicating the presence of different pigments (carotenoids).

Fatty acid profile

The analysis of the fatty acid profile of the three investigated seed oils was performed using CM GC×GC-QMS. One of the major beneficial characteristics of CM GC×GC-QMS was the high sensitivity making this technique particularly suitable for trace-level fatty acids detection in oil from fruits [17] or seeds. The bidimensional plot of the fatty acids detected in the endemic *H. indica* seed oil is shown in Figure 5.3.2.

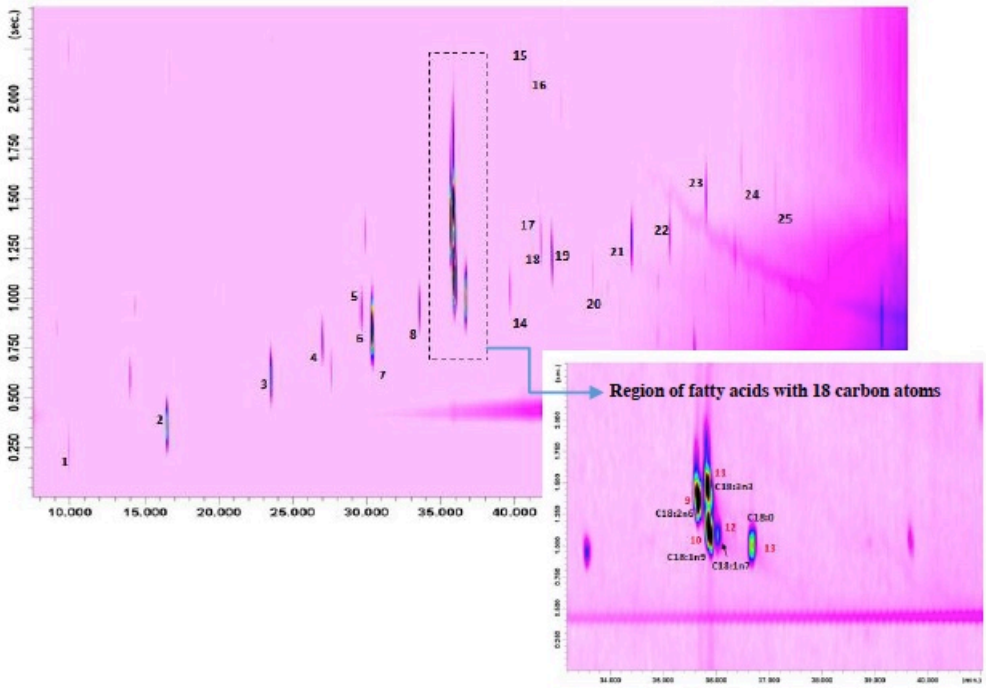

Figure 5.3.2. *Bidimensional plot of the fatty acids detected in the endemic Hyophorbe indica Gaertn. seed oil*

The identification of peaks is reported in Table 5.3.2 together with similarity (Sim.) and linear retention index (LRI).

Table 5.3.2. *Peak assignment, MS database similarity and linear retention index for Hyophorbe indica seed oil.*

Hyophorbe indica Gaertn. seed oil					
Peak	**Compound (fatty acid methyl esters)**	**Sim. %**	**LRIexp**	**LRIlibr**	**ΔLRI**
1	Me. C10:0; Caprate	93	1321	1322	-1
2	Me. C12:0; Laurate	94	1523	1523	0
3	Me. C14:0, Myristate	95	1723	1724	-1
4	Me. C15:0; Pentadecanoate	94	1824	1825	-1
5	Me. C16:1n9; (7Z)-hexadecenoate	90	1898	1897	1
6	Me. C16:1n5; 11(Z)-hexadecenoate	93	1902	1912	-10
7	Me. C16:0; Palmitate	92	1925	1925	0
8	Me. C17:0; Heptadecanoate	92	2025	2026	-1
9	Me. C18:2n6; Linoleate	96	2093	2096	-3
10	Me. C18:1n9; Oleate	95	2099	2098	1
11	Me. C18:3n3; alpha-Linoleate	90	2099	2107	-8
12	Me. C18:1n7; (E)-Vaccenate	91	2105	2107	-2
13	Me. C18:0; Stearate	93	2127	2126	1
14	Me. C19:0; Nonadecanoate	90	2226	2227	-1
15	Me. C20:2n4; Eicosa-(13,16)-dienoate	87	2273	2280	-7
16	Me. C20:2n6; Eicosa-(11,14)-dienoate	85	2295	2293	2
17	Me. C20:1n9; Eicos-(11Z)-enoate	91	2299	2298	1
18	Me. C20:1n7; Eicos-(13)-enoate	90	2300	2300	0
19	Me. C20:0; Arachidate	90	2327	2326	1
20	Me. C21:0; Heneicosanoate	90	2427	2429	-2
21	Me. C22:0; Behenate	95	2529	2528	1
22	Me. C23:0; Tricosanoate	90	2629	2629	0
23	Me. C24:0; Lignocerate	93	2730	2729	1
24	Me. C25:0; Pentacosanoate	90	2831	2830	1
25	Me. C26:0; Cerotate	85	2932	2931	1

Results indicated that twenty-five FAMEs were identified in the *H. indica* seed oil, attained through CM GC×GC-QMS (instead of 13 by 1D GC-FID; data not shown). The fatty acid compositions of *H. indica* seed oil and the two other unconventional palm oils, obtained by relative quantification from CM GC×GC-QMS peak areas, are shown in Table 5.3.3. To the best of the authors knowledge, this is the first report on the seed oil composition of these three endemic *Arecaceae* species from Reunion island.

Interestingly, *H. indica* seed oil contained approximately 50% PUFAs, 23% monounsaturated fatty acids (MUFAs), and only 27% saturated fatty acids (SFAs). Results indicated that fatty acids with 18 carbon atoms were predominant. *H. indica* seed oil contained mainly linoleic acid ($C_{18:2\omega6}$; 33.7%), oleic acid ($C_{18:1\omega9}$; 20.3%), alpha-linolenic acid ($C_{18:3\omega3}$; 16.5%), palmitic acid ($C_{16:0}$; 15.8%) and stearic acid ($C_{18:0}$; 4.5%). These findings are quite unusual and possibly a unique fatty acids composition in species belonging to the *Arecaceae* family. In fact, previous studies conducted on seed oil extracted from different palm species, including the African oil palm (*Elaeis guineensis*), indicated that palm oils are often rich in palmitic acid (43.5%) and oleic acid (36.6%), and contain some traces of ω-3 PUFAs (<0.5% to total fatty acids) [18]. Another study conducted on oil extracted from *Phoenix canariensis* date seeds, belonging to *Arecaceae* family as well, indicated that the main fatty acids of oil were oleic (50.1%), linoleic (19.2%), lauric (10.2%), palmitic (9.8%) and stearic (7.5%) acids [16]. Furthermore, the *H. indica* seed oil investigated here

presented an optimal ω6/ ω3-PUFAs ratio close to 2:1. Ideally, a fatty acid profile rich in PUFAs with a ω6/ ω3-PUFAs ratio lower than 4:1 in diet is recommended to reduce the risk of chronic diseases [19]. By comparison, edible palm oil showed an ω6/ ω3-PUFAs ratio of about 47:1 because the palm oil contained only 10% ω6-PUFAs and <0.5% ω3-PUFAs (and approximatively 50% SFAs and 40% MUFAs) [18].

Table 5.3.3. *Fatty acids identification and composition (%) of the three seed oils obtained from endemic Arecaceae species from Reunion Island.*

Peak number (Fig.S2)	Fatty acid methyl ester (FAMEs) identification	*H. indica* (%)	*D. album* (%)	*L. lontaroides* (%)
n.i	C6:0, Caproate	*n.d*	*n.d*	*n.d*
n.i	C8:0, Caprylate	*n.d*	*n.d*	*1.77*
1	C10:0, Caprate	*0.14*	*0.93*	*1.05*
2	C12:0, Laurate	*1.89*	*20.93*	*34.14*
3	C14:0, Myristate	*1.18*	*16.14*	*22.96*
4	C15:0, Pentadecanoate	*0.39*	*0.08*	*n.d*
7	C16:0; Palmitate	*15.80*	*13.62*	*9.90*
8	C17:0: Heptadecanoate	*0.51*	*0.10*	*0.04*
13	C18:0; Stearate	*4.49*	*5.4*	*4.20*
14	C19:0; Nonadecanoate	*0.17*	*n.d*	*n.d*
19	C20:0; Arachidate	*0.61*	*0.21*	*0.09*
20	C21:0; Heneicosanoate	*0.10*	*n.d*	*n.d*
21	C22:0; Behenate	*0.74*	*0.10*	*0.03*
22	C23:0; Tricosanoate	*0.26*	*0.007*	*n.d*
23	C24:0; Lignocerate	*0.52*	*0.35*	*0.09*
24	C25:0; Pentacosanoate	*0.08*	*n.d*	*n.d*
25	C26:0; Cerotate	*0.04*	*0.18*	*n.d*
	∑ SFAs	**26.9 %**	**58.0 %**	**74.3 %**
	- MUFA Omega-9:			
5	C16:1ω9; cis-7 hexadecenoate	*0.07*	*0.06*	*n.d*
10	C18:1ω9; Oleate	*20.29*	*22.49*	*21.01*
17	C20:1ω9; Gondoate	*0.08*	*0.32*	*0.09*
	- MUFA Omega-7:			
12	C18:1ω7; cis-Vaccenate	*1.78*	*0.38*	*0.04*
18	C20:1ω7; Paulinate	*0.05*	*0.24*	*0.10*
	- MUFA Omega-5 & Omega-11			
6	C16:1ω5; 11(Z)-hexadecenoate	*0.43*	*0.38*	*n.d*
	∑ MUFAs	**22.7 %**	**23.9 %**	**21.2 %**
	- PUFA Omega-6:			
9	C18:2ω6; Linoleate	*33.70*	*16.91*	*4.46*
16	C20:2ω6; Eicosa-(11Z,14Z)-dienoate	*0.11*	*0.05*	*n.d*
	- PUFA Omega-3:			
11	C18:3ω3; alpha-Linolenate	*16.46*	*1.13*	*0.03*
	- Other PUFA :			
15	C20:2ω4; Eicosa (13,16)-dienoate	*0.12*	*n.d*	*n.d*
	∑ PUFAs	**50.4 %**	**18.1 %**	**4.5 %**
	ω6/ω3-PUFA ratio	**2 : 1**	**15 : 1**	**n.d**
	Edible oil equivalent	Oil rich in ω3	Oil rich in SFA	Oil rich in SFA

n.i.: not identified; n.d: not quantified/not detected; Peak numbers only refer to the identifications reported in Figure 5.3.2 relative to the bidimensional plot of *H. indica* seed oil. SFAs: saturated fatty acids. MUFAs: monounsaturated fatty acids. PUFAs: polyunsaturated fatty acids (unsaturation ≥2). ω6/ω3-PUFA ratio: ratio between ω-6 and ω-3 PUFA fatty acids.

Some trace-level long-chain MUFAs and PUFAs fatty acids [e.g. the (E)-vaccenic acid ($C_{18:1\omega7}$; 1.8%), the eicos-(11Z)-enoic acid or gondoic acid ($C_{20:1\omega9}$; 0.08%), the eicos-(13)-enoic acid or paulinic acid ($C_{20:1\omega7}$; 0.05%), the eicosa-(11,14)-dienoic acid ($C_{20:2\omega6}$; 0.11%), and the eicosa-(13,16)-dienoic acid ($C_{20:2\omega4}$; 0.12%)] were also identified by CM GC×GC-QMS in *H. indica* seed oil, with others long-chain SFAs like arachidic acid ($C_{20:0}$; 0.61%), behenic acid ($C_{22:0}$; 0.74%), and lignoceric acid ($C_{24:0}$; 0.52%) (Figure 5.3.2). Some of these long-chain fatty acids, in particular,

gondoic acid, paulinic acid and the eicosa-(13,16)-dienoic acid, can rarely be found in seed oils. The high content of ω6-PUFAs (linoleic acid; 34%), ω3-PUFAs (alpha-linolenic acid; 17%) and MUFAs (oleic acid; 20%), made the *H. indica* oil attractive for its potential use in healthy formulations, paint and coatings, or oleochemical applications. However, from a nutraceutical point of view, research on the chemical composition of the *H. indica* seed oil was very limited, if any at all, and it could be considered to be reasonably foreseeable that this unconventional palm oil might be toxic by ingestion (the toxicological profile of this oil was not known). For example, some ornamental palms, for instance sago and betel nut palms, both belonging to *Arecaceae* family as well, were poisoning, due to the presence of cycasin and arecoline [20, 21]. So, clinical trials are needed before the *H. indica* seed oil can be recommended to treat any health conditions.

The seed oil extracted from *Dictyosperma album* (Bory) Scheff. (8.8% dry weight of oil) had a similar fatty acid composition to edible palm oil. In fact, *D. album* seed oil contained approximately 58% saturated fatty acids, 24% monounsaturated fatty acids, and 18% polyunsaturated fatty acids (Table 5.3.3). The seed oil contained mainly lauric acid ($C_{12:0}$; 20.9%), myristic acid ($C_{14:0}$; 16.1%), palmitic acid ($C_{16:0}$; 13.6%), oleic acid ($C_{18:1\omega9}$; 22.5%), and linoleic acid ($C_{18:2\omega6}$; 16.9%). The *Latania lontaroides* (Gaertn.) H.E. Moore seed oil (8.7% dry weight of oil) showed even higher SFA content (74% *w/w* of total fatty acids) (Table 5.3.3), and its fatty acid composition was approaching the one of the palm kernel oil. These findings suggested that unconventional seed oils of *D. album* and *L. lontaroides* can be useful for oleochemical applications at least, like the palm oil already used in Europe for these purposes.

Seed oil carotenoids composition

The HPLC carotenoid profiles of the three investigated seed oils are shown in Figure 5.3.3, and the carotenoids content and their relative composition (%) in oil are shown in Table 5.3.4.

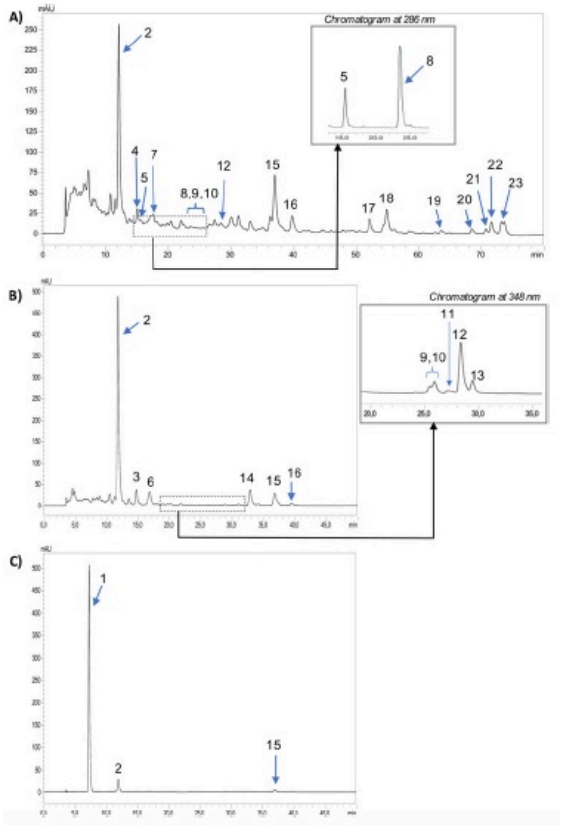

Figure 5.3.3. *HPLC-PDA chromatograms (extracted at λ450 nm) of the carotenoids in the three seed oils obtained from endemic Arecaceae species from Reunion Island: Hyophorbe indica Gaertn. (A), Dictyosperma album (Bory) Scheff. (B), and Latania lontaroides (Gaertn.) H.E. Moore (C). The insert in (A) showing compounds 5 (phytoene isomer-1) and 8 (phytoene isomer-2) was extracted at λ286nm; and insert in (B) showing compounds 9–13 (phytofluene isomers) was extracted at λ348nm. For compounds identification, see Table 5.3.4.*

Lutein was by far the most abundant carotenoid in the seed oils of *H. indica* (A) and *D. album* (B), respectively 41% and 70% to total carotenoids, followed in both oils by also a good percentage of β-carotene (21% and 7%, respectively, in *H. indica* and *D. album* seed oil); this is in agreement with the generally reported higher content of lutein compared to the other carotenoids in oilseeds of many plants that often store carotenoids in specialized plastids [22]. Lutein was considered extremely important in the prevention of macular diseases and cognitive function [23, 24], while β-carotene was being the most important provitamin A carotenoid. The seed oil of *L. lontaroides* also showed the presence of lutein and β-carotene, but its main carotenoid (88%) was a very early eluting compound which has not yet been identified. The author

hypothesis is that it might be an apocarotenoid. Further work is in progress aimed at its structure elucidation.

Table 5.3.4. *Carotenoids content and relative carotenoids composition (%) of the three seed oils obtained from endemic Arecaceae species from Reunion Island.*

				H. indica		*D. album*		*L. lontaroides*	
Unsaponifiable content in oil (g/100g)				13.41 ± 1.50		2.76 ± 0.22		0.74 ± 0.31	
Oil color:				orange-red		dark-green		pale-green	
Peak number	**t_R (min)**	**Carotenoids**	**[M]$^+$ (m/z)**	**Quantification in mg kg^{-1} oil** (rel.% in brackets)					
1	7.3	n.i. (unknown compound)	411	n.d.	–	n.d.	–	5.1	(87.9%)
2	**12.2**	**all-*trans*-lutein**	**568**	**45.2**	**(41.1%)**	**14.2**	**(70.0%)**	**0.5**	**(8.6%)**
3	14.7	9-*cis* or 9′-*cis*-lutein	568	n.d.	–	1.2	(5.9%)	n.d.	–
4	15.1	n.i. (unknown compound)	n.d.	n.q.	–	n.d.	–	n.d.	–
5	15.5	phytoene isomer-1	n.d.	n.q.	–	n.d.	–	n.d.	–
6	16.6	9-*cis* or 9′-*cis*-lutein	568	n.d.	–	1.5	(7.4%)	n.d.	–
7	17.2	phytofluene isomer-1	542	n.q.	–	n.d.	–	n.d.	–
8	23.5	phytoene isomer-2	n.d.	n.q.	–	n.d.	–	n.d.	–
9	25.4	phytofluene isomer-2	542	n.q.	–	n.q.	–	n.d.	–
10	25.8	phytofluene isomer-3	542	n.q.	–	n.q.	–	n.d.	–
11	27.2	phytofluene isomer-4	542	n.q.	–	n.q.	–	n.d.	–
12	28.4	phytofluene isomer-5	541	n.q.	–	n.q.	–	n.d.	–
13	29.4	phytofluene isomer-6	541	n.q.	–	n.q.	–	n.d.	–
14	33.0	*all*-trans-α-carotene	536	n.d.	–	1.5	(7.4%)	n.d.	–
15	**37.1**	***all*-trans-β-carotene**	**536**	**22.9**	**(20.8%)**	**1.5**	**(7.4%)**	**0.2**	**(3.4%)**
16	39.8	9-*cis*-β-carotene	536	7.1	(6.4%)	0.4	(2.0%)	n.d.	–
17	52.2	n.i. (unknown compound)	536	n.q.	–	n.d.	–	n.d.	–
18	**54.9**	***cis*-lycopene isomer-1**	**536**	**11.5**	**(10.4%)**	n.d.	–	n.d.	–
19	63.7	*cis*-lycopene isomer-2	536	2.5	(2.3%)	n.d.	–	n.d.	–
20	68.5	*cis*-lycopene isomer-3	536	3.1	(2.8%)	n.d.	–	n.d.	–
21	70.8	*cis*-lycopene isomer-4	536	2.9	(2.6%)	n.d.	–	n.d.	–
22	71.7	*cis*-lycopene isomer-5	536	5.8	(5.3%)	n.d.	–	n.d.	–
23	73.2	*cis*-lycopene isomer-6	536	9.1	(8.3%)	n.d.	–	n.d.	–
		Total carotenoids (mg kg^{-1} oil):		**110.1**		**20.3**		**5.8**	

n.i.: not identified; n.d.: not detected; n.q.: detected, but not quantified; Peak numbers refer to the identifications reported in Figure 5.3.3.

Interestingly, only in the seed oil of *H. indica* was detected a good amount (34.9mg/kg oil, i.e. 23% to total carotenoids) of different lycopene isomers; both *D. album* and *L. lontaroides* did not show the presence of lycopene. Lycopene has been related to the prevention of some type of cancer and cardiovascular diseases [25]. Furthermore, the HPLC carotenoid profile relative to *H. indica* seed oil (Figure 5.3.3) shows the detection of different isomers of phytofluene (carotenoid precursor) and two isomers of one other 'invisible' carotenoid precursor, phytoene (detected, but not quantified). Phytoene has lately received greater attention in the literature [26] as evidence is accumulating that it may provide health and cosmetic benefits. So, the health beneficial properties attributed to lutein, β-carotene, lycopene, and phytoene, certainly provide very interesting properties to the studied seed oils, especially the *H. indica* one which contained 110mg of total carotenoids per kg of crude oil (Table 5.3.4).

The roles of carotenoids in oilseeds are less clear than in other tissues, but there are evidences of their important role for the abscisic acid (ABA) production, seed

dormancy and their contribution to the antioxidant system in the oilseeds [22]. For example, the crude red palm oil from *E. guineensis* [27] and the unconventional crude seed oils of *Brazilian Passiflora* species [28] have been reported to contain very high amounts, in the order of several hundred mg/kg oil, of total carotenoids content. Then taking into consideration that according to the classification proposed by Britton and Khachik [7], the carotenoid content in fruits and vegetable can be regarded as low (0-100 mg/100 g), moderate (100-500 mg/100 g), high (500-2000 mg/100 g) and very high more than 2000 mg/100 g, the high content of carotenoids determined in *H. indica* oil (110mg/kg oil, i.e. approximatively 357 mg/100 g seeds, taking into account the oil yield), provides evidence for the potential use of these natural compounds in healthy formulations. From a nutraceutical point of view, and provided that this endemic palm oil was not toxic for humans, these high-value carotenoids in *H. indica*, in particular, lutein, β-carotene, and lycopene, which were detected in a high content (respectively 45.2, 22.9 and 34.9mg/kg oil in crude oil) might be use to formulate new nutraceutical and pharmaceutical products.

5.3.4 Conclusions

The works presented in this study investigated for the first time the chemical characterization of three unconventional seed oils from endemic *Arecaceae* species from Reunion Island. First, results revealed the particular composition of the unconventional red seed oil from the ripe fruits of *Hyophorbe indica* Gaertn. This seed oil contained a high degree of unsaturation (50% of polyunsaturated fatty acids), which is possibly a unique fatty acid composition in the *Arecaceae* family. The crude *H. indica* seed oil was interesting because it is high in ω6-PUFAs (linoleic acid; 34%), in ω3-PUFAs (alphalinolenic acid; 17%), in MUFAs (oleic acid; 20%), and very rich in valuable carotenoids, such as lutein, β-carotene and lycopene, that could be exploited due to their beneficial properties on human health. However, the food safety and toxicology of the red oil from this endemic palm species of Reunion Island was not known, and clinical trials are needed before the *H. indica* oil can be recommended to treat any health conditions.

Then, the two other unconventional *D. album* and *L. lontaroides* seed oils contained high level of saturated fatty acids very similar to that of the palm and palm kernel oil,

respectively. So, they can be useful for oleochemical applications at least, like the palm oil used in Europe for these purposes. Although unconventional seed oil crops could offer new opportunities, properties and functionalities for the global market, they lack the years of research, improvements, and experience that have been invested in conventional oilseeds. An important need for any industrial applications is to increase productivity, and enhance the oil and unsaponifiable yields.

References:

[1] P.C. Calder, Eur. J. Lipid Sci. Technol. 116 (2014)1280.

[2] K.J. Bowen, W.S. Harris, P.M. Kris-Etherton, Curr Treat. Options Cardiovasc. Med. 18 (2016) 16.

[3] J.M. Kremer, Am. J. Clin. Nutr. 71 (2000) 349.

[4] J.C. Maroon, and J.W. Bost, 2006. Surg. Neurol. 65 (2006) 326.

[5] R. Zárate, N. El Jaber-Vazdekis, N. Tejera, J.A. Pérez, C. Rodríguez, Clin. Transl. Med. 6 (2017) 19.

[6] H.J. Lee, Y.M. Han, J.M. An, E.A. Kang, Y.J. Park, J.Y. Cha, K.B. Hahm, Expert Rev. Anticancer Ther. 18 (2018) 1189.

[7] G. Britton, and F. Khachik, in: Carotenoids, Birkhäuser (2009).

[8] R.K. Saini, S.H. Nile, S.W. Park, Food Res Int. 76 (2015) 735.

[9] E.M. Yahia, J. de Jesús Ornelas-Paz, T. Emanuelli, E. Jacob-Lopes, L.Q. Zepka, B. Cervantes-Paz, in: Fruit and vegetable phytochemicals: chemistry and human health, John Wiley & Sons Ltd (2017).

[10] L. Cassiday, Inform. 29 (2018) 6.

[11] M. Friedman, J. Agric. Food Chem. 61 (2013) 10626.

[12] D.A. Ofori, K. Kehlenbeck, M. Munjuga, R. Jamnadass, E.K. Asaah, C. Kattah, F. Rutatina, Acta Hortic. 979 (2013) 311.

[13] S.L. Crockett, Int. J. Mol. Sci. 16 (2015) 22333.

[14] A.M.M. Guedes, R. Antoniassi, A. Ferreira de Faria-Machado, OCL. 24 (2017) 507.

[15] R.M. Ojeda-Amador, G. Fregapane, M.D. Salvador, Food Chem. 240 (2018) 123.

[16] I. Nehdi, S. Omri, M.I. Khalil, S.I. Al-Resayes, Ind. Crops Prod. 32 (2010) 360.

[17] P.Q. Tranchida, A. Giannino, M. Mondello, D. Sciarrone, P. Dugo, G. Dugo, L. Mondello, J. Sep. Sci. 31(2008) 1797.

[18] V. Dubois, S. Breton, M. Linder, J. Fanni, M. Parmentier, OCL. 15 (2008) 56.

[19] A.P. Simopoulos, Nutrients 8 (2016) 128.

[20] A.D: Kinghorn, in: Handbook of natural toxins, Marcel Dekker (1983).

[21] G.M. Williams, Food Addit. Contam. 1 (1984) 173.

[22] C.A. Howitt, and B.J. Pogson, Plant Cell Environ. 29 (2006) 435.

[23] N.I. Krinsky, J.T. Landrum, R.A. Bone, Annu. Rev. Nutr. 23 (2003) 171.

[24] M. Le, and L. Xiao-Ming, J. Sci. Food Agric. 90 (2010) 2.

[25] L. Arab, and S. Steck, Am. J. Clin. Nutr. 71 (2000) 1691.

[26] A. Melendez-Martinez, P. Mapelli-Brahm, C.M. Stinco, J. Food Comp. Anal. 67 (2018) 91.

[27] J.M. Lecerf, OCL. 20 (2013) 147.

[28] F.C. De Santana, F.B. Shinagawa, E.D.S. Araujo, A.M. Costa, J. Mancini-Filho, J. Food Sci. 80 (2015) 2647.

5.4 Towards the determination of an equivalent standard column set between cryogenic and flow-modulated comprehensive two-dimensional gas chromatography†

This preliminary research is focused on the task of defining an equivalent standard column set between cryogenic and flow-modulation GC×GC combined with MS. Cryogenic modulation was carried out by using a loop-type device, while the flow modulator used was a seven-port wafer chip, equipped with an external accumulation loop.

Initially, a common low-polarity + mid-polarity CM GC×GC column set was selected (30 m × 0.25 mm ID × 0.25 μm d_f + 1.5 m × 0.25 mm ID × 0.25 μm d_f), a method was developed, and a GC×GC-MS fingerprint was attained (on a sample of bio-oil derived from coconut fibers). After, a column set with the same stationary phases was selected for the flow modulation GC×GC-MS method (20 m × 0.18 mm ID × 0.18 μm d_f + 5 m × 0.32 mm ID × 0.25 μm d_f), with the capability to provide a-similar-as-possible separation. A side-by-side measurement of several chromatography parameters (efficiency, peak capacity, resolution, peak widths, retention factors, elution temperatures) was made.

†This section has been adapted from the following publication: **I. Aloisi**, T. Schena, B. Giocastro, M. Zoccali, P.Q. Tranchida, E.B. Caramão, and, L. Mondello in "Towards the determination of an equivalent standard column set between cryogenic and flow-modulated comprehensive two-dimensional gas chromatography", Analytica Chimica Acta, 1105, (2020) 231-236.

5.4.1 Introduction

Comprehensive two-dimensional gas chromatography separations are carried out on two columns linked in sequence, with a modulator located at some point between them [1]. The modulator, it being either flow or cryogenic, enables continuous (throughout the analysis) processes of isolation and re-injection of chromatography bands from the first to the second column.

Several cryogenic and flow modulation devices have been described over the past two decades, with thorough details reported in the literature [2,3]. Focus will be herein given to cryogenic loop-type modulation [2,3], and to a flow modulation model, stemming from an approach introduced by Seeley et al. in 2006 [4]; the latter transfer device was constructed by using two T-unions (one upstream, and the other downstream), three fused-silica capillary columns, and a two-way solenoid valve (positioned outside the GC oven), with the latter linked to an auxiliary gas source. Two capillaries linked the unions to the valve outlet ports, while the remaining capillary bridged the two unions and acted as accumulation loop. The remaining port of each union was connected to the ^{1}D – upstream, and to a 10 cm segment of 0.25 mm ID capillary tubing (downstream union), which in turn was linked to a T union, this being connected to two ^{2}D columns. During the accumulation step, the gas flow from the auxiliary source was directed to the downstream union allowing the ^{1}D effluent to enter the loop. At the end of the accumulation process, the gas flow from the auxiliary source was directed to the upstream union, enabling the rapid flushing of the loop (re-injection step). The accumulation and re-injection steps were performed in 1.4 s and 0.1 s, respectively. A gas flow of 20 mL min^{-1} was used for efficient loop flushing, and was split equally between two ^{2}D 5 m × 0.25 ID columns, each connected to a flame ionization detector (FID).

In later research, and following the FM model proposed by Seeley et al., a seven-port wafer chip, with internal micro-channels and an external accumulation loop, was evaluated in FM GC×GC- FID applications [5]. In this and other FM studies, high ^{2}D gas flows were used [5-8]. The generation of high gas flows can be considered as a main drawback, especially if MS detection is required.

In recent work, it has been shown that an efficient re-injection process can be performed at greatly reduced gas flows (6–8 mL min^{-1}) simply by extending the re-

injection period [9]. The straightforward concept is that a re-injection period of 100 ms, at a gas flow of 24 mL min^{-1}, is equivalent to a re-injection period of 300 ms, at a gas flow of 8 mL min^{-1}. In following related FM GC×GC-MS research, a 0.53 mm ID ^{2}D column was used to benefit from the vacuum outlet conditions, leading to the introduction of the term "low-pressure comprehensive 2D GC" (GC×LP GC). Additionally, it was demonstrated that the use of a longer accumulation loop, enabling two accumulation + two re-injection processes (dual stage), had a beneficial effect on peak shape [10].

This preliminary investigation is based on the task of determining an equivalent standard column set between cryogenic- and flow-modulation GC×GC. Cryogenic modulation was carried out by using a loop-type device; the FM device used was a seven-port wafer chip, with the seventh port closed [the seventh port is normally used if dual detection (e.g., MS and FID) is required]. The flow modulator used can be considered as a compact version of the device introduced by Seeley et al. [4].

5.4.2 Experimental

Sample, standard compounds, and sample preparation

A sample of bio-oil (produced through pyrolysis of coconut fibers) was diluted in dichloromethane at a concentration of 10,000 and 20,000 ppm (*v/v*). Two internal standards (ISs) were used (naphthalene-d_8 and acenaphthene-d_{10}), each at a concentration of 166 mg L^{-1}. The presence of the ISs for the scope of quantification was not exploited in the present research. The standard compounds were purchased from Merck Life Science (Merck KgaA, Darmstald, Germany).

Instrumentation

Cryogenic-modulation GC×GC-MS

The CM GC×GC-MS analysis was performed on a loop-type modulator Shimadzu GC×GC-MS system, consisting of two independent (GC2010) gas chromatographs (GC1 and GC2) [11], and a QP2010 Ultra single quadrupole mass spectrometer (Kyoto, Japan). The first GC system was equipped with a split/splitless injector, which was maintained at a temperature of 280°C. Injected volume was: 1 μL (of the 10,000 ppm solution), at a split ratio of 20:1.

The capillary columns used were: 30 m × 0.25 mm ID × 0.25 μm d_f [SLB-5ms - silphenylene polymer with similar polarity to poly(5% diphenyl/95% dimethyl siloxane)] in the 1D and 1.5 m × 0.25 mm ID × 0.25 μm d_f [SLB-35ms - proprietary polymer with similar polarity to poly(35% diphenyl/65% dimethyl siloxane) in the 2D. An uncoated capillary column, with dimensions 1.5 m × 0.18 mm ID, was used as delay loop. The columns were heated as follows: 50°C-330°C at 6°C min^{-1} (in both GC ovens). Such a choice was also related to the fact that the FM GC×GC-MS instrument was composed of a single GC oven.

Carrier gas (He) conditions: constant linear velocities of approx. 18.5, 80.4, and 103.9 cm s^{-1}, were generated in the first dimension, the delay loop, and the second dimension, respectively. Gas flow was approx. 0.41 mL min^{-1} (injection pressure: ≈ 9 kPa) at the beginning and 0.35 mL min^{-1} (injection pressure: ≈ 72 kPa) at the end of the analysis. Such gas velocity and flow values can be calculated as previously described [12], by considering the pressures at the ^{1}D column inlet and outlet (or inlet of the delay loop), and the ^{2}D column inlet (or outlet of the delay loop) and outlet (vacuum conditions). A simple alternative, exploited in this case, was to use a dedicated software (GC×GC flow calculation software, Shimadzu).

Modulation was carried out by using a liquid nitrogen free chiller unit (ZX2 - under license from Zoex Corporation). The loop-type modulator is characterized by a vertical cold jet, which operates continuously throughout the GC×GC-MS analysis, and a horizontal hot jet which is activated for a specific time at pre-determined intervals. Both jets are directed onto two overlapping points of the delay loop, one upstream and the other downstream. Modulation period was 4.0 s, with a hot pulse (280°C) duration of 0.2 s.

Mass spectrometry conditions: interface and ion source temperatures were maintained at 250°C; ionization was performed through electron ionization (70 eV), over the mass range *m/z* 35-500. Spectral generation frequency was 33 Hz.

Data processing was performed by using the ChromSquare software v. 2.3 (Shimadzu). Mass spectral databases used were FFNSC 3.0 and Wiley registry 11th edition/NIST 2017 mass spectral library.

Flow-modulation GC×GC-MS

The FM GC×GC-MS applications were carried out on a Shimadzu GCMS-TQ8040 system. The GC system was equipped with a split/splitless injector, which was maintained at a temperature of 280°C. The injected volume was: 1 μL (of the 20,000 ppm solution), at a split ratio of 10:1.

The capillary columns used were: 20 m × 0.18 mm ID × 0.18 μm d_f(SLB-5ms) in the first dimension and 5 m × 0.32 mm ID × 0.25 μm d_f (SLB-35ms) in the second dimension. The columns were heated as follows: 50°C-330°C at 6°C min^{-1}.

A seven-port wafer chip was located inside the GC oven and was connected to a three-way solenoid valve by using two symmetric 1.07 m stainless steel tubings of dimensions 0.97 m × 0.51 mm ID + 0.10 m × 0.25 mm ID. Gas flow was supplied to the solenoid valve through an auxiliary pressure control (APC) unit. The modulator loop (stainless steel) was of dimensions 40 cm × 0.51 mm ID (volume = 78.6 μL). The seventh port was blocked. The modulator used in the present study was characterized by 5 ports on the front face and by 2 ports on the back, with the latter connected to the valve via the stainless steel tubing.

Carrier gas (He) conditions: average ^{1}D gas velocity was 12.3 cm s^{-1} [gas flow was approx. 0.24 mL min^{-1} (injection pressure: ≈ 61 kPa) and 0.20 mL min^{-1} (injection pressure: ≈ 155 kPa) at the beginning and at the end of the analysis, respectively]; loop gas velocity was about 1.9 cm s^{-1} during accumulation and approx. 68.0 cm s^{-1} during re-injection; the average ^{2}D gas velocity was approx. 257 cm s^{-1} [gas flow was approx. 8.4 mL min^{-1} (re-injection pressure: ≈ 13 kPa) and 7.1 mL min^{-1} (re-injection pressure: ≈ 79 kPa), at the beginning and at the end of the analysis, respectively].

Approximate gas flows (and velocities) were derived with the support of the HP flow calc. 2.0 (Hewlett–Packard) software, and were calculated as follows: ^{1}D gas flow: ^{1}D column inlet pressure and the APC pressure (as outlet pressure), with a pressure reduction due to the 0.10 m × 0.25 mm ID stainless steel tubing linked to the modulator (the contribution of the 0.97 m × 0.51 mm ID portion on the APC pressure drop was considered to be negligible); ^{2}D gas flow: the APC pressure as inlet pressure, with a pressure reduction due to the 0.10 m × 0.25 mm ID stainless steel tubing linked to the modulator (the contribution of the 0.97 m × 0.51 mm ID portion on the APC pressure drop was considered to be negligible) and the outlet vacuum conditions; loop flow

during accumulation: ^{1}D gas flow; loop flow during re-injection: ^{2}D gas flow. It is noteworthy that the calculations were made by not considering restrictions inside the wafer chip (internal channels).

Modulation period was 4.0 s, with a re-injection period of 0.4 s.

Mass spectrometry conditions (the triple quadrupole mass spectrometer was used in the scan mode): interface and ion source temperatures were maintained at 220°C; ionization was performed through electron ionization (70 eV), over the mass range *m/z* 45-450. Spectral generation frequency was 33 Hz.

5.4.3 Results & Discussion

Outline of the research

The CM GC×GC-MS applications were carried out by using a single quadrupole mass spectrometer, whereas a triple quadrupole one (in the scan mode) was used in the FM ones. The ion sources in the two MS systems were the same. Furthermore, in the triple quadrupole MS instrument the first quadrupole and the collision cell were operated only as "fly through" zones, while the second quadrupole was operated by using the same acquisition frequency as that of the single quadrupole MS instrument. Such a procedure was considered as acceptable because the objective of the research was to define an equivalent standard column set, in terms of the overall separation performance.

Very simply, and initially, a standard CM GC×GC-MS column set was selected, a method was developed, and a GC×GC-MS fingerprint was attained (on a sample of bio-oil derived from coconut fibers). After, a column set was selected for the FM GC×GC-MS method, with the capability to provide a-similar-as-possible separation. With the FM column combination providing a comparable result with respect to that of the standard CM column set, then these can be considered (to a certain degree) as equivalent. In view of the results hereafter reported, the FM set of columns is proposed as a possible standard column combination.

The CM GC×GC-MS method

Cryogenic-modulation GC×GC-MS analyses are usually carried out by using a 30-60 m × 0.25 mm ID column in the first dimension and a 1-2 m ^{2}D column characterized

by a 0.1 mm ID or the same ID as that of the 1D column [13]. Such a selection can be considered as a standard choice.

In the present study, a (low-polarity + mid-polarity) 30 m × 0.25 mm ID × 0.25 µm d_f + 1.5 m × 0.25 mm ID × 0.25 µm d_f combination of columns was used, with a 1.5 m × 0.18 mm ID uncoated column used as delay loop, to enable two accumulation and two re-injection processes (dual-stage modulation). The phase ratio of both analytical dimensions equaled approx. 250. The GC×GC-MS system was operated in the constant average linear velocity (ALV) mode: the ^{1}D gas ALV was approx. 18.5 cm s^{-1} (void-time: ≈ 162 s), the intra-loop one about 80 cm s^{-1}, and the ^{2}D gas ALV circa 100 cm s^{-1} (void-time: 1.5 s).

The He ^{1}D velocity was lower than the ideal value (≈ 30-40 cm s^{-1}), with a potential highest column efficiency of about 120,000 theoretical plates (N). With regards to the ^{2}D, a 1.5 m × 0.25 mm ID × 0.25 µm d_f column, operated under optimum GC-MS conditions, should generate about 6000 N [14]. The modulation period was 4.0 s, with a re-injection time of 0.2 s (280°C). Both columns were heated from 50°C to 330°C, at 6°C min^{-1}.

The developed CM GC×GC-MS method was applied to the analysis of bio-oil, the resulting chromatogram of which is shown in Figure 5.4.1A. Considering an analyte elution time window of 40 min (2400 s), corresponding to 600 modulations, this would lead to an overall potential N value of: 600 × 6000 = 3,600,000. In this approximate calculation, the ^{1}D N value has not been included.

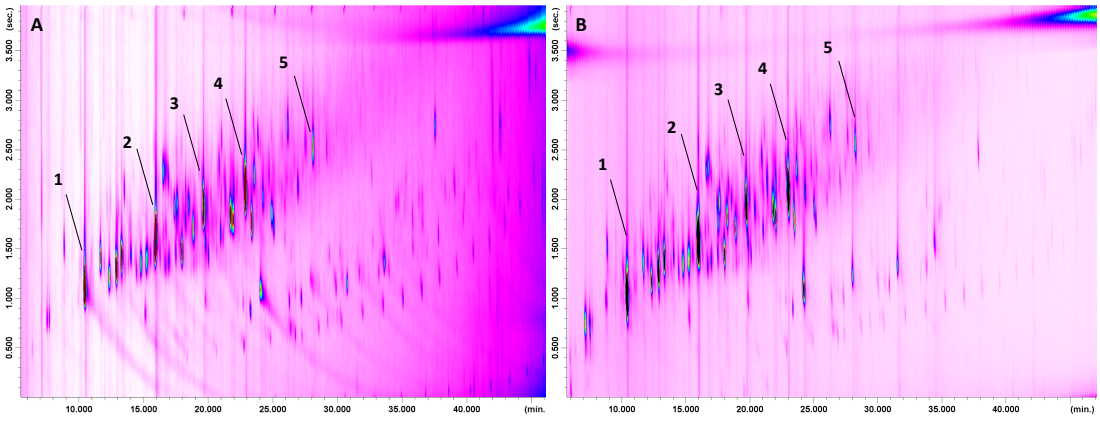

Figure 5.4.1. *A cryogenically-modulated (in A) and a flow-modulated (in B) GC×GC-MS chromatogram of coconut-derived bio-oil. Peak identity can be found in Table 5.4.1.*

The FM GC×GC-MS method

In FM applications, it is widespread practice to use a rather long wider-bore column in the second dimension [5-10], to accommodate the rather large sample volumes deriving from the modulator loop. Even so, there is no real standard set of columns used in FM GC×GC.

In the present study, a 20 m × 0.18 mm ID × 0.18 μm d_f column was used in the first dimension and a 5 m × 0.32 mm ID × 0.25 μm d_f one in the second dimension. The types of stationary phase and the temperature program were obviously the same as used in the CM analysis. The phase ratio of the ^{1}D column was approx. 250, while that of the second column was approx. 320. Ideally, and if available in the laboratory, a ^{2}D column with a phase ratio of 250 would have been used. A sample amount 4× higher was introduced onto the ^{1}D column in the FM analysis, to compensate for the higher sensitivity of CM. Such a choice was made purely on the basis of previous experience made on the two types of modulators.

The injector pressure applied generated a ^{1}D ALV of approx. 12.3 cm s^{-1} (a flow of about 0.24 mL min^{-1} at the beginning of the analysis), corresponding to a void time of about 163 s. The ^{1}D outlet pressure considered was that provided by the APC unit during accumulation (with a pressure reduction due to the stainless steel tubing linked to the modulator; see section 5.4.2.2.2.). With regards to the ^{2}D, a constant ALV of approx. 260 cm s^{-1} was generated by the auxiliary pressure, corresponding to a void time, in this case, of about 1.9 s. The ^{2}D outlet pressure was obviously that of the mass spectrometer. The ^{1}D void times in the CM and FM applications can be considered as equal. On the other hand, the ^{2}D void time in the FM method was slightly higher (1.9 s *vs.* 1.5 s), a factor in part counterbalanced by the higher phase ratio (retention factors will slightly decrease).

The ^{2}D column used was operated at a very high gas linear velocity, and presumably far from its ideal separation potential (≈ 15,600 *N*). On the other hand, the use of low ^{1}D gas flow conditions is related to the necessity to avoid the occupation of an excessive volume of the loop, during the accumulation step (a factor leading to breakthrough). Such ^{1}D He velocity conditions were again lower than ideal, with a potential highest column efficiency of ≈ 110,000 *N*. The ^{2}D gas flow was calculated to be 8.4 and 7.1 mL min^{-1}, at the beginning and at the end of the analysis, respectively.

Such values are admittedly high, but well within the pumping capacity of the mass spectrometer used (15 mL min^{-1}). Moreover, the use of a relative long accumulation loop (40 cm × 0.51 mm ID) enabled two accumulation and two re-injection processes, with the scope of improving peak shape as previously demonstrated [10]. Modulation period was 4.0 s, with a pulse time of 0.4 s. More specifically, an accumulation (3.6 s) ➔ re-injection (0.4 s) ➔ accumulation (3.6 s) process occurred within the loop, prior to the final re-injection step (0.4 s) which enabled the transfer of the chromatography band onto the 2D. On the basis of flow calculations (see section 5.4.2.2.2.) it was anticipated that the leading edge of the chromatography band, at the end of the second accumulation step, could have been released from the loop leading to breakthrough. Such a factor, visible as a baseline raise prior to the sharp modulated peak, was not observed. It is noteworthy that such tuning of the FM flow conditions (^{1}D, accumulation loop, ^{2}D), which has been previously described [9,10], must be considered as a useful approximation, also because restrictions inside the wafer chip (internal channels) were not considered.

The developed FM GC×GC-MS method was applied to the analysis of coconut bio-oil, the resulting chromatogram of which is shown in Figure 5.4.1B. In this case, an overall potential *N* value of about 9,360,000 (600 × 15,600) could be attained.

Comparison of the results

Considering the combined potential efficiency of the columns used in the FM GC×GC-MS analyses, then this was nearly three times higher than that of the CM GC×GC-MS set of columns. However, two advantages must be accounted for in the CM method, compared to the FM one: I) the gas flow conditions were nearer to optimum in the second dimension; II) the re-injection conditions are much better due to chromatography band re-concentration.

The CM and FM GC×GC-MS chromatograms reported in Figures 5.4.1A-B have been aligned (as will be seen ^{2}D retention times differed a little), after being corrected for wrap-around.

In first instance, the elution temperatures were very similar for the 5 numbered peaks in Figure 5.4.1A-B, as can be seen from the information listed in Table 5.4.1. The elution temperatures were calculated from the total (^{1}D + ^{2}D) retention times provided

by the GC×GC-MS software used (the most intense modulated peak is considered). Across the elution temperature range 112.3-219.7°C, corresponding to a time period of approx. 18 min, the maximum difference was 0.8°C for peak 5, corresponding to 8 s. The elution temperature for phenol was slightly higher in the CM application (0.5°C, corresponding to 5 s) and, on the other hand, slightly lower for the other four compounds. Such differences can also be related to the modulation phase and, hence, to the position of the most intense modulated peak for a specific compound.

Table 5.4.1. *Information related to compound identity, elution temperatures (Elution temp.), ^2D retention times (t_R), peak widths at half height (w_h) for the 5 compounds indicated in the cryogenic modulation and flow modulation applications (Figure 5.4.1A-B).*

Peak/Compound	Cryogenic modulation			Flow modulation		
	Elution temp. (°C)	^2D t_R (s)	w_h (ms)	Elution temp.	^2D t_R	w_h
1. Phenol	112.8	4.16	190	112.3	3.47	190
2. Naphthalene-d_8	146.1	4.67	230	146.4	4.01	190
3. 2,6-Dimethoxyphenol	168.1	4.97	220	168.4	4.43	180
4. Acenaphthene-d_{10}	187.7	5.18	230	188.4	4.52	200
5. Syringylacetone	218.9	5.63	250	219.7	5.06	180
Average			*224*			*188*

Peaks widths (at half height - w_h) for the five compounds listed in Table 5.4.1 were derived by considering only non-overloaded modulated peaks. The measured values were rounded to the first ten due to the fact that one data point every 30.3 ms was acquired. Consequently, the w_h results listed in Table 5.4.1 are to be considered as approximations. In general, the w_h values were similar, even though always lower in the flow modulation experiments (apart from phenol), with an average value of 188 ms against 224 ms. The peak capacities, calculated using the two average w_h values and the modulation period, were approx. 18 and 21 in the CM and FM applications, respectively.

Besides peak capacity, peak-to-peak resolution is a further important factor, and was found to be generally similar in both types of applications. For example, CM and FM chromatogram expansions between approx. 15.1 and 15.4 minutes are shown in Figures 5.4.2A and 5.4.2B, with the (spectrally-similar) compounds indicated by a asterisk characterized by resolution values of 1.4 and 1.5, respectively.

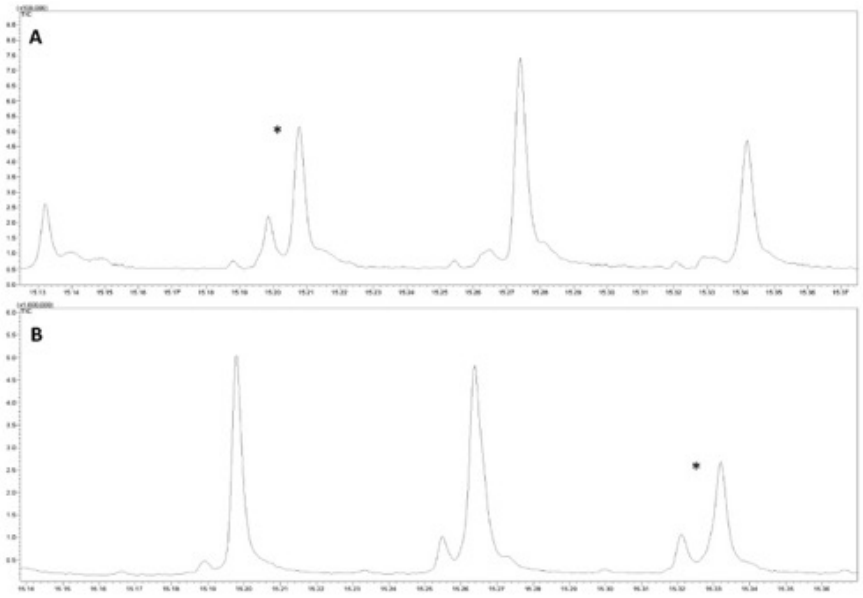

Figure 5.4.2. *Cryogenically-modulated (in A) and flow-modulated (in B) GC×GC-MS untransformed chromatogram expansions relative to the analysis of coconut-derived bio-oil.*

Retention factors were measured for the 5 compounds numbered in Figure 5.4.1, and were obviously found to be higher in the CM analysis, with all compounds characterized by a difference of approx. a single *k* unit (Table 5.4.2). Column efficiencies were also calculated for the 5 compounds (^{2}D separations can be considered as isothermal), with them being altogether comparable (Table 5.4.2): the average *N* values were approx. 2700 and 3000 in the CM and FM analyses, respectively.

Table 5.4.2. *Retention factor and theoretical plate number values for the 5 compounds indicated in the flow modulation and cryogenic modulation applications (Figure 5.4.1).*

Peak/Compound	**Cryogenic modulation**		**Flow modulation**	
	k	*N*	*k*	*N*
1. Phenol	1.8	2658	0.8	1849
2. Naphthalene-d_8	2.1	2286	1.1	2470
3. 2,6-Dimethoxyphenol	2.3	2830	1.3	3359
4. Acenaphthene-d_{10}	2.5	2813	1.4	2832
5. Syringylacetone	2.8	2812	1.7	4382
Average		*2680*		*2978*

The GC×GC profiles illustrated in Figure 5.4.1, even at a first glance, are very similar. As seen, such a fact was confirmed by measuring various chromatographic parameters, with focus on the ^{2}D separations, in particular. With regard to the ^{1}D separations, again these were entirely comparable as can be seen in the two 6.45 min expansions (range: 10.00-16.45 min) derived from the chromatograms shown in Figure 5.4.1 (Figure 5.4.3). Three dashed lines connect the same peaks (α, β, γ) in the two chromatogram expansions emphasizing the altogether similar elution profile along the x axis. The upper part of each dashed line was positioned at the peak apex in the CM result. The observation of the lower ends of the dashed lines highlight the fact that first dimension retention times for the three compounds were slightly lower in the FM analysis. However, in the two types of applications the retention time differences between compound β and α, as well as between compound β and γ, were very similar.

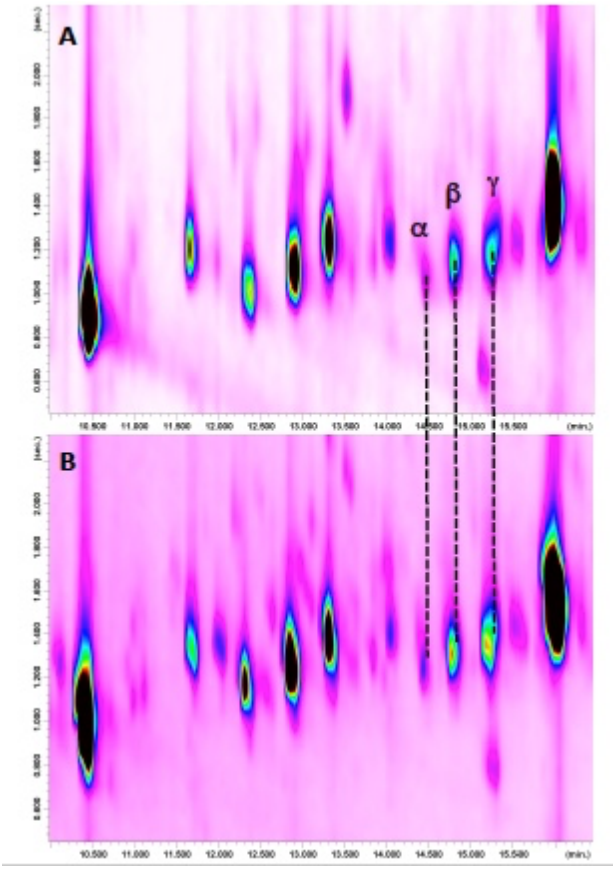

Figure 5.4.3. *Chromatogram expansions derived from the chromatograms shown in Figure 5.4.1. The CM and FM expansions are shown in A and B, respectively.*

5.4.4 Conclusions

A preliminary attempt to determine an equivalent standard column set for cryogenic and flow-modulation GC×GC-MS has been herein described. The term “preliminary attempt” is used because the CM and FM approaches provided an altogether similar, even though not equal, separation performance. Furthermore, the determination of “equivalence” would require a more in-depth evaluation of the GC×GC-MS fingerprints. Finally, a specific view on the analytical potential of FM GC×GC-MS, compared to the more powerful CM GC×GC-MS, has been given. In such a respect, obviously the use a ^{2}D 1.5 m × 0.10 mm ID × 0.10 μm d_f column would have provided a superior result (potentially 9,000,000 *N*), but such an evaluation would have been outside the scope of the present investigation.

References:

[1] Z. Liu, and J.B. Phillips, J. Chromatogr. Sci. 29 (1991) 227.

[2] M. Edwards, A. Mostafa, T. Góreki, Anal. Bioanal. Chem. 401 (2011) 2335.

[3] H.D. Bahaghighat, C.E. Freye, R.E. Synovec, TrAC Trend. Anal. Chem. 113 (2019) 379.

[4] J.V. Seeley, N.J. Micyus, J.D. McCurry, S.K. Seeley, Am. Lab. 38 (2006) 24.

[5] P.Q. Tranchida, G. Purcaro, A. Visco, L. Conte, P. Dugo, P. Dawes, L. Mondello, J. Chromatogr. A 1218 (2011) 3140.

[6] M. Poliak, M. Kochman, A. Amirav, J. Chromatogr. A 1186 (2008) 189.

[7] P.Q. Tranchida, F.A. Franchina, P. Dugo, L. Mondello, J. Chromatogr. A 1255 (2012) 171.

[8] J.V. Seeley, S.K. Seeley, E.K. Libby, Z.S. Breitbach, D.W. Armstrong, Anal. Bioanal. Chem. 390 (2008) 323.

[9] P.Q. Tranchida, F.A. Franchina, P. Dugo, L. Mondello, J. Chromatogr. A 1359 (2014) 271.

[10] P.Q. Tranchida, F.A. Franchina, P. Dugo, L. Mondello, J. Chromatogr. A 1372 (2014) 236.

[11] L. Mondello, A. Casilli, P.Q. Tranchida, M. Lo Presti, P. Dugo, G. Dugo, Anal. Bioanal. Chem. 389 (2007) 1755.

[12] P.Q. Tranchida, M. Zoccali, F.A. Franchina, A. Cotroneo, P. Dugo, L. Mondello, J. Chromatogr. A 1314 (2013) 216.

[13] M.S. Klee, J. Cochran, M. Merrick, L.M. Blumberg, J. Chromatogr. A 1383 (2015) 151.

[14] F. David, D.R. Gere, F. Scanlan, P. Sandra, J. Chromatogr. A 842 (1999) 309.

5.5 Evaluation of the fatty acid content in dietary supplements by using a fully-automated robotic station and gas chromatography with simultaneous mass spectrometry and flame ionization detection

5.5.1 Introduction

The present investigation is based on the lipid characterization, in term of fatty acid methyl esters, of dietary supplements. Fatty acid derivatization was performed by using a direct derivatization protocol [1]. In detail, a robotic preparative station enabled derivatization in a fully automatic manner. With regards to the GC separation, a medium-polarity ionic liquid column was used. Dual detection was performed by splitting the eluate between a triple quadrupole mass spectrometer (in this case used as a single quadrupole) and a flame ionization detector. This choice allowed the possibility to obtain quali-quantitative results, in a single run. A comparison without manually and automatic sample preparations was carried out.

The sample was derivatized by using an hot methylation procedure and subjected to GC-MS-FID analysis.

The reliable and simple strategy proved its suitability for the qualitative and quantitative (if required) screening of fatty acids in dietary supplements.

5.5.2 Experimental

Sample, standard compounds, and sample preparation

The dietary supplement sample was purchased in a Pharmacy located in Messina and were stored at room temperature. The internal standard $C_{18\text{-}d35:0}$ was solubilized in *n*-heptane at a final concentration of 5,000 ppm (*w/v*). The presence of the ISs for the scope of quantification was not exploited in the present research. In a vial (volume 2 mL) with a propylene screw-cap and a polytetrafluoroethylene/silicone septum were weighed approx. 25 mg of the sample. An amount of 100 µL of a 5000 ppm solution of the internal standard ($C_{18\text{-}d35:0}$) was added.

The derivatization procedure was carried out by using AOC-6000 Shimadzu robotic station (Shimadzu, Duisburg, Germany). In detail, the preparative station added to samples 500 µL MeONa in methanol (0.5% *w/v*), 100 seconds of vortex and 900

seconds in the oven at the temperature of 95°C. In a second stage, the procedure involved the addition of 500 µL of BF_3 derivatizing reagent, 100 seconds of vortex and 900 seconds in the oven (95°C). 350 µL of *n*-heptane were used for the extraction of FAMEs fraction. To facilitate the gravitational separation of the by-phasic system (methanol and heptane), 250 µL of saturated NaCl solution were added to the reaction mixture. The *n*-heptanic upper layer was collected from robotic system and injected directly in GC-MS-FID instrument. The same procedure was also carried out manually. The sample was analyzed in triplicate.

Instrumentation

The separation and identification of FAME compounds was carried out by using a GCMS-TQ8050 NX instrument (Shimadzu, Duisburg, Germany) equipped with a split-splitless injector (280°C) and the AOC-6000 system. The separation of analytes was conducted by using a liquid ionic (IL) capillary column, namely SLB-IL60 30 m × 0.25 mm ID, 0.20 µm d_f(Merck Life Science). An Y union was installed at the end of the column, in order to split the flow between the two detectors. Two uncoated columns allow the connection to the detectors (1 m × 0.1 mm ID to QqQMS; 0.35 m × 0.1 mm ID to FID). Initially, the flow was divided with a ratio of 5.9:4.1 between FID and QqQMS, respectively. At the end of the analysis the ratio values change to a ratio of 6.6:3.4 between FID and QqQMS, respectively.

The temperature program was as follows: 50°C to 180°C (10 min) at 3.0°C/min and from 180°C to 280°C maintaining the same temperature program. Injection volume was 0.5 µL with a split ratio of 1:100. Helium was used as carrier gas, at an initial inlet pressure of 218 kPa and at an average linear velocity of 30 cm s^{-1}.

The triple-quad spectrometer worked in full scan mode (3 Hz). The MS parameters were as follows: the mass range was 40–550 amu, the ion source temperature was 220°C, and the interface temperature was 250°C. The GCMSsolution software (version 4.50 Shimadzu) was used for data collection and handling. FAMEs peak assignment was carried out through the application of two different parameters: spectral similarity (over 80 %) and a LRI tolerance window (± 10). C_4-C_{24} reference standard mixture was used for determining LRIs of target compounds. A lab-constructed MS spectra database, containing also reference LRIs were used.

The FID temperature was set at 280°C (sampling rate: 200 ms), while the gas flows were 40 mL min^{-1} for H_2, 30 mL min^{-1} for the make-up gas (N_2) and 400 mL min^{-1} for air.

5.5.3 Results & Discussion

The chromatogram relative to the dietary supplement sample is shown in Figure 5.5.1. Similarity values and LRIs for the twenty-eight compounds identified are listed in Table 5.5.1. Looking at the chromatogram, and as expected, is evident that more unsaturated fatty acids were found than saturated fatty acids. The base peak is relative to the linolenic acid ($C_{18:3n3}$) followed by linoleic fatty acid ($C_{18:2n6}$) and oleic fatty acid ($C_{18:1n9}$).

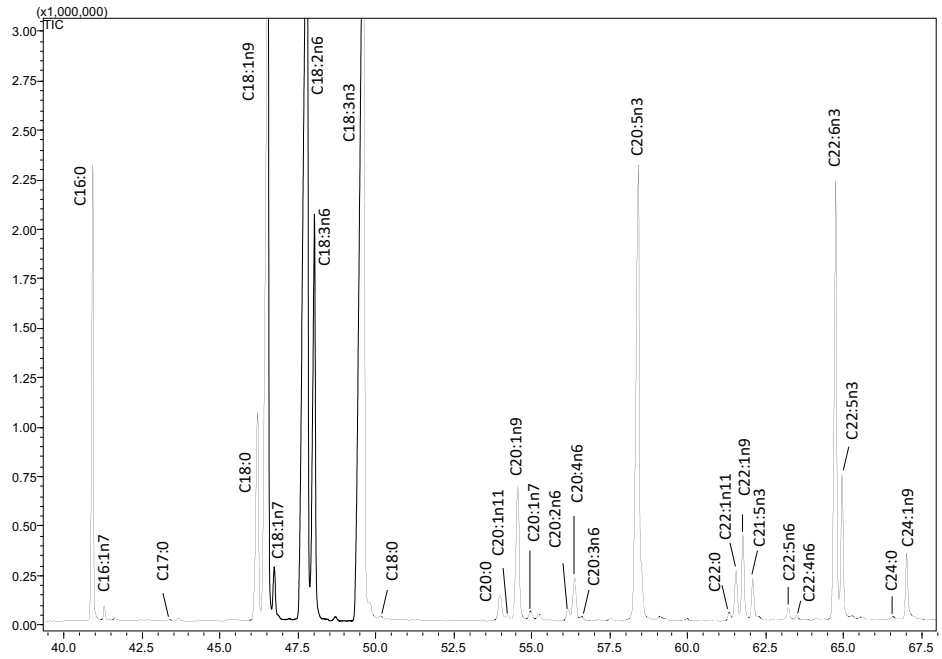

Figure 5.5.1. *FAMEs GC-MS chromatogram of dietary supplement sample.*

Table 5.5.1. *Identification of FAMEs detected in dietary supplement sample. LRI_{lib} are linear retention index values present in the mass spectra library, LRI_{exp} are those obtained experimentally, while Δ is the difference between LRI_{lib} and LRI_{exp}. Sim represents the percentage of similarity between experimental and library spectra.*

Peak	Compound	Sim.	LRI_{exp}	LRI_{lib}	Δ
1	Me. C16:0; Palmitate <methyl->	97	1601	1600	-1
2	Me. C16:1n7; Palmitoleate <methyl->	91	1615	1615	0
3	Me. C17:0; Heptadecanoate <methyl->	94	1695	1700	5
4	Me. C18:0; Stearate <methyl->	96	1803	1800	-3
5	Me. C18:1n9; Oleate <methy->	96	1811	1809	-2
6	Me. C18:1n7; Vaccenate <(E)-, methyl->	97	1816	1820	4
7	Me. C18:2n6; Linoleate <methyl ->	98	1842	1845	3
8	Me. C18:3n6; Linolenate <gamma-, methyl->	97	1848	1856	8
9	Me. C18:3n3; Linolenate <alpha-, methyl->	97	1888	1898	10
10	Me. 9,10-methylene C18: 0; Dihydrosterculate <methyl->	86	1902	1903	1
11	Me. C20:0; Arachidate <methyl->	94	2000	2000	0
12	Me. C20:1n11; 9Z-Eicosenoate <methyl->	89	2006	2005	-1
13	Me. C20:1n9; Eicos-(11Z)-enoate <methyl ->	94	2015	2011	-4
14	Me. C20:1n7; Eicos-(13Z)-enoate <methyl>	94	2026	2018	-8
15	Me. C20:2n6; Eicosa-(11Z, 14Z)-dienoate < methyl ->	96	2059	2053	-6
16	Me. C20:4n6; Arachidonate <methyl>	90	2065	2063	-2
17	Me. C20:3n6; 5(Z),11(Z),14(Z)-eicosatrienoate <methyl->	94	2071	2066	-5
18	Me. C20:5n3; Eicosa-(5Z,8Z,11Z,14Z,17Z)-pentaenoate <methyl->	97	2120	2119	-1
19	Me. C22:0; Behenate <methyl->	95	2199	2200	1
20	Me. C22:1n11; Docos-(11Z)-enoate <methyl>	95	2207	2210	3
21	Me. C22:1n9; Erucate <methyl ->	96	2216	2216	0
22	Me. C21:5n3; 6(Z),9(Z),12(Z),15(Z),18(Z)-Heneicosapentaenoate <methyl->	93	2228	2235	7
23	Me. C22:5n6; 4,7,10,13,16-Docosapentaenoate (all-Z)- <methyl->	93	2271	2275	4
24	Me. C22:4n6; (7Z,10Z,13Z,16Z)-docosatetraenoate <methyl->	94	2282	2285	3
25	Me. C22:6n3; Docosa-(4Z,7Z,10Z,13Z,16Z,19Z)-hexaenoate <methyl->	95	2329	2333	4
26	Me. C22:5n3; Docosa-(7Z,10Z,13Z,16Z,19Z)-pentaenoate <methyl->	96	2337	2341	4
27	Me. C24:0; Lignocerate <methyl->	93	2399	2400	1
28	Me. C24:1n9; Nervonate <methyl->	92	2415	2416	1

The elution order in GC depends primally on the relative vapor pressure of the analytes. For fatty acid compounds the relative vapor pressure increase proportionally with the carbon number present in the chain. For this reason the C_{18} family elutes after than C_{16} and so on. Another separation parameter is the interaction of double bonds of fatty acids with the stationary phase. The medium polarity of the stationary phase used in this application allows the separations of compounds in terms of double bonds. Therefore, SFAs, MUFAs, and PUFAs, belonging to the same family (e.g. C_{18}) are totally resolved. The more double bonds are present the more the compounds are retained.

Usually, the GC analysis of FAMEs is carried out on capillary column with a polar stationary phase. Recently, several applications, related to the GC analysis of FAMEs,

have been carried out using IL columns [2-4]. Compared to common polar stationary phase utilized for FAME separations, such as polyethylene glycol or cyanopropyl-based phases, IL columns have lower bleeding with the advantage of enabling the quantification of low concentration analytes [5].

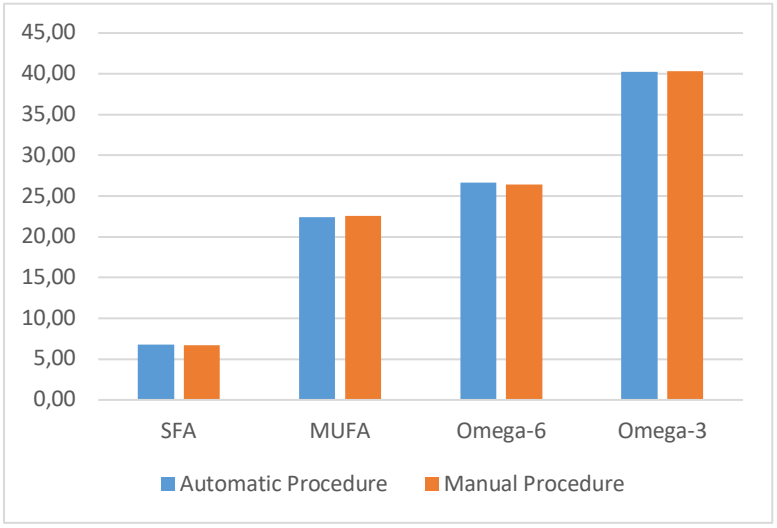

Figure 5.5.2. *Graph reporting the relative percentages of the different fatty acid families by the use of GC-FID instrument. The relative percentages obtained by an automatic sample preparation procedure are reported in blue, while the one obtained by the manual sample preparation procedure are reported in orange.*

The percentages relative to the different fatty acid families are reported in Figure 5.5.2. No substantial difference between the automatic and manual sample preparation procedures were found. As reported into the dietary supplement leaflet, the amount of unsaturated fatty acids it was higher than that of saturated fatty acids.

5.5.4 Conclusions

A GC-MS-FID approach for the detailed profiling of fatty acid content in dietary supplements has been developed.

The method herein reported allows the automatic sample preparation and the simultaneous identification and quantification (if required) of fatty acid compounds present in dietary supplements, by the use of a robotic preparative station coupled to GC-MS-FID. Certainly, the methodology can be easily applied for the analysis of the fatty acid profile present in other food related samples.

References:

[1] G. Micalizzi, E. Ragosta, S. Farnetti, P. Dugo, P.Q. Tranchida, L. Mondello, F. Rigano, Anal. Bioanal. Chem. 412 (2020) 2327.

[2] J. Kováčik, V. Antos, G. Micalizzi, S. Dresler, P. Hrabák, L. Mondello, J. Hazard Mater. 347 (2018) 168.

[3] J. Kováčik, G. Micalizzi, S. Dresler, P. Babula, J. Hladký, A. Chemodanov, Luigi Mondello, Chemosphere 213 (2018) 384.

[4] J. Kováčik, S. Dresler, G. Micalizzi, P. Babula, J. Hladký, L. Mondello, Nitric Oxide 89 (2019) 11.

[5] C. Fanali, G. Micalizzi, P. Dugo, L. Mondello, Analyst 142 (2017) 4601.

5.6 Thin layer chromatography-bioassay screening for the identification of acetylcholinesterase inhibitor terpenoids from orange by-products

5.6.1 Introduction

Neurodegenerative disorders are a debilitating conditions that result in progressive degeneration and dysfunction of nerve cells. Alzheimer's disease (AD) is the most common of this neurodegenerative disorder among the elderly, affecting up around 75% of all cases of dementia [1]. Alzheimer's disease is a etiology neurological pathology characterized by memory loss, cognitive impairment amnesia and disorientation [2]. Nowadays, the cholinergic hypothesis remains the basis on the treatment of AD. Cholinergic hypothesis consists in degeneration of cholinergic neurons and their axons projected to cerebral cortex [3]. In consequence, levels of the neurotransmitter acetylcholine (ACh) decrease, leading to synaptic reduction and cognitive impairment. In addition, cholinergic deficits have also been shown to interact with acute proinflammatory mechanisms to exacerbate damage in brain tissue [3, 4]. Moreover, several authors underline the capacity of acetylcholinesterase enzyme (AChE) to promoting amyloid-beta (Aβ) plaques formation and hyper-phosphorylation of tau protein and their aggregation into neurofibrillary tangles, increasing neurotoxicity in AD patients [5-7].

Low levels of ACh, inflammatory response, Aβ plaques and neurofibrillary tangles cited above, formed the principal hallmarks of AD [7]. In this context, acetylcholinesterase inhibitors (AChEi) play a key role in AD therapy, trough increase synaptic acetylcholine (ACh) levels and improve cholinergic function by reduction of AChE activity in the brain [8].

A few extract from plant material was studied as AChEi, some of them, such as *Salvia officinalis* or *Crocus sativus L.* extracts, were used in clinical trials with promising results [9]. Actually, galantamine is a naturally source AChEi widely use in AD pharmacology therapy. Galantamine is alkaloid extract and purify from *Amaryllidaceae family* [9]. However, the cultivation and the collection of plant material and after that extract and isolation of compounds, sometimes can be lead to

high consumption of resources and unfavorable cost-efficient process. In this way, the revalorization of by-product from agricultural wasted, can be exploit to obtain interest bioactive compounds. *Citrus sinensis* (orange) by-products from orange juice industrial production represent one of the most abundant citric residues in Southern Europe, and a promising source of health-promoting compounds like terpenoids [10]. Terpenoids are a large and diverse family of organic compounds based on isoprene units. In addition, terpenoids usually contain additional functional groups and be part of other natural molecules like phenols, alkaloids, vitamins or phytosterols. Under this description, more than 50,000 molecules have been discovered like terpenoid structure [11]. Previous works described terpenoids like a promising AChEi and can be studied as a tool to prevent AD [12-14]. However, this large amount of type compounds in a plant material matrix difficult the correlation between compounds and their bioactivity in experimental assays. In this way, thin layer chromatography (TLC) can provide the separation of study compounds in a complex plant extract like orange by-product extract.

Thin layer chromatography is a partition chromatography technique based on a dynamic equilibrium of molecules between the mobile and stationary phases. It represents a very fast, sensitive, and cheap method that permit to obtain several results depending on what is the task object. Paper chromatography was the first type of partition chromatography on a planar surface and the first experiment was carried out in 1945 [15]. During the years TLC replaced paper chromatography and became a widely used and inexpensive technique [16].

The main uses of TLC are: to verify the identity and purity of a compound; to check the progress of a reaction; to define the number of components present in a mixture (analytical TLC); to study the progress of an enzymatic reaction (TLC bioautographic assay); and to achieve the best separation of compounds in a complex mixture with the purpose of purify as many compounds as possible (preparative TLC). These last three points are related to the present research work, for the characterization of orange-by product samples to evaluate the activity of acetylcholinesterase enzyme and to purify some terpenes which demonstrated enzyme-inhibiting activity for further characterization.

TLC bioautographic is an useful and inexpensive technique appeared in 1961 [17, 18]. The main purpose is the biological screening of complex extracts for the characterization of bioactive compounds [19]. The most common bioactivity monitored are: antioxidant [20], antienzyme [21], antibacterial [22], and antifungal [23].

TLC, as others form of chromatography, possesses a high separation power but, at the same time, do not give any molecular information about the resolved compounds. For this reason, the use of some form of detection is mandatory. Several reagent-detector were developed, some universal and some others specific to certain classes. Reagent-detectors, often, allows the class identification but, rarely, can be useful for the identification of a specific compounds. The best way to achieve an identification is the use of spectrometric technique such as MS. Thin layer chromatography could be coupled with MS directly on-line or also in off-line manner. The latter, usually, is the easiest way and is carried out scratching from the plate the compounds of interest, solubilizing it in a suitable solvent (with an affinity higher than the stationary phase) and, at the end, analyzed. If available, is also common to analyze, the spot removed from the plate, by GC or LC coupled with MS. The addition of chromatography allows to find and resolve, some possible coelutions issue that could make difficult the identification by MS and that reduce the purity of a compound. Whit this knowledge, the extraction condition of AChEi terpenoids from plant material can be studied whit the aim of enhance their extraction yield and concentrate the interest compound to improve de AChEi extract capacity.

Hence, the main objective of this research work is to investigate the principal bioactive terpenoids whit capacity AChEi from orange juice by-product industry. Different range of polarity extraction solvents were used in order to increase spectrum and selectivity of terpenoidal compund extracted. The present research work is still in progress. Up to now only the separation of terpenes has been totally optimized.

5.6.2 Experimental

Sample, reagents, and standard compounds

Orange samples were obtained by maceration method. Briefly, 5 g of raw material of orange by-products was mixed with 45 ml of solvent. The solvents used were *n*-

heptane, ethyl acetate (EtOAc), acetone and ethanol. The mixture was placed in an orbital shaker (Compact digital mini rotator, Thermo Scientific, Massachusetts, USA) at 200 rpm for 24 hours (at room temperature out of direct light.). Extracts were filtered by using 0.45 μm Nylon filter (Agilent Technologies, California, USA) and evaporated by nitrogen stream (TurboVap® LV Biotage, Uppsala, Sweden). Finally, the extracts were stored at -20°C until their analyses. Each solvent extraction was performed in triplicate.

HPLC-grade solvents acetonitrile, *n*-heptane, EtOAc, acetone, ethanol, dichloromethane (DCM), acetic acid and sulphuric acid were purchased from VWR Chemicals (Barcelona, Spain) while toluene was acquired from Riedel-de Haën.

TLC Silica gel 60 F_{254} 20×20 cm plates were purchased from Merck. For achieve a fast response, the plates were cut in shorter dimension. To perform a ^{1}D TLC the dimension of the plates were 5×10 cm, while for the ^{2}D TLC the dimension of the plates were 10×10 cm. From a single 20×20 cm whole plate it was possible to obtain 8 plates for ^{1}D TLC or 4 plates for ^{2}D TLC. Two different chambers were used: a 500 mL beaker to carry out the ^{1}D TLC while two TLC chambers from Panreac for the ^{2}D TLC. The mobile phase volumes were 10 mL and 50 mL, respectively. To spot the sample on the plate, a capillary spotter was obtained from a glass Pasteur pipette.

Instrumentation

^{1}D TLC

Analytical mono-dimensional TLC was carried out on a TLC plates cut to 5×10 cm. This allowed the development of four samples for each plate. The starting line was placed at 1 cm from the bottom of the plate, while the solvent front was nearly the top-end of the plate (0.5 cm to the upper part of the plate). A 500 mL beaker was used as chamber. The chamber was filled with 10 mL of mobile phase. An aliquot of extract was spotted on the silica gel plate and dried for few minutes before the analysis.

^{2}D TLC

Analytical bi-dimensional TLC was carried out on a TLC plates cut to 10×10 cm. The starting line was placed at 1 cm from the bottom (1D) and at 1 cm from the left-side (2D) of the plate while the solvent front was marked at 0.5 cm to the upper part

of the plate for each dimension. The total bi-dimensional space that could be occupied was 8.5 cm^2. Two TLC chamber were employed to fill them with two different mobile phases. Each chamber was filled with 50 mL of mobile phase.

Detection

The detection was performed using two different UV light (254 nm and 365 nm) and a universal vanillin-based detector. The TLC visualization reagent was prepared dissolving 0.5 g of vanillin in a mixture of 85 mL of methanol, 10 mL of acetic acid and 5 mL of sulphuric acid (97%) on an ice bath. The main compounds that could be monitored are: terpenes (all classes), flavonoids, phenols, and fatty acids. Two different ways have been tried for applying the detection solution: spraying the solution on the plate or dipping the plate in a beaker containing the detection solution. The latter shown a better and more uniform result. After the detector application, the plate was heated for few minutes (between 2 min and 5 min) on a heater (110°C) to reveal the compounds. Before the application of the vanillin solution, the plates were placed under UV lights (254 nm and 365 nm) looking for compounds containing chromophores.

5.6.3 Results & Discussion

TLC and design of experiment description

In order to carry out a TLC separation, a small amount of sample is located near to the bottom part of the plate and the chamber is filled with a low amount of solvents (mobile phase). Once that the plate is dried, it is placed inside of the chamber, paying attention to avoid the direct contact between the sample spotted and the mobile phase. The mobile phase, usually, is a mixture of two or more pure solvents. Afterwards, the chamber is closed and the compounds starts the migrations from the start-zone. It is important to generate a chamber-saturation, due to an equilibrium between the liquid mobile phase and its vapor. The migration depends on the interaction of the components between the stationary phase (usually silica) and the mobile phase. The interaction with the stationary phase that determining the retention are: hydrogen bonding, ion-ion, ion dipole, charge transfer, and van der Waals interaction. At the end of the chromatographic process, the plate is collected and is dried for few minutes. The

detection is carried out by the use of UV light, applying reagent-detector (by spraying or dipping) or by the use of a spectrometric technique. Analytes containing chromophore groups can be detected by inspection under 254-365 nm UV light. While many specific reagent-detector allows a tentative identification. As reported in the introduction, the best way to achieve a reliable identification is the use of spectrometric techniques.

Two-dimensional TLC is very useful for the analysis of complex sample. The mechanism of 2D TLC is the same of 1D TLC, even if, in this case two different separation analysis are performed, sequentially and using two different mobile phases. The plate, usually, has a square shape and the sample is spotted in a corner of the plate. After the first analysis, the plate is dried and then turned 90° and developed again using a different mobile phase. The advantage is due to the different separation power of the mobile phases.

A scheme of the design of experiment is illustrate in Figure 5.6.1. After the sample extraction, the first step (TLC 1) is related to the optimization of the separation by the use of 1D TLC or 2D TLC, depending on the complexity of the sample. The use of a selective and destructive detector, such as vanillin, allows to see if the analytes of interest were resolved or not. Afterwards, the second step (TLC 2) is conducted on another TLC plate but, in this case, the Ellman detector will be used (TLC-bioassay) in order to look at possible compounds having AChEi activity. If any compounds will give a positive result to this step it is important to record its retention factor. The latter will be useful in order to scratch in the proper position of the next plate (TLC 3). Finally an identification by the use of GC-MS will be carried out, in order to identify the compound/s with AChEi activity. As reported previously, to now, only the first step were totally optimized and the research work is still in progress.

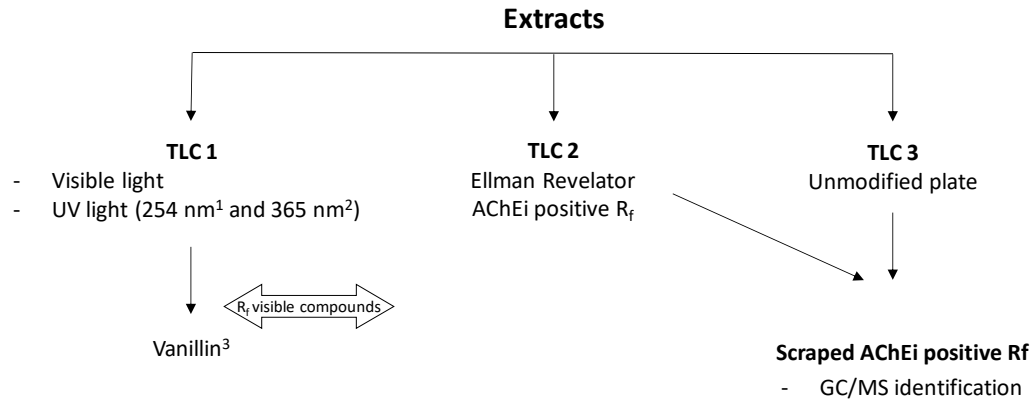

Figure 5.6.1. *Design of experiment.*

1D TLC

Analytical mono-dimensional TLC was carried out on a TLC plates cut to 5×10 cm to develop four samples in each plate. The starting line was placed 1 cm from the bottom of the plate while the solvent front was nearly the top-end of the plate. A 500 mL beaker was used as chamber. The chamber was filled with 10 mL of mobile phase. An aliquot of extract was spotted on the silica gel plate and dried for a few minutes before the analysis. In order to find out the best mobile phase, the TLC plate was developed using several solvent mixtures, starting from the more polar (ethanol-acetic acid with a ratio of 7:3) to the more apolar (DCM-ethyl acetate with a ratio of 9.3:0.7).

In Figure 5.6.2 are illustrated seven TLC plates developed reducing the polarity of the mobile phase to elute all the compounds detected from the starting line. The samples analyzed were extracted from orange, by using the following solvents: O_1 ethanol; O_2 ethyl acetate; O_3 acetone, and O_4 heptane. It is possible to highlight that the use of polar mobile phase (Fig. 5.6.2a) allows to all compounds to move from the starting point but, at the same time, leads to a massive co-elution of the apolar ones on the top of the plate. For this reason, reducing the polarity of the mobile phase allow to achieve a better resolution. The best result seems to be the one obtained with the most apolar mobile phase (Fig. 5.6.2g), in particular for the O_4 extract.

In an effort to resolve all the compounds, for the remaining extracts, in a single plate the only reasonable solution is to perform a 2D TLC. Repeatability was also evaluated in duplicate with satisfactory results. The detection was carried out using UV light and a universal vanillin detector as mentioned before.

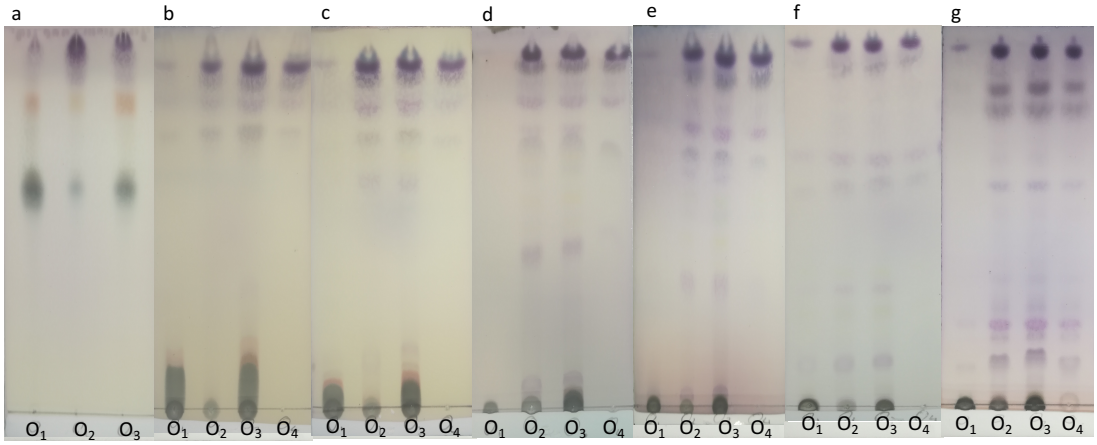

Figure 5.6.2. . *Illustration of seven plates developed using different mobile phases reducing the polarity from the left to the right. The mobile phase used are: a) ethanol-acetic acid 70:30; b) acetone 100; c) EtOAc-acetone 50:50; d) EtOAc 100; e) toluene-EtOAc 7:93; f) toluene-EtOAc 50:50; g) DCM-EtOAc 93:7. The orange by-products were extracted with: O_1 ethanol; O_2 ethyl acetate; O_3 acetone; O_4 heptane.*

2D TLC

Analytical bi-dimensional TLC was carried out on a TLC plates cut to 10×10 cm. The starting line was placed at 1 cm from the bottom (1D) and at 1 cm from the left-side (2D) of the plate while the solvent front was marked at 0.5 cm to the upper part of the plate for each dimension. The total bi-dimensional space that could be occupied was 8.5 cm^2. Two TLC chamber were employed to fill them with two different mobile phases. Each chamber was filled with 50 mL of mobile phase. The first dimension separation was carried out by the use of a mid-polar mobile phase (DCM/EtOAc 9:1) with an approximate elution time of 25 minutes. Instead, the second dimension process was carried out using a high polar mobile phase (Ethanol/Acetic Acid 7:3). In the latter case the elution time was nearly 50 minutes.

In order to optimize the 2D TLC separation were selected the best mobile phases with different polarity reported in the 1D TLC method optimization. For what concerns the sample, 2D TLC were carried out on the most analyte-rich sample that is the orange peels extract O_2 (EtOAc).

In Figure 5.6.3 is illustrate the bi-dimensional plate relative to the orange peels extract.

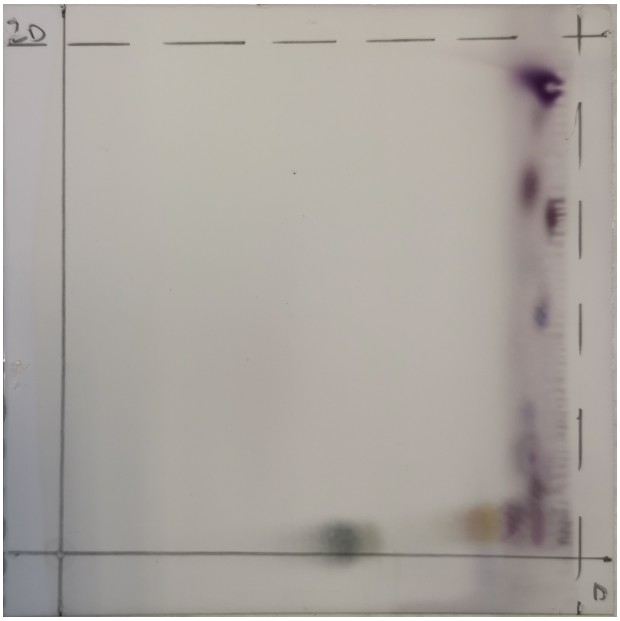

Figure 5.6.3. *Bidimensional TLC plate relative to the EtOAc orange extract. Mobile phases: DCM/EtOAc 9:1 (1D)); Ethanol-Acetic Acid 7:3 (2D).*

Looking at the bidimensional TLC plate and comparing it with the 1D TLC plates eluted using the two mobile phases herein reported, it is well evident that a better resolution of polar compounds (compared to Figure 5.6.1g) and apolar compounds (compared to Figure 5.6.1a) is achieved.

5.6.4 Conclusions

As already reported, the research work is still in progress. The results herein reported are related only to the first step of the design of experiment. Thin layer chromatography 1D and 2D methods were already developed in order to resolve as many compounds as possible in an orange extract.

References:

[1] H. Niu, I. Álvarez-Álvarez, F. Guillén-Grima, I. Aguinaga-Ontoso, Neurologia 32 (2018) 523.

[2] C. Reitz, and R. Mayeux, Biochem. Pharmacol. 88 (2014) 640.

[3] H. Hampel, M.M. Mesulam, A.C. Cuello, M.R. Farlow, E. Giacobini, G.T. Grossberg, A.S. Khachaturian, A. Vergallo, E. Cavedo, P.J. Snyder, Z.S. Khachaturian, Brain 141 (2018) 1917.

[4] E.D. AlFadly, P.A. Elzahhar, A. Tramarin, S. Elkazaz, H. Shaltout, M.M. Abu-Serie, J. Janockova, O. Soukup, D.A. Ghareeb, A.F. El-Yazbi, R.W. Rafeh, N.Z. Bakkar, F. Kobeissy, I. Iriepa, I. Moraleda, M.N.S. Saudi, M. Bartolini, A.S.F. Belal, Eur. J. Med. Chem. 167 (2019) 161.

[5] G.V. De Ferrari, M.A. Canales, I. Shin, L.M. Weiner, I. Silman, N.C. Inestrosa, Biochemistry, 40 (2001) 10447.

[6] R.H. Field, A. Gossen, C. Cunningham, J. Neurosci. 32 (2012) 6288.

[7] M. Gohar, H.G. Nigel, A.K. Jalaluddin, A.K. Mohammad, CNS Neurol. Disord. Drug Targets 13 (2018) 1432.

[8] M. Singh, M. Kaur, H. Kukreja, R. Chugh, O. Silakari, D. Singh, Eur. J. Med. Chem. 70 (2013) 165.

[9] T.C. Santos, T.M. Gomes, B.A.S. Pinto, A.L. Camara, A.M. de Andrade Paes, Front. Pharmacol. 9 (2018) 1192.

[10] B. Alquézar, A. Rodríguez, M. de la Peña, L. Peña, Front. Plant Sci. 8 (2017) 1481.

[11] K.G. Ramawat, and J.M. Merillon in: Natural products: phytochemistry, botany and metabolism of alkaloids, phenolics and terpenes (2013).

[12] A. Cutillas, A. Carrasco,R. Martinez-Gutierrez, V. Tomas, J. Tudela, Plant Biosyst. 152 (2018) 1282.

[13] F. Burčul, I. Blažević, M. Radan, O. Politeo, Curr. Med. Chem. 25 (2018) 1.

[14] P. Williams, A. Sorribas, M.J.R. Howes, Nat. Prod. Rep., 28 (2011) 48.

[15] R. Consden, A.H. Gordon, A.J. Martin, Biochem. J. 39 (1945) 351.

[16] L.S. Ettre, and H. Kalász, LC-GC North America 19 (2001) 712.

[17] R. Fischer, and H. Lautner, Archiv. Der Pharmazie 294 (1961) 1.

[18] B.J.R. Nicolaus, C. Coronelli, A. Binaghi, Experientia 17 (1961) 473.

[19] S. Dewanjee, S. Dewanjee, N. Bhattacharya, R. Khanra, T.K. Dua, J. Pharm. Anal. 5 (2015) 75.

[20] L. Jaime, J.A. Mendiola, M. Herrero, C. Soler-Rivas, S. Santoyo, F.J. Señorans, A. Cifuentes, E. Ibáñez, J. Sep. Sci. 28 (2005) 2111.

[21] O. Galarce-Bustos, J. Pavón, K. Henríquez-Aedo, M. Aranda, Phytochem. Anal. 30 (2019) 679.

[22] D.L. Valle, J.J.M. Puzon, E.C. Cabrera, W.L. Rivera, Evid-Based Compl. Alt. 2016 (2016) Art. 4976791.

[23] Q. Favre-Godal, E.F. Queiroz, J.L. Wolfender, J. AOAC Int. 96 (2013) 1175.

5.7 Evaluation of the modulation performance of a novel commercial diverting flow modulator in the context of comprehensive two-dimensional gas chromatography time-of-flight mass spectrometry analysis of a fish oil sample

5.7.1 Introduction

This research is manly focused on the evaluation of an innovative FM GC×GC LR ToFMS system for the analysis of fatty acids in complex food sample.

The modulation parameters were optimized, trying to find a good compromise between instrumental sensitivity and peak capacity in the second analytical dimension. For this purpose, a certified reference material containing FAMEs, from a fish oil (menhaden oil) was analyzed.

A measurement of chromatography parameters, such as peak capacity, modulation period, peak widths, elution order, was made.

The approach herein reported proved itself as being a powerful analytical platform, benefiting from the high performance, selectivity and resolving power, of both the GC and MS sides.

5.7.2 Experimental

The sample analyzed, PUFA No.3, is a standard mixture of FAMEs derived from menhaden oil (Merck KGaA). Menhaden oil is a fish oil rich in PUFAs content and in particular of ω3-PUFAs.

The sample was diluted in *n*-hexane to a final concentration of 100,000 ppm (*v/v*).

The FM GC×GC LR ToFMS application was performed on a Pegasus BT 4D system (LECO, Mönchengladbach, Germany). The following set of columns was used: an apolar ^{1}D column, namely SLB-5ms, [equivalent in polarity to poly(5% diphenyl/95% dimethyl siloxane)] with dimensions 30 m × 0.25 mm ID × 0.25 μm d_f and an intermediate polarity ^{2}D one, namely an SLB-35ms, with dimensions 1 m × 0.10 mm ID × 0.10 μm d_f [equivalent in polarity to poly(35% diphenyl/65% dimethyl siloxane)], with 0.3 m inside the MS transfer line. The carrier gas was He and was used under a constant flow of 0.8 ml min^{-1}. The system was equipped with a

split/splitless injector (280 °C), while the injection volume was 1 μL (split ratio was 20:1). The temperature program was 150 °C to 280 °C at 3 °C min^{-1} with a negative secondary oven offset of -10 °C. Transfer line temperature: 280 °C. The modulation period was set at 2 s, setting different reinjection time (30 ms, 50 ms, and 80 ms).
The ^{2}D eluate was monitored by the LR ToFMS instrument by using electron ionization (70 eV), at a source temperature of 250 °C, and a mass range of 45-400 amu with a spectral production frequency of 200 Hz. Data analysis were acquired and processed by using the LECO ChromaToF software (v. 5.50.55.0). Mass spectral matching was performed by using the Lipids database.

5.7.3 Results & Discussion

The hyphenation of GC×GC with ToFMS generate a very powerful analytical tool. As already reported, the main objective of the present research work was the performance evaluation of a novel commercial type of diverting flow modulation, named FLUX, commercialized by LECO. This modulator was already described in the paragraph devoted to modulators (see section 4.6.2). Briefly, the modulation process consists of two phases: i) re-injection step, during which the auxiliary gas flow is directed straight to waste, thus enabling the flow from ^{1}D column to be transferred directly into ^{2}D column; ii) diverting step, during which the auxiliary gas flows in the opposite direction with respect to the ^{1}D column flow, sending the latter to the waste. The P_M is represented by the sum of the re-inject and divert phases. Maintaining constant the diverting time and increasing the re-injection step, an higher amount of effluent from ^{1}D column reaches the ^{2}D column, leading to an increase in sensitivity. The same effect can be obtained keeping constant P_M and increasing the re-injection step. From the software it is possible to set the re-injection step in a range between 30 ms (high peak capacity – low sensitivity) and 80 ms (low peak capacity – high sensitivity). Three analyses were carried out using the same analytical method but setting three different re-injection time (30, 50, and 80 ms). The P_M was set to 2 s. In Figure 5.7.1 are illustrated two bidimensional plot relative to the PUFA No.3 sample, acquired by using two different re-injection times: 50 ms (a) and 80 ms (b). It is quite clear that increasing the re-injection time, an higher amount of effluent reaches the ^{2}D column and, consequently, the detector.

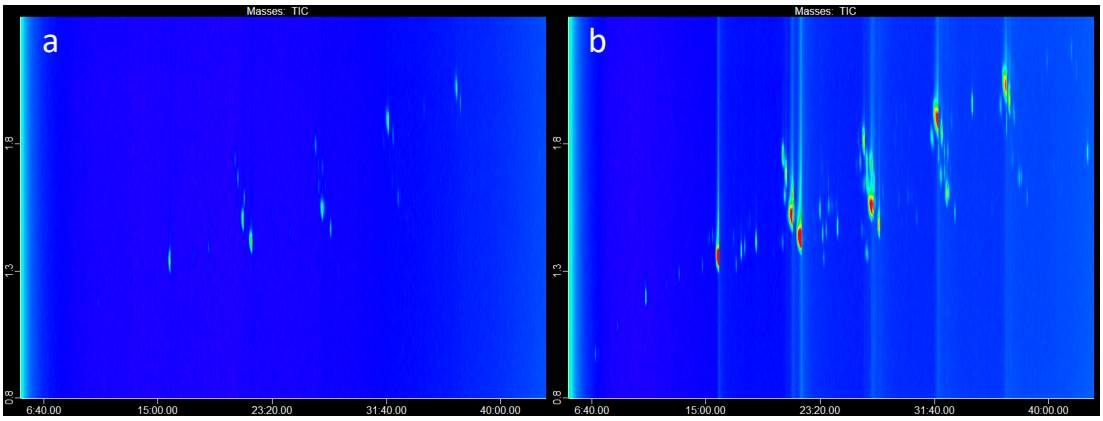

Figure 5.7.1. *GC×GC-ToFMS chromatogram of* PUFA No.3 sample by using 50 ms (a) and 80 ms (b) of re-injection time.

The overall analytical performance of FM GC×GC-LR ToFMS was evaluated, in relation to MS similarities, ^{2}D peak widths, and peak capacity.

The GC×GC bidimensional plot expansion of C_{20} fatty acids family is reported in Figure 5.7.2.

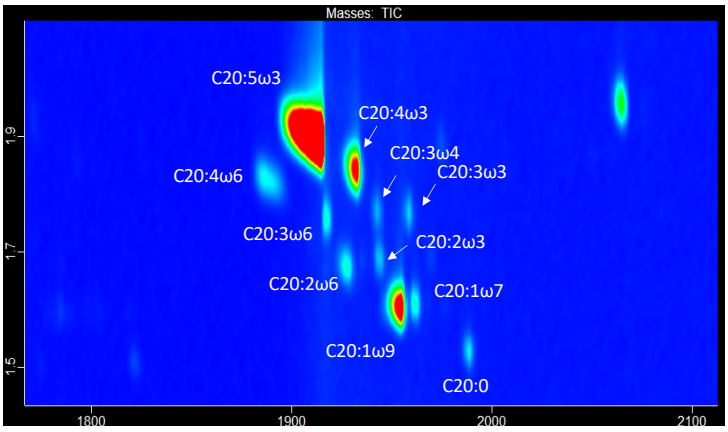

Figure 5.7.2. *GC×GC-ToFMS bidimensional plot expansion relative to C_{20} fatty acids family.*

Looking at the bidimensional plot expansion it is well evident the ^{2}D separation between $C_{20:2\omega3}$ and $C_{20:3\omega4}$. These compounds result totally coeluted in the first analytical dimension (near equal vapor pressures) but, thanks to the different interaction with the ^{2}D stationary phase, they were resolved. Due to the presence of an additional double bond, the analyte $C_{20:3\omega4}$ interact more with the ^{2}D polar stationary phase compared to $C_{20:2\omega3}$.

In table 5.7.1 are reported similarity values and peaks widths relative to the eleven compounds belonging the C_{20} fatty acid family.

Table 5.7.1. *Identification of C_{20} fatty acid FAMEs detected in* PUFA No.3*sample. In table are reported the MS similarity values, and peak widths at the base (w_b) and at half eight (w_h)*

Compound	Similarity	w_h (msec)	w_b
C20:4ω6	883	56	95
C20:5ω3	947	62	105
C20:3ω6	922	55	93
C20:2ω6	903	53	90
C20:4ω3	946	56	95
C20:3ω4	860	53	90
C20:2ω3	927	51	87
C20:1ω9	929	51	87
C20:3ω3	901	53	90
C20:1ω7	909	52	88
C20:0	903	48	82
average	912	54	91

The average peak widths were 91 ms (w_b) and 54 ms (w_h). The peak capacity, calculated using the w_b value, was approx. 21.

With regards to the MS similarity, an average value of 910 was calculated, with a range between 860 and 947.

5.7.4 Conclusions

A FM GC×GC-LR ToFMS approach for the analysis of fatty acid content has been developed. The overall analytical performance related to the method, in its various aspects, can be considered as satisfactory. Despite more than 90% of eluate from the ^{1}D column do not reach the second analytical dimension, the instrument provided a satisfactory result in terms of sensitivity. In this case the use of a ToFMS system is indispensable, especially for the high acquisition frequency (200 Hz) that allows a correct reconstruction of chromatographic peaks with narrow widths.

List of publications

1. *"Current state of comprehensive two-dimensional gas chromatography-mass spectrometry with focus on processes of ionization"* Peter Q. Tranchida, **Ivan Aloisi**, Barbara Giocastro, Luigi Mondello, Trends in Analytical Chemistry, 105 (2018) 360-366.

2. *"Comprehensive two-dimensional gas chromatography-mass spectrometry using milder electron ionization conditions: a preliminary evaluation"* Peter Q. Tranchida, **Ivan Aloisi**, Barbara Giocastro, Mariosimone Zoccali, Luigi Mondello, Journal of Chromatography A, 1589 (2019) 134-140.

3. *"Chemical characterization of unconventional palm oils from Hyophorbe indica and two other endemic Arecaceae species from Reunion Island"* Yanis Caro, Thomas Petita, Isabelle Grondin, Patricia Clerc, Hermann Thomas, Daniele Giuffrida, Barbara Giocastro, Peter Q. Tranchida, **Ivan Aloisi**, Daniella Murador, Luigi Mondello, Laurent Dufossé, Natural Product Research, 34 (2020) 93-101.

4. *"Towards the determination of an equivalent standard column set between cryogenic and flow-modulated comprehensive two-dimensional gas chromatography"* **Ivan Aloisi**, Tiago Schena, Barbara Giocastro, Mariosimone Zoccali, Peter Q. Tranchida, Elina Bastos Caramão, Luigi Mondello, Analityca Chimica Acta, 1105 (2020) 231-236.

5. *"Recent application and instrumental trends in comprehensive two-dimensional gas chromatography"* Peter Q. Tranchida, **Ivan Aloisi**, Luigi Mondello, LC GC Europe, 33, (2020) 172-178.

6. *"Analysis of organic sulphur compounds in coal tar by using comprehensive two-dimensional gas chromatography-high resolution time-of-flight mass spectrometry"* **Ivan Aloisi**, Mariosimone Zoccali, Peter Q. Tranchida, Luigi Mondello, Separations, 7 (2020) 1-9.

7. *"Fingerprinting of the unsaponifiable fraction of vegetable oils by using cryogenically-modulated comprehensive two-dimensional gas chromatography-high resolution time-of-flight mass spectrometry"* **Ivan Aloisi**, Mariosimone Zoccali, Paola Dugo, Peter Q. Tranchida, Luigi Mondello, Food Analytical Methods 13 (2020) 1523-1529.

8. *"Cryogenic- and flow-modulation comprehensive two-dimensional gas chromatography-mass spectrometry: obtaining similar chromatographic performance"* Barbara Giocastro, **Ivan Aloisi**, Mariosimone Zoccali, Peter Q. Tranchida, Luigi Mondello, LCGC North America, 38 (2020) 548-558.

La borsa di dottorato è stata cofinanziata con risorse del
Programma Operativo Nazionale Ricerca e Innovazione 2014-2020 (CCI 2014IT16M2OP005),
Fondo Sociale Europeo, Azione I.1 “Dottorati Innovativi con caratterizzazione Industriale”

UNIONE EUROPEA
Fondo Sociale Europeo

Ministero dell’Istruzione,
dell’Università e della Ricerca

PON
RICERCA
E INNOVAZIONE
2014 - 2020